TU Clausthal

Clausthal University of Technology

Drillbotics® -Phase 1 Design Report International University Competition 2021/2022 Group B (Physical Rig)

Clausthal University of Technology
Institute of Subsurface Energy Systems
Date: December 22^{nd} , 2021

Table of Contents

List of Figures

List of Tables

List of Abbreviations

IMU	Inertial Measurement Unit
ISR	Interrupt Service Routine
MOSFET	Metal Oxide Semiconductor Field Effect Transistor
FFT	Fast Fourier Transformation
LSB	Least Significant Bit
ITM	Institute of Applied Mechanics
CAD	Computer Aided Design
FEMM	Finite Element Method Magnetics
PCB	Printed Circuit Board
SMD	Surface Mount Device
PLC	Programmable Logic Controller
DP	Drill pipe
BHA	Bottom hole assembly
bbl	Barrel
DHM	Down Hole Motor
RT	Rotary Table
RPM	Revolutions per Minute
ROP	Rate of Penetration
LWD	Log while Drilling
MWD	Measurement While Drilling
TD	Total Depth
MD	Measured Depth

Symbol register

Symbols used

Θ	Magnetomotive force
A	Area
N	Number of turns
I	Current
Φ	Magnetic flux
F	Force
μ_0	Vacuum permeability
μ_r	Relative permeability
B	Magnetic flux density

Guidelines taken into account

Guidlines

i. Student Biographies

Included in Chapter: **2**, Page **4**

ii. A description of your safety plan that is appropriate for the project

Included in Chapter: **9**, Page **80** and in Chapter **3.4,** Page **11**

iii. Engineering sketches or drawings of the rig concept, mechanical and electrical and auxiliary systems, if any, that explain your design assumptions

Along the whole report as an example the full BHA setup is shown in Figure **3.13**

iv. Include any design notes and calculations regarding rig, drillstring and other limitations for the particular modules used in your models.

Cutting transport Calculation given in Chapter: **3.6**

Pressure Loss Calculation given in Chapter: **3.7**

Whole DP-Calculations are given in Chapter: **4**

v. A block diagram/flowchart of the modeled control system architecture. Describe the key features. The response time of measurements, data aggregation and control algorithms should be estimated. Explain how individual measurements are used are in the control code. Are they all given equal weight, and if not, what criteria is used to assign importance?

Included in Chapter: **7** and Page: **54-55**

vi. Since this is a directional drilling problem, be sure to include how downhole data is used for steering and other drilling aspects? Judges are looking for a description of the principles being applied to directionally steer the wellbore and hit the required targets with the intent to score the maximum number of points.

Trajectory is explained in Chapter: **7.2.2**

Exact calculations for the Steering are given on Page: **99 -106**

vii. Proposed user interface/data display that shows the drilling progress in real time.

An example of the planned GUI is shown on Page: **70-71**

viii. Cost estimate and funding plan

Funding Plan and Price list are given in Chapter: **8.4**

ix. Key features for any models/modules and control software. What drilling dysfunctions are addressed?

Included in Chapter **6.3**

x. Proposed data handling, i.e., inherent time delays and uncertainty.

Included in Chapter: **7.1.1**

xi. The Phase I design report should include a discussion regarding the major design concept as modeled (mechanical and otherwise) with respect to the feasibility for use on today's working rigs? If not, what would be needed to allow implementation?

Included in Chapter: **8.5**

1 Introduction and Objectives

The 2022 Drillbotics® competition marks the sixth year that a team from the Clausthal University of Technology (TU Clausthal), Germany is participating in the competition. The TU Clausthal is opting to participate in Group B (physical rig) challenge, which, according to the 2022 Drillbotics® competition guidelines, states its objective as to "design and build a miniature drilling rig and autonomously drill a directional well through a homogeneous rock sample to a given plan". Drilling automation is more and more gaining an increased interest from the oil and gas industry, equipment manufactures, and research organizations. Automating and digitizing the drilling process is considered to offer safety improvements during drilling operations, less drilling time requirements, increasing accuracy in data acquisition, better well placement and quality, and a reduction of costs. In automated drilling systems, the operating parameters are optimized by acquiring relevant data, assessing the data, and adjusting the operating parameters without human interference. Ideally, the automation level reaches tier three, which describes a stage in which the automation has evolved to decide and act autonomously. The purpose of this proposal is to showcase a well-conceived design plan of a small-scale drilling robot that incorporates important features which are essentially encountered in the field. Emphasis has been placed on implementing different, new ideas and solutions in the design, that are not commonly or frequently used in the conventional drilling process to fulfill the demands of directional drilling; utilizing an automated process, which from a human intervention point of view only knows the activation of the start button. This proposal consists of several chapters as follows:

1.1 Introduction and Objectives

The Introduction and Objectives of this report sets the objectives of the proposal and the project. A brief description of the proposal content is explained herein.

1.2 Team and workflow

Team members, as well as supervising and advising staff, are introduced here. Also, workflow and distribution of workload is described.

1.3 Rig Design

This chapter explains the rig structure design, the machine bed, the fluid system, the hoisting system, the sled, and the top drive system. The section's dimensions are listed. Further, calculations for pressure loss and cutting transport are presented.

1.4 Drill Pipe Design

In this chapter the drill pipe characteristics and limit calculations are presented to determine the maximum values for operating the rig.

1.5 BHA design

This chapter explains the bottom hole assembly (BHA) design including the, steering unit, the drill bit and sensor chambers. The developing history leading to the final concept is described. Finally, the chapter includes a brief simulation for the final concept's potential dogleg severity.

1.6 Mechatronic System Architecture

Within this chapter the mechatronic system, the used sensors, the different actuators and as well the bus system that distributes the operational data will be described. Also, the calibration of the sensors before the drilling operations are discussed.

1.7 Algorithmic

This chapter describes how the acquired sensor dataflow will be processed. Filtration and synchronization of the data as well as the algorithms to use this data for drilling optimization and wellbore trajectory are part of this chapter. Also, the possibility for a third-party interface will shortly be mentioned.

1.8 Further Rig Considerations

This chapter includes the anticipated total power consumption of the rig, a funding and budgeting plan, a calculation for the rig's shipping weight and a discussion how the rig's design concept could be upscaled.

1.9 Safety Consideration and Risk Analysis

This chapter discusses the risks and potential harmful events that could occur during the test. Precaution and mitigation plan are set to prevent undesirable events, including the rig structure design and drilling automation system. This report is an update of the previous design report submitted for the Drillbotics® international university competition 2020.

1.10 Future applications

In this chapter we are going to present what we are planing for the future and what may be useful to implement in the current rig design.

2 Team and workflow

This year's team of the TU Clausthal's Drillbotics® team will be again working under the supervision of the senior researchers of the drilling and production department at the Institute of Subsurface Energy Systems.

Supervisors:
Prof. Dr. Philip Jaeger
Erik Feldmann, M.Sc

One staff member of the drilling and production department of the Institute of Subsurface Energy Systems, who was himself three times a participant in previous Drillbotics® competitions, will serve as advisor to the current team.

Advisors:
Wolfgang Hollstein, M.Sc.

The competition team of the TU Clausthal consists of five students from different engineering backgrounds.

Student Team:
Shakhrukh Arbobov

Previously attained degree:	B.Sc Mechanical Engineering, major in Mechanical Design Engineering
Current degree:	M.Sc Mechanical Engineering, major in Mechanical Design Engineering
Expected graduation date:	Fall 2022
Role and responsibilities:	Teamleader, programming, mechanics

Charalampos Soilemezidis

Current degree:	B.Sc. Energy and Resources, major in Petroleum Engineering
Expected graduation date:	Winter 2022
Role and responsibilities:	Administrative activities and electronics

Lilav Koro

Current degree:	B.Sc Energy and Resources, major in Petroleum Engineering
Expected graduation date:	Summer 2022
Role and responsibilities:	Administrative activities and mechanics

Ahmed Fulais

Current degree:	B.Sc Energy and Resources, major in Petroleum Engineering
Expected graduation date:	Summer 2022
Role and responsibilities:	Mechanics and programming

Samet Gürses

Current degree:	B.Sc Mechanical Engineering, major in Mechatronics
Expected graduation date:	Fall 2022
Role and responsibilities:	Mechatronics and mechanics

Based on the previous experiences of the teams from Clausthal University of Technology in the Drillbotics® competition, it showed, that distinct distribution of workload and clear communication between the team members is crucial for success. That led to the conclusion, that when working on a project of this scale with a relatively small team, setting clear objectives and a splitting the workload is necessary for success. The team is composed of three petroleum engineers and two mechanical engineers. This season, a decision was made, so that every team member had to approach the project in an interdisciplinary manner. That means, that certain tasks are split between two or more team members. This way the team has a better overview over the whole project and mistakes done by a single individual can be held better in view and thus avoided. For example, the tasks in the mechanics of the rig were split between three people, the programming was done by two individuals and administrative activities were split up between three members also anything related to mechatronics and automation was split evenly throughout two members. The team leader ensures that the communication between the team members flows smoothly and keeps track of the progress. Weekly meetings are scheduled on Tuesdays, as well as smaller working groups, that take place regularly during the week. The weekly team meetings help all the team members as well as the advisor to keep an overview of the current stand of the project. The arising uncertainties are discussed with the advisor and can this way be

rectified effectively. For the purpose of project management and progress overview, the team uses an online cloud-based platform, which also makes it possible for every Team-member to work from home.

3 Rig Design

3.1 Rig Overview

For the 2022 competition the previous rig design was expanded and proposed to accommodate the rotary BHA system. This years rig, as illustrated in **Figure 3.1**, will consist mainly of a traverse which can be disconnected from the main construction. The traverse is mounted on four pivots and supports drilling in any pre-defined position, i.e. in vertical or horizontal starting position. A higher grade of transportability is achieved with this specific design choice. A surface power pack is used to rotate a flexible shaft which is located in the drill pipe. The bottom part of the shaft is connected to the bit. This design allows to rotate the bit via the flexible shaft without rotating the drill pipe. As a push-the-bit system is used (see **Chapter 5.2.3**), rotation of the drill pipe needs to be prevented. The overall size of the rig and its components are displayed in **Table 3.1**. For this chapter, **Mitchell u. Miska (2011)** is used as a reference.

3.2 Rotary Table and Power Pack

To be able to point the drill bit into any desired spherical coordinate, the BHA must be rotated in the desired direction. To achieve this, a rotary table has been incorporated into the design of the rig. A form-locked and friction locked connection to the drill string by means of a collet chuck assembly is applied and, thus, can position the drill string to achieve a precise angle. Azimuth corrections are also enabled by steering the drill string. In contrast to the concept of last year, this year's construction features a rotary table mounted driving motor. As a driving motor, this year a IHS v60 Servomotor as shown in **Figure 3.2**

Component	Height (cm)	Length (cm)	Width (cm)	Volume (L)
Rock sample reciever	60	68	38	155
Mounting System	80	200	79	
Traverse System	200	40	40	
Topdrive	28	9,5	9,5	
Syringe System	15	14	20	
BHA	15,4	3,3	3,3	

Table 3.1: Rig components‘ dimensions

Figure 3.1: Rig overview

was chosen, which has enough power and rpm to propel the flex shaft in order to provide downhole torque and speed. As the flexible shaft runs within the drill pipe, cables and hoses cannot be accommodated within the pipe. The data and power supply cables as well as the hoses for drilling mud and hydraulic fluids are therefore attached outside to the drill pipe and connected to the BHA. A rotary decoupler is attached to the motor, allowing the hoses and cables to rotate with the rotary table and hence the drill pipe.

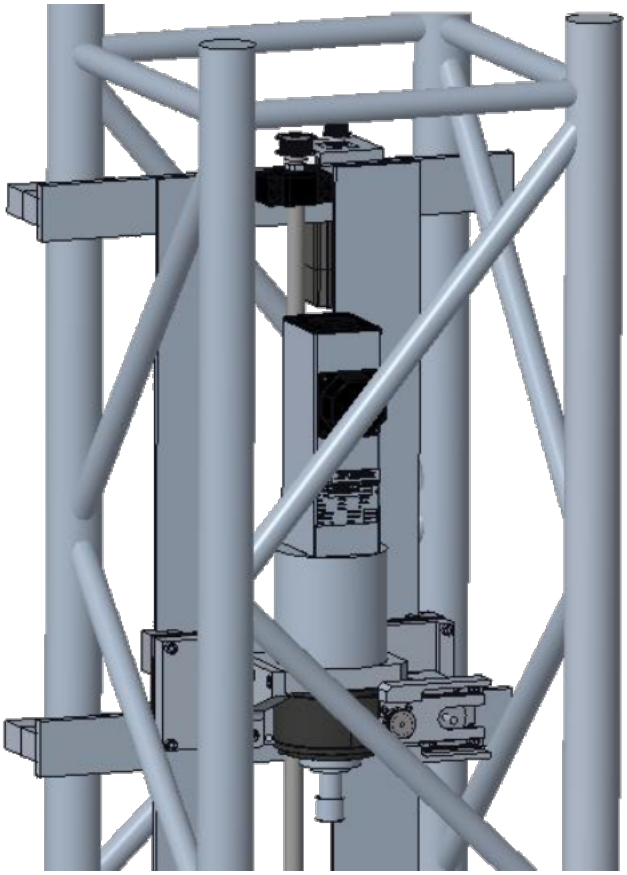

Figure 3.2: Rotary Table and Servomotor

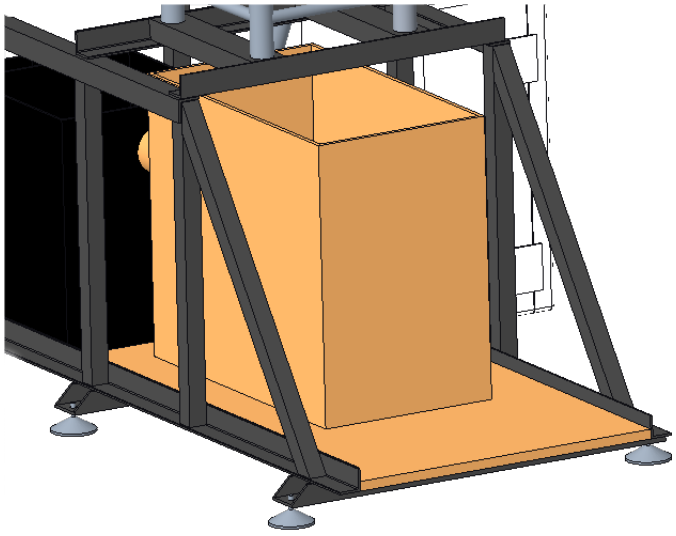

Figure 3.3: Rock sample receiver

3.3 Rock Sample Receiver

The rock sample receiver **Figure 3.3** of this year's rig is a simple cuboid, as illustrated in the image beneath the section, where the rock sample will be hoisted in. The sampling receiver is connected to the mud filtration to separate the drilling fluid into its different components. In contrast to last year's installation, this year's receiver will feature a mounted beam on top with a centralizer tube in order to stabilize the BHA before it enters the rock sample completely. A reliable measurement of the earth's natural electromagnetic field to determine the azimuth is difficult due to the electromagnetic noise and interference created by the nearby electrical devices and electrical motors. To solve this problem, a decision was taken to create an own electromagnetic field through placement of two square coils with 185 winding's of copper wire and a diameter of 1 mm, on the outer walls of the rock sample receiver. The length of each side of the square coils amount to 400 mm. These coils will create a much stronger magnetic field which leads to a better environment for the magnetometer and therefore it can be assured, that the measured azimuth is reliable and correct. As the coils are self made, the electric resistance for each coil is calculated as follows:

$$R = \frac{\rho * l}{A} = \frac{17,86 * 10^{-3}\Omega\text{mm}^2/\text{m} * 0.4m * 4 * 185}{\pi * 0,5mm^2} = 6.722\Omega \tag{3.1}$$

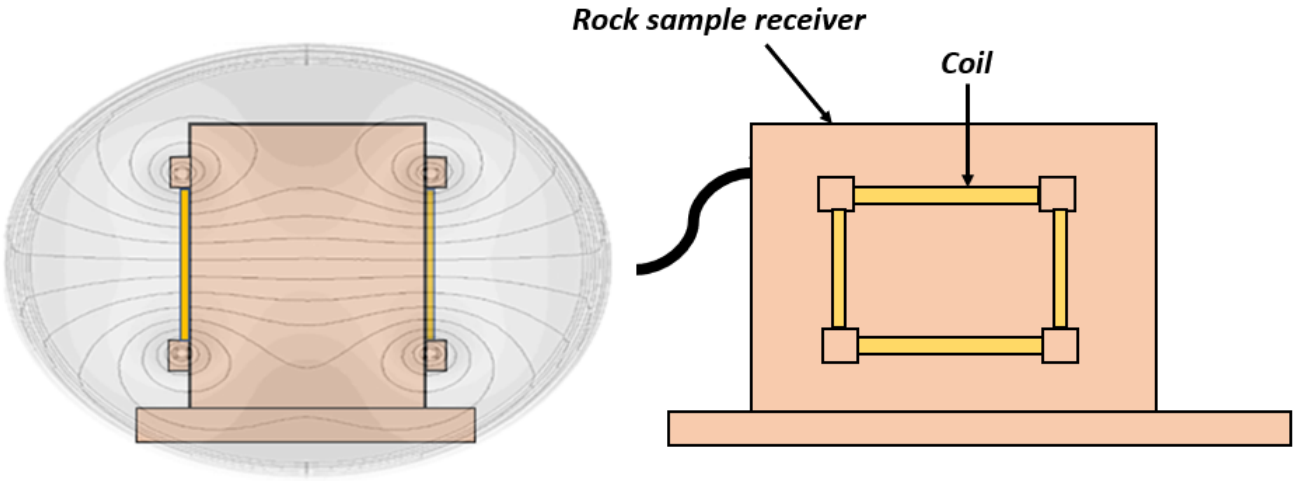

Figure 3.4: Rock sample receiver with coil

3.4 Rig Electronics

The electronics are housed in a switch-cabinet under the rig table and protected against water. In addition, multiple FI circuit breakers are installed to interrupt the power supply immediately in the event of a failure. It was decided to use a **TN-S network** as it is one of the safest networks according to German standards (**DIN VDE 0100**) which, due to the separately laid **PE** and **N** conductors, reliably switches off in the event of a failure. Furthermore, all those involved in working on the mini-rig system were instructed in electrical-engineering and encouraged to follow the 5 safety rules according to **DIN VDE 0105**. To start the rig there is a Main-switch on the right side of the switch-cabinet which is directly connected with the first FI-circuit breaker that cuts off all three phases in case of a failure, to detect in which phase the failure occurred there are three separate FI-circuit breakers that are switching of independently. An emergency switch is placed with reach, which can be accessed immediately in case a human or a system error occurs and the machine has to be turned off instantly. This switch is installed according to **EN ISO 13850** standards, and it is clearly distinguished from the second emergency stop switch, which only sends a signal through the BUS to stop all moving and or working parts. A small overview of how the individual components of the rig are connected is shown on **Page 54**, This is only a process-flow diagram and not a circuit diagram. The main computer with the human machine interface is located on the table next to the main controller. So that the current state during drilling can be easily tracked and monitored.

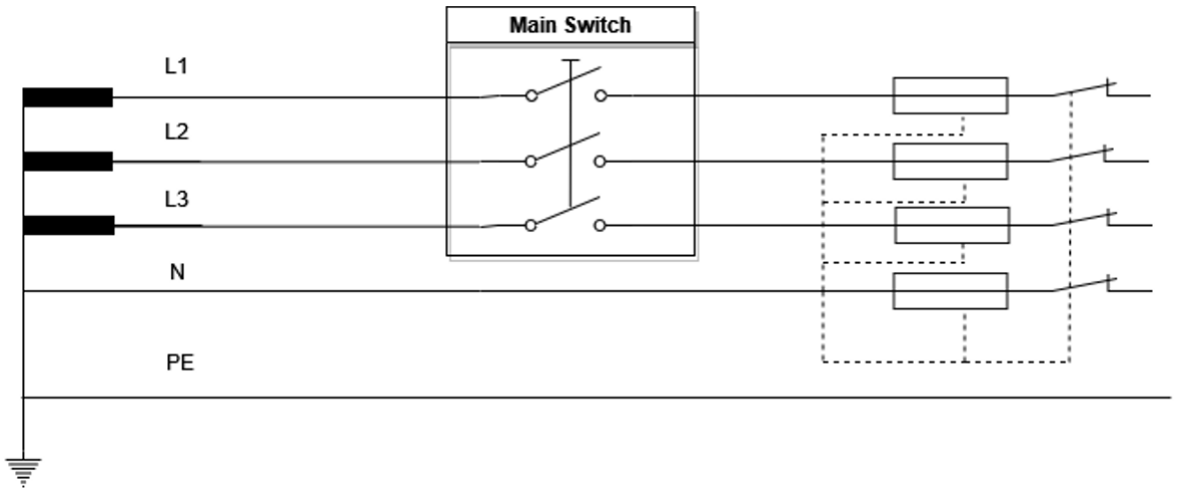

Figure 3.5: TN-S network

3.5 Rig Plumbing and Mud Handling

A drilling mud preparation container is installed next to the drilling sample container. Behind the filter, a pump is connected which generates the necessary pump pressure for drilling. The pumps used for the setup are a combination of a pre charging pump (2-3 bar pre-pressure), that feeds a positive displacement pump with a maximum pressure capacity of 120 bar. In between both pumps a flow meter is placed, which detects the amount of fluid that is being fed to the positive displacement pump. Further details about the flow meter will be discussed. in **Chapter 6.4.2** The drilling mud will be pumped through a plastic hose that is laid parallel to the drill pipe. The hose will lead into the BHA and the drilling mud is then directed to the bit and leaves the bit through its nozzles. The returning drilling mud is handled by a two-chambered separation tank system. The drilling mud is then drawn out of the rock sampling receiver directed into the first mud tank. In there, the heavier components are separated due to the gravitational force and only the liquid components enter the next filtering tank. Due to the slow flow rate of the systems fluid, enough time is available for the separation of the solid from the liquid components of the mud. The last tank is connected to a pumping system to reinject the filtered drilling mud into the hose. Inside the mud tanks, filtration packs consisting of plastic granules are installed to increase filtration performance of the mud handling system. Water with no additives will be used as drilling mud. Any other decision would lead to higher environmental impacts and to the need of a very thorough and complex sealing and leakage prevention. Also, the need for additives or an oil-based mud is not seen for the given application. Basis for the circulation system were the cutting transport and pressure loss calculations which are presented in the following sub-chapters. The used values can be found in the **Appendix**.

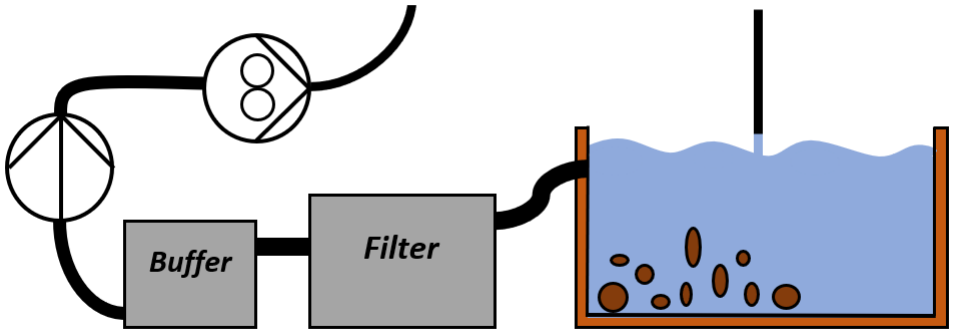

Figure 3.6: Mud Handling

3.6 Cutting Transport Calculation

The following section sets the flow rate calculation required for the drilling operation with a Newtonian fluid. References are **PhD u. Liu (2011)** and **Aadnoy (2006)** The minimum flow rate of the mud v_{mud} must be greater than the terminal slip velocity $v_{rittinger}$ expressed in **equation 3.2**.

$$v_{mud} > v_{rittinger} \tag{3.2}$$

The slip velocity can be calculated by Moore's correlation for a vertical well. The slip velocity of a small spherical particle settling (slipping) through a Newtonian fluid under laminar flow condition, v_{slip} is given by Stoke´s law **3.6**.

$$\begin{aligned} v_{slip} &= \frac{g * (\rho_s - \rho_w) * d_s^2}{\mu_w * 18} \\ &= \frac{9.81\,\mathrm{m\,s^{-2}} * 0.000\,000\,01\,\mathrm{m} * (2650\,\mathrm{kg\,m^{-3}} - 1000\,\mathrm{kg\,m^{-3}})}{18 * 0.001\,\mathrm{Pa\,s}} \\ &= 0.5394\,\mathrm{m\,min^{-1}} \\ (&= 0.0295\,\mathrm{ft\,s^{-1}}) \end{aligned} \tag{3.3}$$

Where:

d_s: Diameter of cutting

ρ_s: Density of the cutting solid

ρ_w: Density of the drilling fluid (Water)

μ_w: Viscosity of the drilling fluid (Water)

Stokes law could be used already to determine the slip velocity, as the Particle Reynolds number is smaller than one. The Particle Reynolds number Re_p is calculated as follows **3.7**.

$$\begin{aligned} Re_p =& \frac{\rho_w \cdot v_{slips} \cdot d_s}{\mu_w} \\ =& \frac{1000\,\mathrm{kg\,m^{-3}} * 0.008\,99\,\mathrm{m\,s^{-1}} * 0.0001\,\mathrm{m}}{0.001\,\mathrm{Pa\,s}} \\ =& 0.899 \end{aligned} \tag{3.4}$$

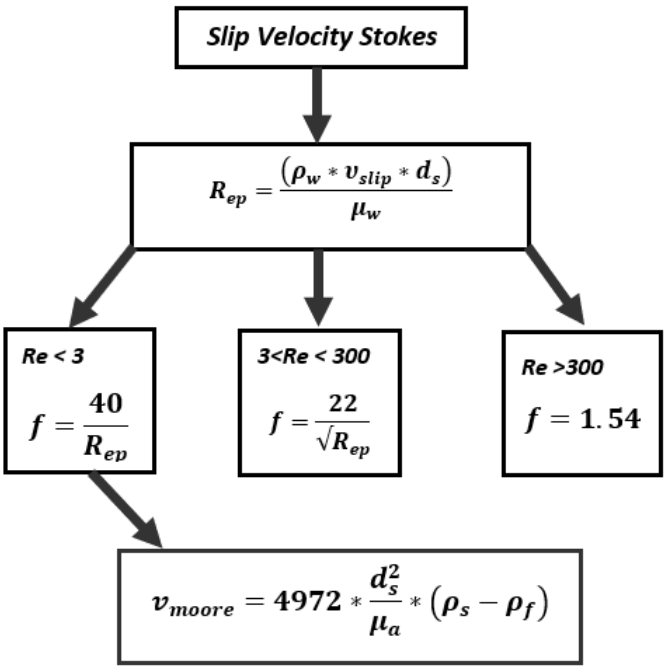

Figure 3.7: Slip velocity derived by Moore´s correlation

The friction factor f is taken as 44.49 according to Moore's correlation **3.8**, with that in mind, the empirical equation **3.5** that applies for particle Reynolds numbers smaller than 3, can be used. This equation only works in field units, so in the following it will be switched from SI units to Oil-field units. This method is used to get a closer approximation to the actual slip velocity by including the friction factor.

$$\begin{aligned} v_{moore} =& 4972 * \frac{d_s^2 * (\rho_s - \rho_w)}{\mu_w} \\ =& 4972 * \frac{0,000016 * (26,55 - 8,34)}{1} \\ =& 1.448 \, \frac{\text{ft}}{\text{min}} \\ =& (0.441 \, \frac{\text{m}}{\text{min}}) \end{aligned} \tag{3.5}$$

The slip velocity is quite low. The reason for that lies in the approximation of the cuttings' diameter. Previously, more of a grinding action was used to bore through the sample, which would lead to **small cuttings** <0.1 mm. Due to the structure of the bit, it is not possible to assure if this method is going to work. For this reason, the slip velocity is calculated for

cuttings as big as 1 mm:

$$\begin{aligned} v_{slipB} &= \frac{g * (\rho_s - \rho_w) * d_s^2}{\mu_w * 18} \\ &= \frac{9.81\,\mathrm{m\,s^{-2}} * 0.000\,001\,\mathrm{m} * (2650\,\mathrm{kg\,m^{-3}} - 1000\,\mathrm{kg\,m^{-3}})}{18 * 0.001\,\mathrm{Pa\,s}} \\ &= 53.49\,\mathrm{m\,min^{-1}} \\ (&= 2.95\,\mathrm{ft\,s^{-1}}) \end{aligned} \tag{3.6}$$

$$\begin{aligned} Re_{pB} =& \frac{\rho_w \cdot v_{slipsB} \cdot d_s}{\mu_w} \\ =& \frac{1000\,\mathrm{kg\,m^{-3}} * 0.899\,\mathrm{m\,s^{-1}} * 0.0001\,\mathrm{m}}{0.001\,\mathrm{Pa\,s}} \\ =& 899 \end{aligned} \tag{3.7}$$

For the bigger cutting diameter ($Re_{pB} > 1000$) the friction factor becomes constant as turbulent flow is approached. This leads to Rittingers equation (f=1.54).

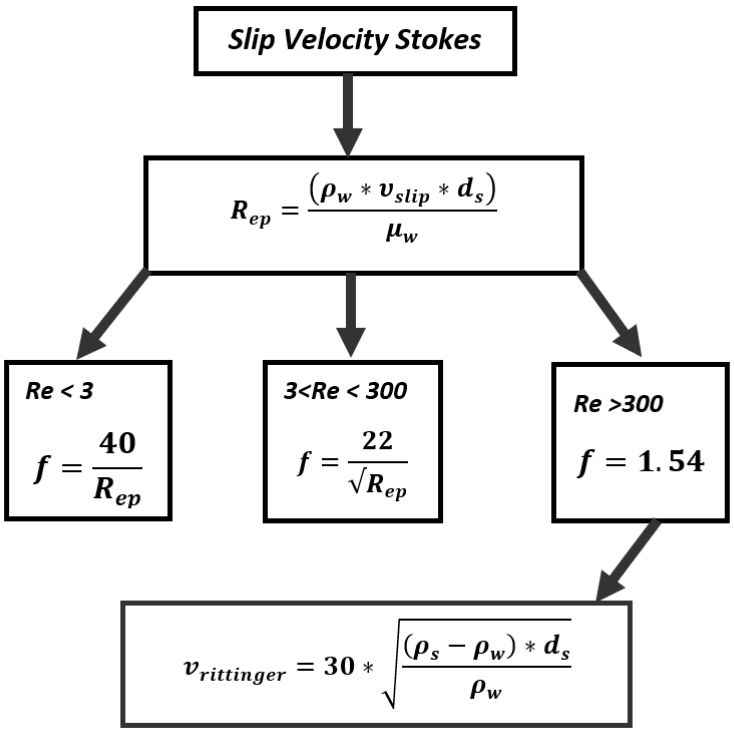

Figure 3.8: Slip velocity derived by Moore´s correlation

$$
\begin{aligned}
v_{rittinger} =& 30 * \sqrt{\frac{(\rho_s - \rho_w) * d_s}{\rho_w}} \\
=& 30 * \sqrt{\frac{(2.65\,\mathrm{g\,cm^{-1}} - 1\,\mathrm{g\,cm^{-1}}) * 0.1\,\mathrm{cm}}{1\,\mathrm{g\,cm^{-1}}}} \\
=& 7.30\,\mathrm{m\,min^{-1}} \\
(=& 0.399\,\mathrm{ft\,s^{-1}})
\end{aligned}
\tag{3.8}
$$

Therefore, the mud velocity must be at least as high as $0.399\,\mathrm{ft\,s^{-1}}$.

A flow rate of 1.85 gpm ($7\,\mathrm{L\,min^{-1}}$) is pumped by the rig pump. The annular velocity v_a is calculated by following formula:

$$
\begin{aligned}
v_a =& \frac{Q}{2,448 * (d_h^2 - d_d^2)} \\
=& \frac{1.85\,\mathrm{gpm}}{2,448 * (2.22\,\mathrm{in} - 0.15\,\mathrm{in})} \\
=& 0.3650\,\mathrm{ft\,s^{-1}} \\
(=& 6.675\,\mathrm{m\,min^{-1}})
\end{aligned}
\tag{3.9}
$$

Where:

Q: Flow rate of drilling fluid

d_h: Diameter of Borehole in inch

d_p: Diameter of Drill pipe in inch

It can be seen that the annular velocity is smaller than the slip velocity, (v_a<$v_rittinger$) which would make an effective cutting transportation impossible. When it is taken into account that a major part of the cross-sectional area, between the drill pipe and the borehole, is going to be taken away by the hoses cables and the drilling fluid supply (as it won't flow through the DP), the difference between inner and outer diameter gets smaller, and therefore the annular velocity gets higher.

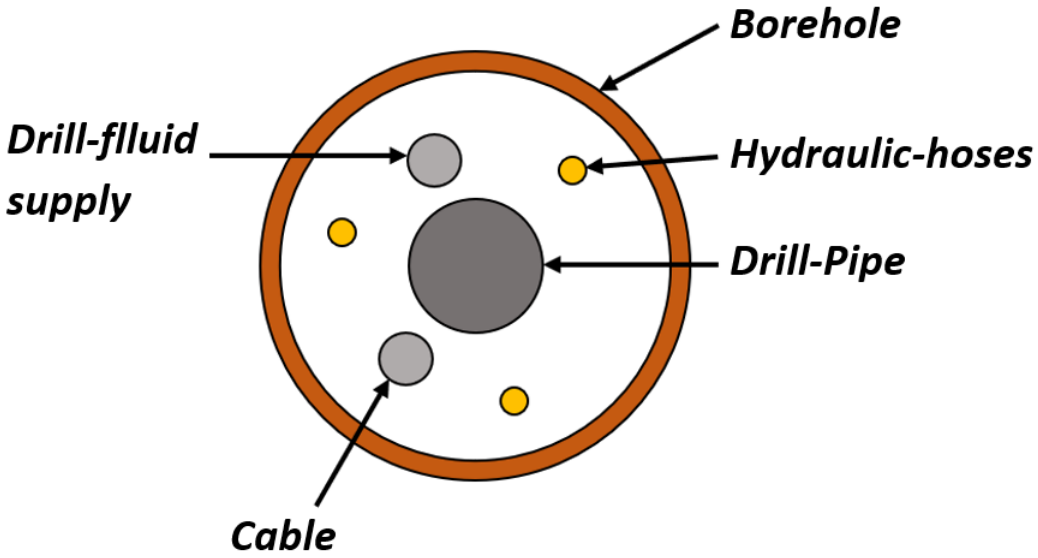

Figure 3.9: Borehole schematic

$$
\begin{aligned}
A_{BO} &= \frac{\pi}{4} * (1,49in)^2 = 2,220in^2 \\
A_{DP} &= \frac{\pi}{4} * (0,4in)^2 = 0,12in^2 \\
A_{HO} &= \frac{3*\pi}{4} * (0,07in)^2 = 0,011in^2 \\
A_{FS} &= \frac{\pi}{4} * (0,314in)^2 = 0,077in^2 \\
A_C &= \frac{\pi}{4} * (0,314in)^2 = 0,077in^2 \\
A_I = A_{DP} + A_{HO} + A_{FS} + A_C &= 0,285in^2 \\
d_{dneu} &= \sqrt{\frac{A_I}{\frac{\pi}{4}}} = 0.60\,\text{in}
\end{aligned}
\tag{3.10}
$$

$$
\begin{aligned}
v_{a,neu} =& \frac{Q}{2,448 * (d_h^2 - d_{d,neu}^2)} \\
=& \frac{1.85\,\text{gpm}}{2,448 * (2.22\,\text{in} - 0.6\,\text{in})} \\
=& 0.4650\,\text{ft}\,\text{s}^{-1} \\
(=& 8.575\,\text{m}\,\text{min}^{-1})
\end{aligned}
\tag{3.11}
$$

For the transport ratio a value of above 50% is empirically recommended to achieve good hole-cleaning during drilling. The transport ratio is calculated as follows and a value of 14.19% is determined. It will be assured that this ratio is sufficient. In case problems with bottom hole clearing arise during testing, a more powerful pump will be purchased.

$$Transport\ ratio = \frac{v_{a,neu} - v_{rittinger}}{v_{a,neu}} * 100 = 14.19\% \tag{3.12}$$

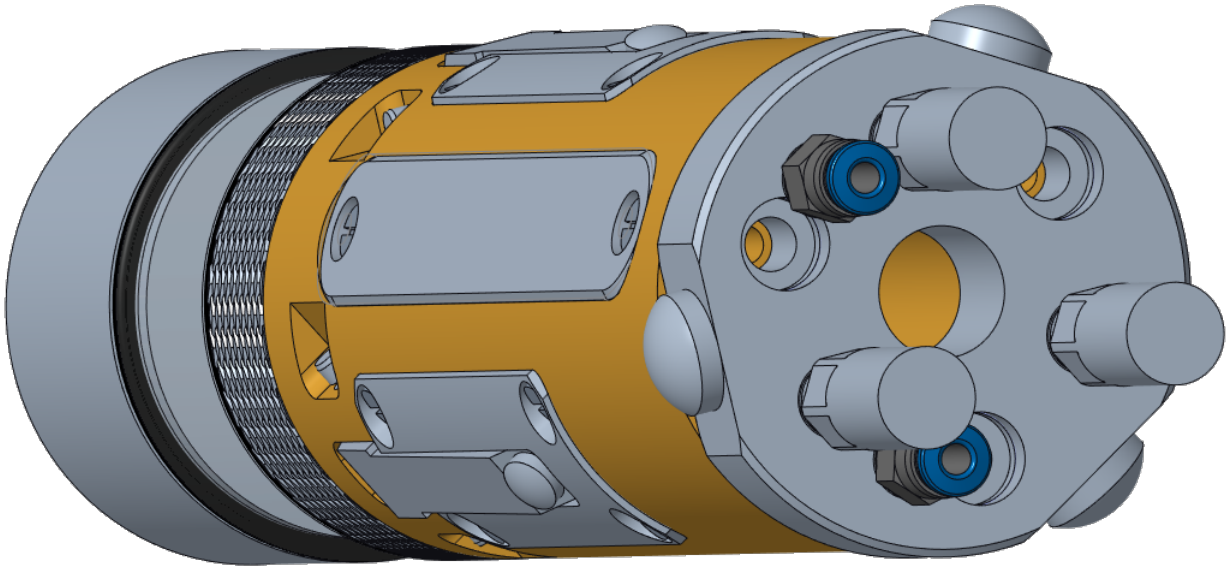

Figure 3.10: Connection for Hoses and Cable

3.7 Pressure Loss Calculation

The following section sets the calculation for conventional, rotary drilling pump requirements with the bit dimensions provided by DSATS. Assuming the Newtonian fluid (water) flows inside the hose around the drill string until it gets to the BHA where it connects to the drill pipe and exits through the bit, which cause the biggest drop in pressure. The pressure loss inside the hose along the drill pipe until it connects to the BHA is neglected. A small overview of how the fluid flows is shown in **Figure: 3.11**.

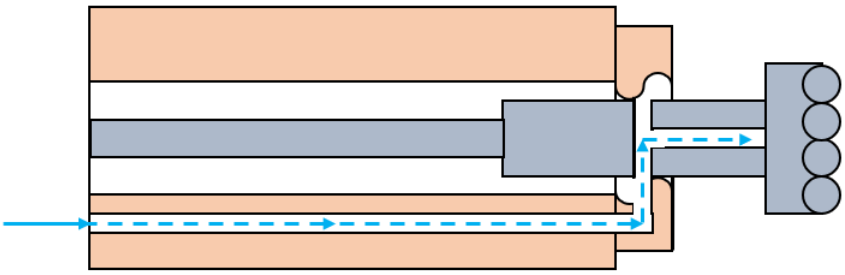

Figure 3.11: Fluid-flow schematic

First the velocity of the fluid in the Flow line v_d is determined:

$$v_d = \frac{Q}{2.448 * id_H^2} = \frac{1,85gpm}{2.448 * 0,15^2\text{in}} = 33.5\,\text{ft}\,\text{s}^{-1}\ (102\,\text{m/s}) \tag{3.13}$$

Where:
Q: Flow rate of drilling fluid

Based on that, the Reynolds number is determined:

$$Re = \frac{928 * \rho_f * v_d * id_p}{\mu_w} = \frac{928 * 8.33ppg * 33.5\,\text{ft}\,\text{s}^{-1} * 0.15\,\text{in}}{1cp} = 38844\ (Turbulent) \tag{3.14}$$

The Required friction factor f can be calculated by the following formula:

$$f = 0.25([log_{10}(\frac{k}{3.7 * id_p} + \frac{5.74}{Re^{0.9}})])^{-2} = 0,25 * ([log_{10}(\frac{0.0006\text{in}}{3.7 * 0,15\text{in}} + \frac{5.74}{38844^{0.9}})])^{-2} = 0.031 \tag{3.15}$$

Where:

k: Roughness of the flow line (assumed with 0,0006in)

Re: Reynolds number

The pressure loss in the flow line inside the BHA parallel to the drill string, P_s is calculated as follows:

$$P_s = \frac{f * \rho_w * v_d^2 * L_{Flowline}}{25.8 * id_p} = \frac{0.0301 * 8.33ppg * 33,5^2\text{ft s}^{-1} * 3.14\,\text{in}}{25.8 * 0.15\,\text{in}} = 228\,\text{psi} \quad (15.72\,\text{bar}) \tag{3.16}$$

Where:

f: Fanning friction factor

$L_{Flowline}$: Length of the drill string

i_{dp}: Internal diameter of the Flow line

In the next part, the losses in the hollow rotating part right beneath the Steering unit as well as the losses inside the small section where the fluid flows through the DP, have to be calculated.

First, the Losses inside the Hollow part are determined.

$$v_{ho} = \frac{Q}{2,448 * id_{ho}^2} = \frac{1,85gpm}{2,448 * 0,118^2\text{in}} = 54.27\,\text{ft s}^{-1} \;\; (16.49\,\text{m s}^{-1}) \tag{3.17}$$

Where:

v_{ho}: Velocity of the drilling fluid inside the hollow part

id_{ho}: Internal diameter of the hollow part

Reynolds Number:

$$R_e = \frac{928 * \rho_w * v_{ho} * id_{ho}}{\mu_w} = \frac{928 * 8.33ppg * 54.27\,\mathrm{ft\,s^{-1}} * 0,118\mathrm{in}}{1cp} = 49503 \quad (Turbulent) \tag{3.18}$$

Friction factor:

$$f = 0.25([log_{10}(\frac{k_{ho}}{3.7 * id_{ho}} + \frac{5.74}{Re^{0.9}})])^{-2} = 0,25 * ([log_{10}(\frac{0.0039\mathrm{in}}{3.7 * 0,118\mathrm{in}} + \frac{5.74}{49503^{0.9}})])^{-2} = 0.051 \tag{3.19}$$

Where:
k_{ho}: Roughness of the hollow part (0.0039in)

Pressure Losses:

$$P_{ho} = \frac{f * \rho_w * v_{ho}^2 * L_{ho}}{25.8 * id_{ho}} = \frac{0.051 * 8.33ppg * 54,27^2\mathrm{ft\,s^{-1}} * 0.35\,\mathrm{in}}{25.8 * 0.118\,\mathrm{in}} = 143.84\,\mathrm{psi} \quad (9.9\,\mathrm{bar}) \tag{3.20}$$

Where:
L_{ho}: Length of the hollow part
Now, only a small section inside the DP remains:

$$v_{dp} = \frac{Q}{2,448 * id_{dp}^2} = \frac{1,85gpm}{2,448 * 0,27^2\mathrm{in}} = 10.36\,\mathrm{ft\,s^{-1}} \ \ (3.13\,\mathrm{m\,s^{-1}}) \tag{3.21}$$

Reynolds Number:

$$R_e = \frac{928 * \rho_w * v_{dp} * id_{dp}}{\mu_w} = \frac{928 * 8.33ppg * 10.36\,\mathrm{ft\,s^{-1}} * 0,27\mathrm{in}}{1cp} = 21623 \quad (Turbulent) \tag{3.22}$$

Friction factor:

$$f = 0.25([log_{10}(\frac{k_{dp}}{3.7 * id_{dp}} + \frac{5.74}{Re^{0.9}})])^{-2} = 0,25 * ([log_{10}(\frac{0.0039\mathrm{in}}{3.7 * 0,27\mathrm{in}} + \frac{5.74}{21623^{0.9}})])^{-2} = 0,045 \tag{3.23}$$

Pressure Losses:

$$P_{dp} = \frac{f * \rho_w * v_{dp}^2 * L_{dp}}{25.8 * id_{dp}} = \frac{0.051 * 8.33ppg * 10,36^2 \text{ft s}^{-1} * 1.3 \text{ in}}{25.8 * 0.275 \text{ in}} = 8.35 \text{ psi} \quad (0.6 \text{ bar}) \tag{3.24}$$

Finally, the previously calculated losses are summed up to acquire the BHA pressure losses:

$$P_{dp} + P_{ho} + P_s = P_{BHA} = 380 \text{ psi} \quad (26.2 \text{ bar}) \tag{3.25}$$

There are three nozzles at the bit with diameter d_n. For that reason, the total area of nozzle, $A_n$is calculated as follows:

$$A_n = 3 * \frac{\pi}{4} * d_n^2 = 3 * \frac{\pi}{4} * 0,118\text{in}^2 = 0.008\text{in}^2 \quad (0.053\text{cm}^2) \tag{3.26}$$

Then, the pressure loss at the bit,P_{bit} can be estimated by following calculation:

$$P_{bit} = \frac{Q^2 * \rho_f}{12031 * A_n^2} = \frac{1,84gpm^2 * 8.33ppg}{12031 * 0,008in^2} = 35.06psi \tag{3.27}$$

The jet impact force, F_j of the bit is:

$$F_j = 0,01823 * C_d * Q * \sqrt{\rho_f * P_{bit}} = 0,01823 * 0,95 * 1,85gpm * \sqrt{8,33ppg * 35.06psi} = 0,54lbf \tag{3.28}$$

Where:
C_d: Discharge coefficient (assumed value 95%)

The jet velocity of the bit, v_{bit} is:

$$v_{bit} = \frac{Q * 144}{448,8 * A_n} = \frac{144 * 1,85gpm}{448,8 * 0,008\text{in}^2} = 73.79 \text{ ft s}^{-1} \quad (22.5 \text{ m s}^{-1}) \tag{3.29}$$

Further, the pressure loss in the annulus, P_a is calculated as follows:

$$P_a = \frac{1,4327 * 10^{-7} * \rho_f * L_{rock} * v_{a,neu}^2}{d_h - d_{d,neu}} = \frac{1,4327 * 10^{-7} * 8,33ppg * 1,97\text{ft} * 27,6^2\text{ftmin}}{0,125\text{ft} - 0,05\text{ft}} = 0,02psi \tag{3.30}$$

The annular velocity was calculated as $28\,\mathrm{ft\,min^{-1}}$. As this is not very fast, the pressure loss in the annulus is negligible. the total downhole pressure loss $P_{downhole}$ is the sum of the following.

$$P_{downhole} = P_{bit} + P_{BHA}(+P_a) = 35.06psi + 380psi = 415,06psi \quad (28.6\,\mathrm{bar}) \tag{3.31}$$

It is assumed that the pump will be connected with the hose line (made from rubber material) to the standpipe with roughness 0.0006 in. The pressure loss in the hose, P_H is calculated by following schematic as applied for the pressure loss calculation before:

$$v_H = \frac{Q}{2,448 * id_H^2} = \frac{1,85gpm}{2,448 * 0,5^2\mathrm{in}} = 3.02\,\mathrm{ft\,s^{-1}} \ \ (0.92\,\mathrm{m\,s^{-1}}) \tag{3.32}$$

$$R_e = \frac{928 * \rho_w * v_H * id_H}{\mu_w} = \frac{928 * 8.33ppg * 3.02\,\mathrm{ft\,s^{-1}} * 0,5\mathrm{in}}{1cp} = 11678 \quad (Turbulent) \tag{3.33}$$

Then, the ratio of the roughness of the pipe divided by the inner diameter of the pipe k_H/id_H calculated to determine the friction factor on the Fanning chart, as shown in Figure **??** :

$$\frac{k_H}{id_H} = \frac{0.0006\,\mathrm{in}}{0.5\,\mathrm{in}} = 0.0012 \tag{3.34}$$

Based on the Fanning chart, see **Figure 3.12**, the friction factor,f is approximately 0.007. The pressure loss inside the hose, P_H is:

$$P_H = \frac{f * \rho_w * v_H^2 * L_H}{25.8 * id_H} = \frac{0.007 * 8.33ppg * 3.02^2\mathrm{ft\,s^{-1}} * 7.5\,\mathrm{in}}{25.8 * 0.5\,\mathrm{in}} = 0.3\,\mathrm{psi} \quad (0.02\,\mathrm{bar}) \tag{3.35}$$

The pressure loss through the hose is negligible, which brings the total pressure loss along the entire system to P_{system}=$P_{downhole}$ or 415,06psi. If additional atmospheric pressure and the hydro static-pressure are added, the pressure which the pump has to deliver can be determined.

$$\begin{aligned} P_{pump} =& P_{system} + P_{atm} + \frac{\rho_w * (v_H - v_a)^2}{2} + \rho_f * g * H_{rig} \\ =& 415,06psi + 14,5 + \frac{8.33ppg * 7,48 * (3.02^2 - 0,46^2)\mathrm{fts}}{2 * 32,174\mathrm{fts^2} * 144} + \frac{8.33ppg * 7.48 * 32,174\mathrm{fts^{-2}} * 7.5}{32,174\mathrm{fts^{-2}} * 144} \\ =& 432.86psi \quad (29.7bar) \end{aligned} \tag{3.36}$$

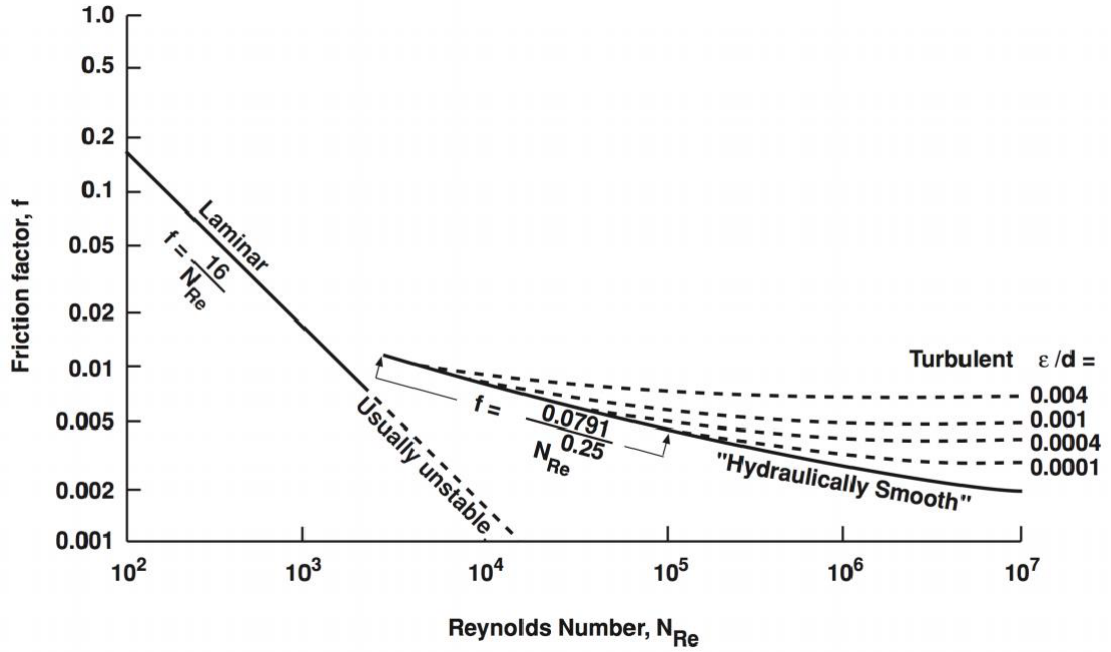

Figure 3.12: Fanning chart

$$Pump_{HP} = \frac{P_{pump} * Q}{1714} = \frac{432,86psi * 1.85gpm}{1714} = 0,46HP \tag{3.37}$$

It is assumed that the efficiency of the pump is 85%, therefore the requirement of the horsepower pump is 0.46 HP. The following **Table 3.2** shows the variation of the pump power requirement according to the flow rate variation:

Table 3.2: Pump power requirement rotary drilling

Flow ratevariation (gpm)	Flow rate variation (Lpm)	Transport ratio (%)	Pump Pressure (bar)	Pump (HP)	Pump (kW)
1,32	5	70	4,82	0,05	0,04
1,84	7	83	8,19	0,12	0,09
2,64	10	85	15,3	0,34	0,25
3,43	13	88	24,89	0,72	0,53

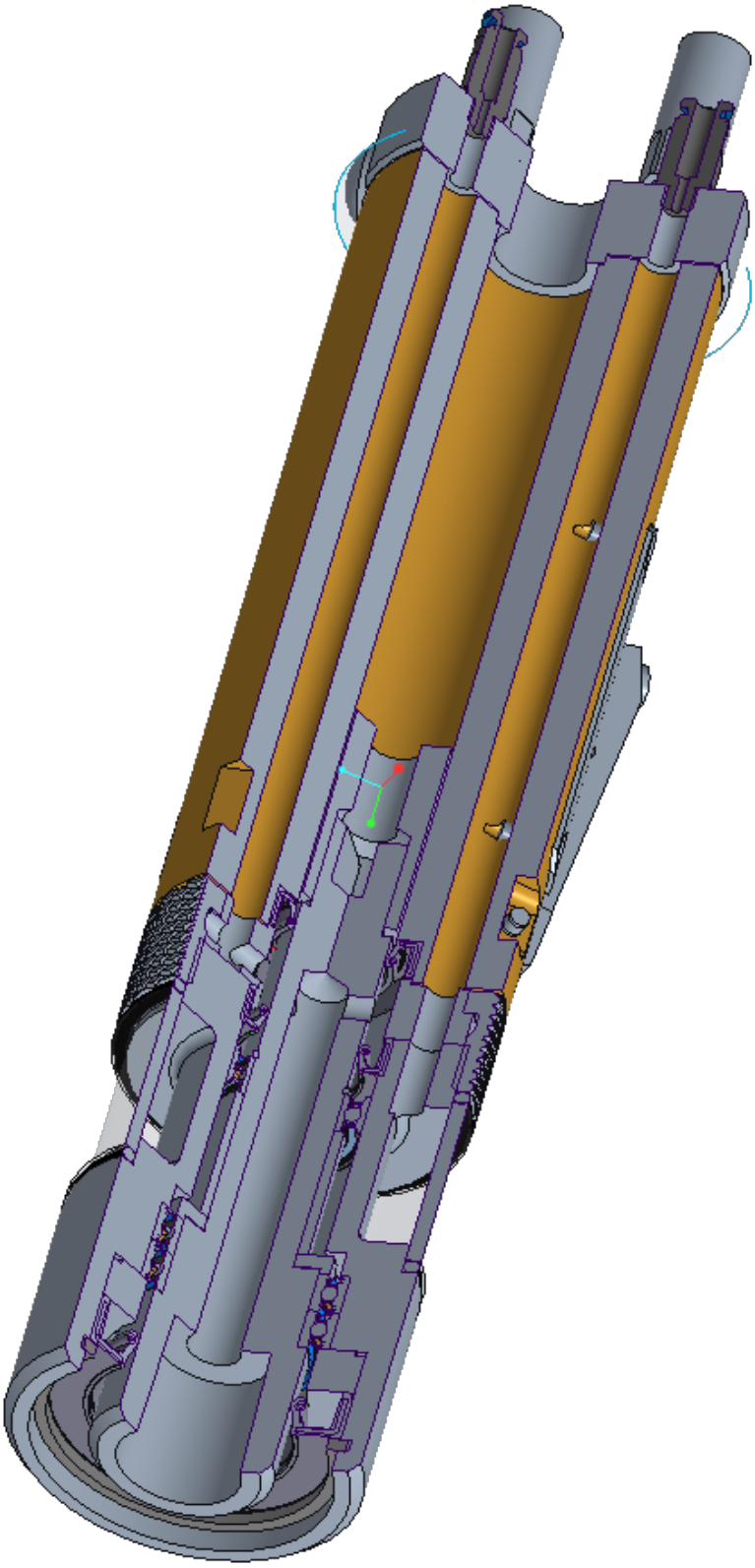

Figure 3.13: Fluid Pathway inside the BHA

4 Drill Pipe

The original rig featured an aluminum drill pipe. Since last year, the guidelines allow for a steel drill pipe to be used for the rig. Due to the higher stability and durability, it was decided to upgrade the rig with a **steel pipe**. The diameters, the density and the Young's Modulus of the selected pipe can be found in the **Appendix**. The 0.91 m long pipe is constructed in one piece and hence does not need tool joints. The pipe is connected with the top drive and the BHA with collect chuck joints. Through the pipe runs the before mentioned flexible shaft. All hoses and cables are attached to the outside of the DP. To accomplish a stable connection, 3D Printed clips that are screwed tightly around the DP with clip-in connections for the hoses, cables and fluid supply are used. Based on the selected pipe, the following limit calculations were conducted. The flexibility of the pipe and its impact on directional drilling will be discussed in **Chapter 5.2.6**, as a reference **5C3 (1994)** and **Bourgoyne (1986)** is used.

4.1 Limit Calculations

The steel drill pipe can be considered as one of the weakest parts in the entire string next to a connection. The following calculated values for buckling, burst and torsion maxima, are based on the scenario that no other forces are acting on the component for the calculation. The maximum values are good indicators, aiding in the selection of the appropriate equipment and parameters for the drilling robot, such as the maximum WOB for the hoisting system, maximum torque value for the downhole motor, and high pump pressures for flushing. The used values can be found in the **Appendix**.

4.2 Buckling Limit Calculation

Buckling is characterized by a lateral deformation or failure of a structural member subjected to high axial compressive stress, where the compressive stress at the point of failure is less than the yield strength that the material can withstand. The critical buckling load limit of the steel drill pipe is calculated by the following Euler equation (assuming both pipe ends are pinned). First the moment of inertia is determined:

$$I = \frac{\pi}{64} * (d_p^4 - id_p^4) = \frac{\pi}{64} * (0,393in^4 - 0,315in^4) = 6.876 * 10^{-4}in^4 \tag{4.1}$$

Where:

d_p: Outside diameter of the drill pipe

id_p: Inside diameter of the drill pipe

Then the critical buckling load, P_{bcr} is calculated:

$$P_{bcr} = \frac{\pi^2 * E * I}{(K * L)^2} = \frac{\pi^2 * 2,901 * 10^{-7} * 6,8790 * 10^{-4}}{(1 * 36)^2} = 151.92lbf \quad (75,77N) \qquad (4.2)$$

Where:

P_{bcr}: Critical buckling load

E: Modulus of elasticity of the steel drill pipe

I: Area moment of inertia

L: Length of the column

K: Column effective length factor

Based on the scenarios of buckling failure, there are several recommendations in respect to the effective length factor (K), as illustrated in **Figure 4.1** and **Table 4.1**. The variation of effective length factor is used to estimate the buckling load limit.

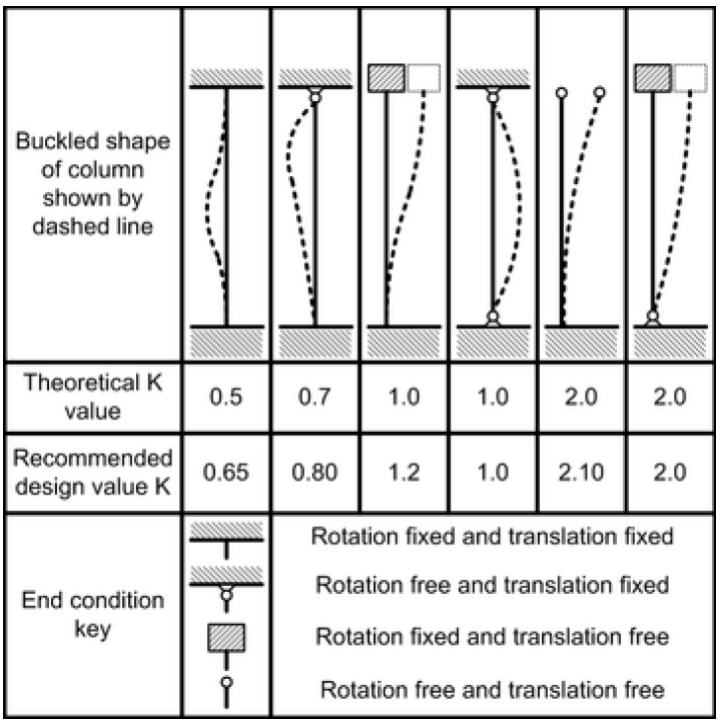

Figure 4.1: Design value K variation

Table 4.1: Buckling limit according to K variation

K variation	Buckling load limit (lbf)	Buckling load limit (N)	Buckling load limit (Kg)
0,5	607,67	2703,05	275,63
0,7	310,04	1379,13	140,63
1	151,92	675,77	68,91
2	37,98	168,94	17,22

4.3 Burst Limit Calculation

Assuming the yield strength of the steel drill pipe is **31183 psi** (215 MPa) and a safety factor of **1.5**, the burst limit P_{burst} of the steel drill pipe can be estimated by following equation (Barlow equation):

$$P_{burst} = \frac{2 * Y_p * t}{d_p * Sf} = \frac{2 * 31183\text{Nin}^2 * 0,0787\text{in}}{0,393\text{in} * 1,5} = 8326.04psi \quad (574.06\,\text{bar}) \tag{4.3}$$

Where:

Y_p: Yield strength of the drill pipe

t: Wall thickness of the drill pipe

d_p: Outside diameter of the drill pipe

Sf: Safety factor

4.4 Torsional Limit Calculation

Assuming the maximum yield stress of the steel drill pipe is **31183 psi** (215 MPa). The maximum limit of torque T_{max} of the steel drill pipe can be estimated by following equation:

$$T_{max} = \frac{\pi}{16} * \sigma_m ax * \frac{(d_p^4 - id_p^4)}{d_p} = \frac{\pi}{16} * 31183\text{Nin}^2 * \frac{(0.393\text{in}^4 - 0,315\text{in}^4)}{0,393\text{in}} = 218.25\text{in}lbf \tag{4.4}$$

Where:

d_p: Outside diameter of the drill pipe

id_p: Inside diameter of the drill pipe

σ_{max}: Yield strength of the drill pipe

4.5 Maximum Inclination

With the maximum force that one wing can exert on to the rock determined by the ANSYS simulation, it is now possible to calculate the maximum deflection of the drill pipe and the BHA. A simple model was defined using a free software for structural analysis. A bar construction was defined with the respective lengths and cross sections of the drill pipe and the BHA. Density and Young's modulus for the used steel were entered. The top of the drill pipe was defined as a fixed bearing and the stabilizer as plain bearing. Finally, the acting forces were an upward force of 150 N for the maximum WOB and 60 N in x-direction for the maximum wing force. By doing that, the deflection could be computed. The result is displayed in **Figure 4.2**, where the bending is depicted ten times larger than the actual value for demonstration purposes. The maximum deflection at the tip of the BHA is 3.36 cm (1.3 inch). With the maximum deflection and the length of the BHA, the maximum inclination can be calculated with

$$\begin{aligned} \varphi =& tan^{-}1(\frac{max.\ deflection}{length\ BHA}) \\ =& tan^{-}1(\frac{3.35\text{cm}}{18.5\text{cm}}) = 10,3^{\circ} \end{aligned} \tag{4.5}$$

This model does not count for bit-rock interaction and is only conducted under static condition. Nevertheless, it gives a good first assumption that the chosen concept and set-up can fulfil the directional drilling task.

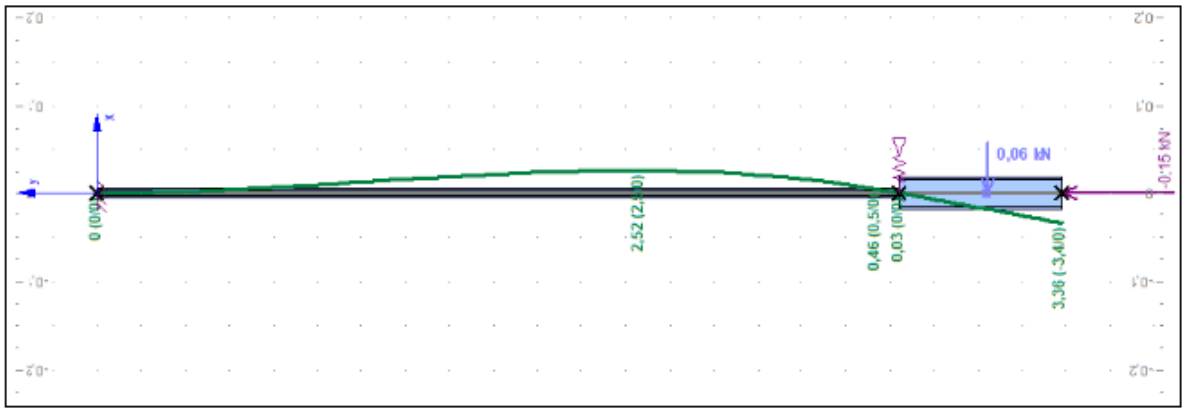

Figure 4.2: Maximum deflection of the drill pipe and BHA

5 BHA Design

Due to the usage of a 1.5 Inch diameter Bit for the 2022 Drillbotics® Competition, the TU Clausthal chose once more a larger diameter for their drill bit and BHA construction. This year´s concept is based around a drill bit propelled by a flexible shaft, which is powered by a surface mounted electric motor used normally for milling applications. The BHA is steerable through three independent wings following a push-the-bit approach and allows an inclination setup of 9 degrees. References for this chapter where based on **Fairhurst (1956)**, **Bruno (2005)** and **Moore (1986)**

5.1 Development History

Different approaches were discussed in the team taking many considerations into account. Until the final concept was decided on, earlier ideas were favored. For the sake of completeness and to better understand the development history, the earlier concepts are described as follows.

5.1.1 Concept 1

The first concept shown in **Figure 5.1** was based around a BLDC Downhole Motor and a radial bending joint, which allowed the setting of a specific inclination towards the central axis. This concept study resulted in a very long BHA setup and therefore it would have been difficult to meet the drilling requirements of the given trajectory. Furthermore, the stresses along the outer borehole wall could have led to a total failure of the construction due to the high axial forces alongside the BHA during the bending process.

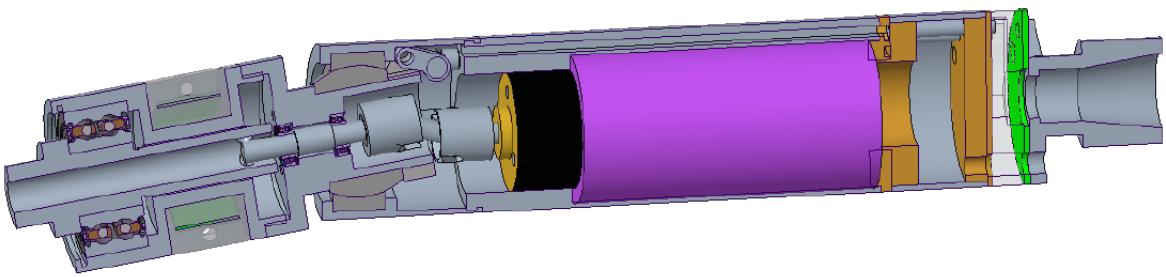

Figure 5.1: Drillbotics Bendable BHA construction

5.1.2 Concept 2

The second concept was as well based around a BLDC Motor but instead of a radial bending joint the steering requirements would have been met with the help of two extendable wings **(Figure 5.2)**, which allowed a correction of inclination towards the borehole wall. The wings could be steered independently from one another with two hydraulic cylinders. The extended wings would have been pressed against the borehole wall and by that it would be ensured, that the inclination correction is carried out.

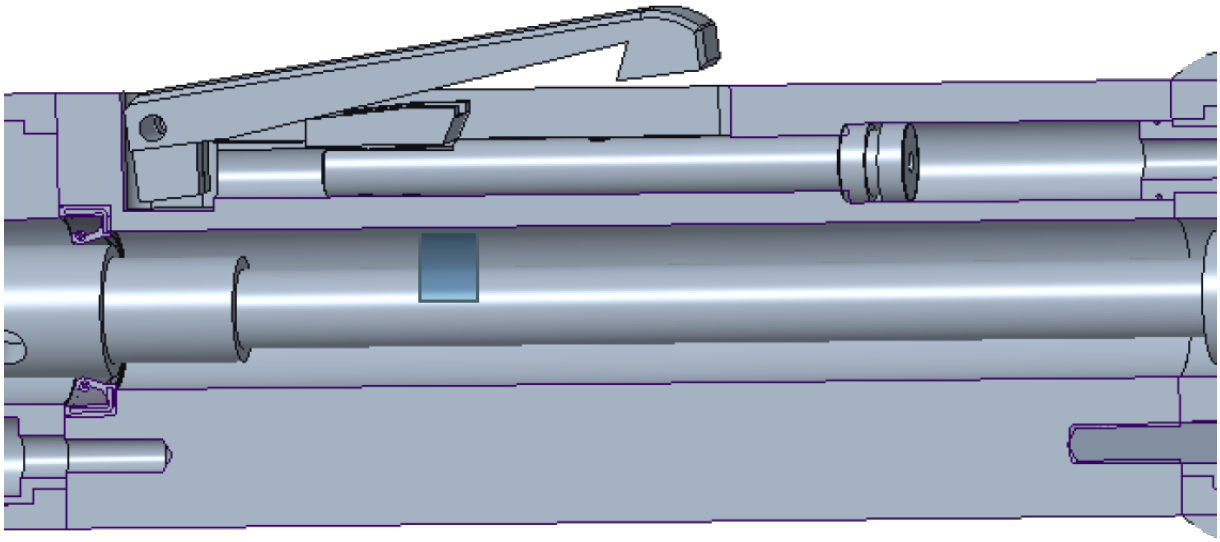

Figure 5.2: Drillbotics Wing Module extended

5.1.3 Concept 3

Finally, it was decided to change the concept drastically due to the limited space of the BHA. The driving Motor is now installed onto the rotary table and is powering the bit with the help of a flex shaft. The concept of the rest of the bottom hole assembly, however, remained the same as in the second development stage. An optional setup consists of three wings instead of two in order to increase stability of the BHA during the drilling operation.

5.2 Description of the Final Concept

This year's BHA consists of a modular system, which allows the team to adjust the arrangement to different wellbore conditions. The upper part of the system consists of a modular guiding plate setup, which manages the incoming fluids from the surface. The fluids are directed to their specific destination with this modular channeling system. In total, the setup consists of five different input ports, three of them for the high-pressure hydraulic lines, one for the drilling fluid and the last one for the electrical cables. The decision to go for a known concept, as wing steering is quite common in nowadays Trajectory drilling procedure, was based around the idea to make the rig as realistic as possible.

5.2.1 Collet Chuck Joint

A notch will be considered to hold a sensor unit in the upper unit. In the same way, this type of notch is also placed directly behind the bearing package in the lower unit. Between drill string and Collet Chuck receiver, there are two O-rings to prevent water from breaking into the electronics compartment. The Collet Chuck is tightened by a union nut. With this type of clamping, the cross section of the drill string is not disturbed, and more force can be transmitted.

5.2.2 Stabilizer

The stabilizer of the Bottom Hole Assembly is attached on the top of the BHA and is responsible for the overall borehole quality. The stabilizer centers the BHA inside the hole and therefore prevents shifting of the BHA during the drilling operation and establishes the fixation of the BHA during downhole operations. The stabilizing element consist of seven convex shaped fins, that can guide the BHA along the drill path. Further, it can reduce the shocks transmitted through the pipe and the rotating shaft onto the BHA and therefore prevents the bit from lateral displacement due to vibrations.

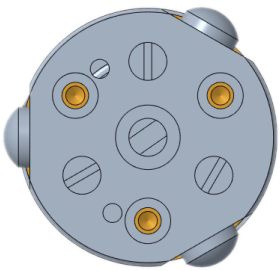

Figure 5.3: Stabilizer unit

5.2.3 Steering Unit

The steering unit is connected to the DP. This year´s steerable component consists of three wings, that can be extended due to the inflow of liquid under high pressure conditions into three independent cylinders. Each wing is independently controllable from one another and can be unfolded by its own cylinder steering unit. The cylinders are attached to a wedge which will drive the wings from its current position. To reduce the current inclination, three springs, one for each cylinder, are included in the construction to reposition the lifting arms of the cylinders. The inflow of the high pressurized liquid into the cylinders will be managed through surface mounted stepper motors, which will allow to control inflow and outflow without a hazard of pumping a vacuum. References where **Construction (2011)** and **Hearn (1997)**

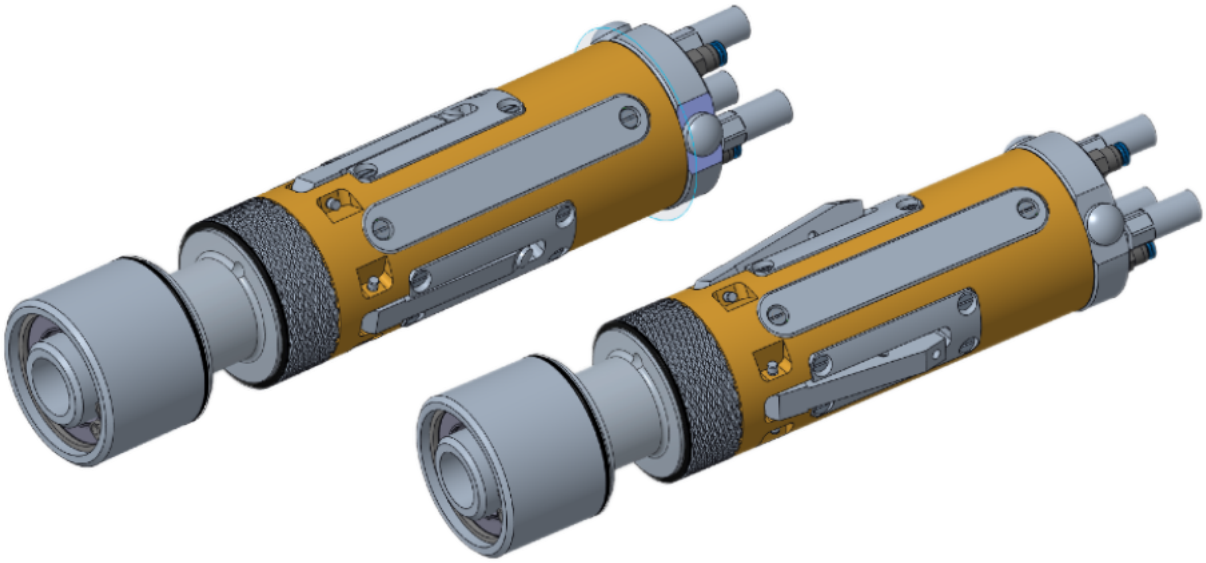

Figure 5.4: Steering unit open and closed

5.2.4 Syringe Unit

The subsurface steering unit is powered by a surface mounted control device **(Figure 5.5)**, allowing the wings to be actuated separately through a hydraulically connected system. The whole subsurface compartment is stored on top of the topdrive and will function through actuated stepper motors, that are connected to the processing unit to adjust the total deflection of the bottom hole setup. The pressure is recorded by a sensor for each of the three hydraulic lines, that enables the processing unit to extrapolate the grade of deflection of the drill curve. If the deflection in one direction should be increased, the stepper motors will transfer their power through a pulley system onto the syringe systems beneath, forcing them to increase the pressure inside the hydraulic system and therefore on to the wing. The pressure is operated by a maximum of 10 MPa in order to create enough power to operate the wings successfully against the force applied by the rock on the BHA. The deflection force was confirmed via an ANSYS simulation **(Figure 5.6)**, taking friction losses into account, to grant the capability of the system. The simulation calculates that the system can transmit a force of 60 N onto the rock surface.

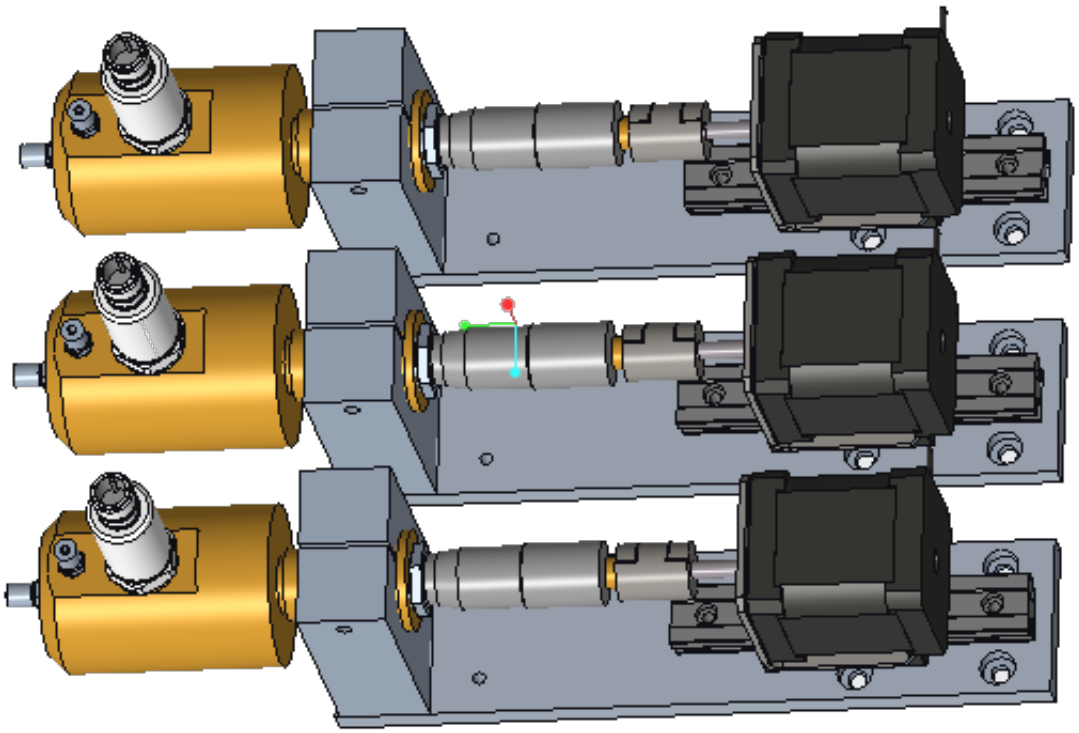

Figure 5.5: Syring deflection unit

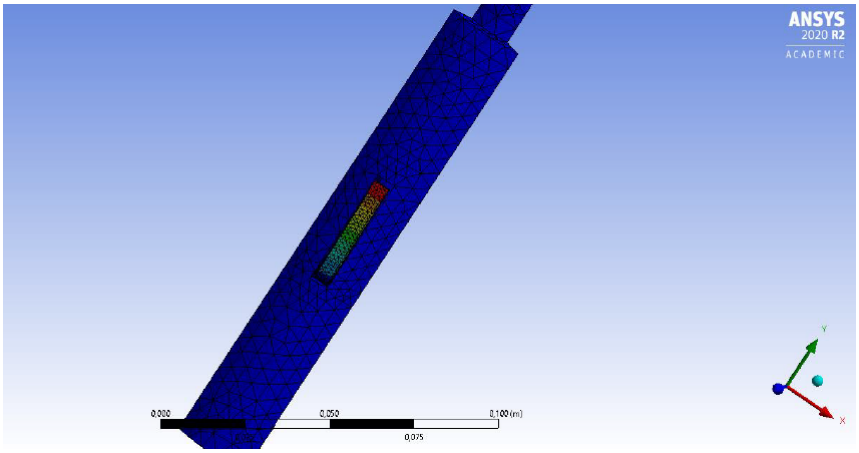

Figure 5.6: BHA ANSYS wing simulation

5.2.5 Sensor unit

The next module connected to the upper part is the sensor unit. This module consists of two half circular shaped parts. The parts are mounted on the BHA beneath the steering unit and are installed in to sense the position of the Bit and the inclination of the BHA. In addition, the downhole weight on the bit is measured here, it is also possible to measure the bending moment in x and y axis and later to determine a force vector of the bit from these values. With this arrangement the actual weight on bit can be determined more precisely, as the friction of the drill pipe and the supporting moment of the BHA wings is omitted. Beneath the sensor unit the drill bit is installed. In order to meet the properties of the driving system, the system is optimized for high rpm counts and low output torque. **Figure 5.7** shows the whole BHA setup.

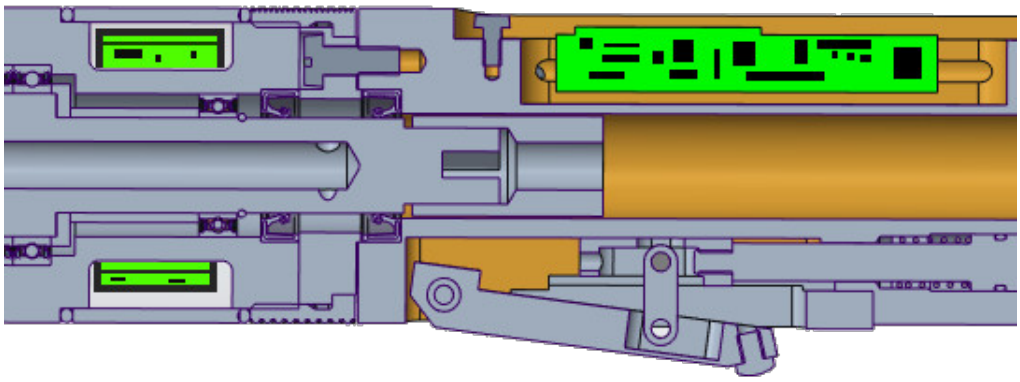

Figure 5.7: Sensor unit

5.2.6 Drill Spindle and Spindle Housing

Directly behind the drill bit, a shaft sealing ring seals the BHA from dirt and drilling fluid. The first sensor module is mounted directly behind the drill bit. This has the advantage, that the drilling process can be recorded more accurately. This year´s bearing construction consists of a classic movable/fixed bearing construction **(Figure 5.8)**. For the two bearing rings behind the drill bit, the "fixed" bearing, the **s61702-2rsr** bearing was chosen. The moveable component consists of one **s61700-2rsr** bearing ring. These two single row ball bearings offer a great stiffness in addition to a limited requirement of installation space, which is beneficial for constructing a miniature drilling rig. Furthermore, the bearing construction can absorb the axial and lateral tilting moments and prevents the BHA from a critical failure because of high stress moments.

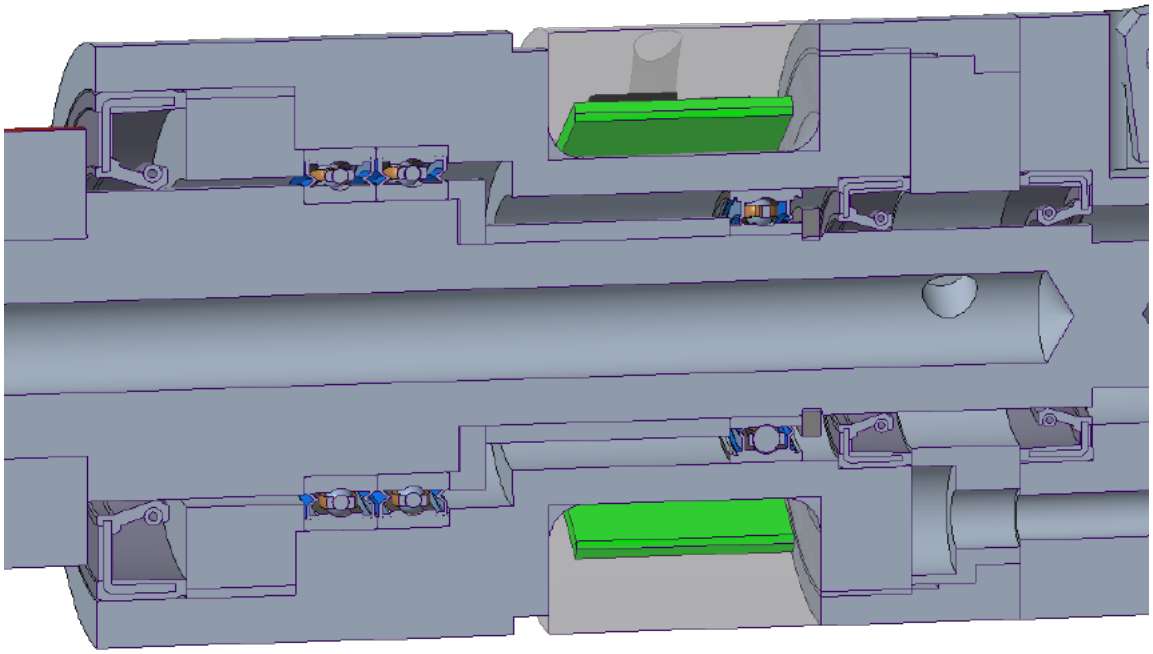

Figure 5.8: Drill spindle and bearing unit

5.2.7 Drill Bit

It was originally planned to design an own impregnated diamond drill bit to be able to drill at high RPM. But since the manufacturing effort of such a bit would be way bigger than initially anticipated, the decision was made to use the drill bit provided by Baker Hughes. This drill bit will deliver the necessary cutting action which is needed for the specifications of the given design. From the two drill bits that are provided, one will be used during trials before the competition and the second drill bit will be held as a spare part in the case that the first drill bit gets damaged. In any case, the second bit will be used for the competition. The bit wear will be analyzed after each run to decide if it can be further used or not. The **IADC** dull bit grading system will be applied after each test run to describe the bit wear. The **IADC** dull bit grading system, after **IADC/SPE 23938-23939**, defines several parameters such as a cutting structure, bearing seals, gauge, or the reason for pulling the bit. From that, a conclusion can be made on the drilling performance of the bit. The wear of PDC bits is also sensitive to the amount of mud cooling the bit across its surface. Thus, it is of most importance, to keep a continuous and high amount of mud flow during drilling to protect the bit from wear.

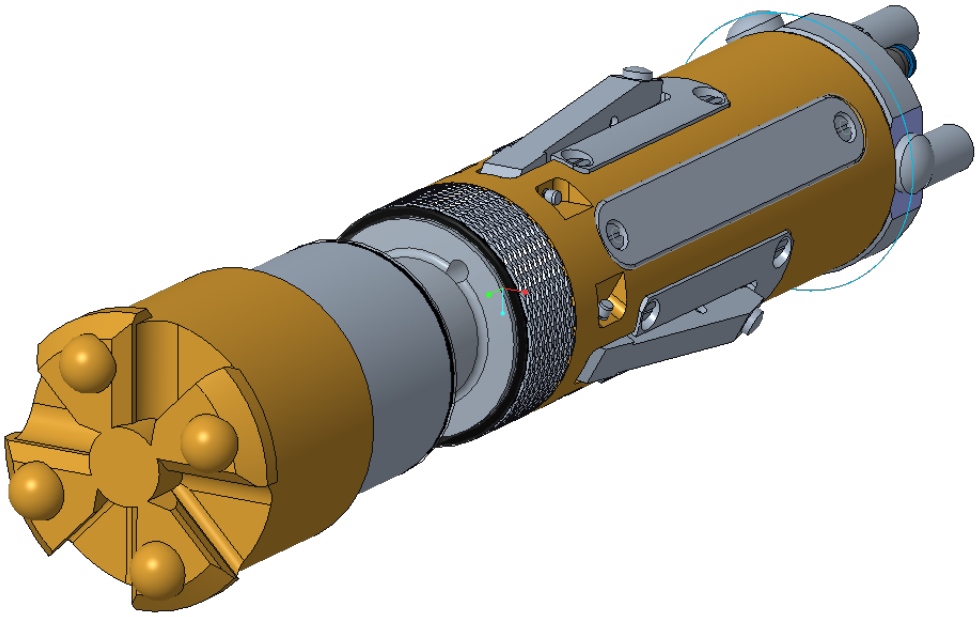

Figure 5.9: Full BHA

6 Mechatronic System Architecture

6.1 CAN Bus

A universal, error-resistant bus system is necessary, since many subsystems in the arrangement are required to communicate with each other without interference. Therefore, a decision was made in favor of the controller area network protocol, which is widely used in the automotive industry.

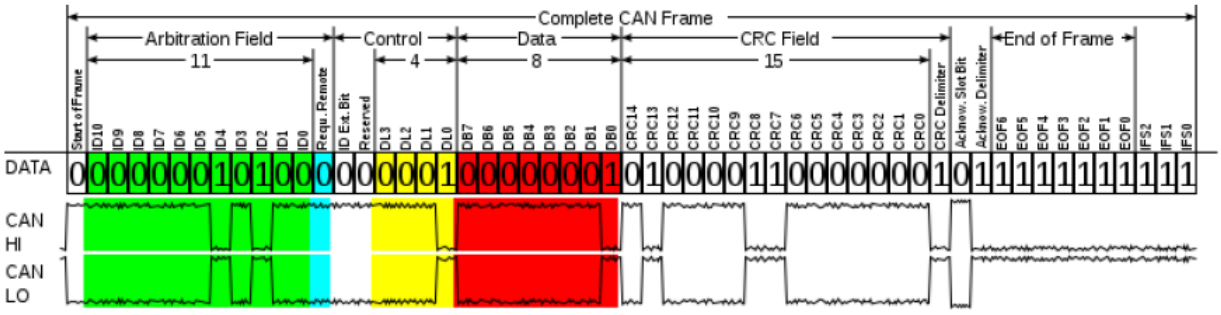

Figure 6.1: CAN bus schematic

The structure essentially consists of two redundant data lines, CAN High and CAN Low. To write a "one", the CAN High line goes to zero voltage while it is normally on supply voltage, the CAN Low line goes from zero voltage to supply voltage. To write a ”zero”, CAN High stays on supply voltage and CAN Low stays on zero voltage. This mechanism results in an opposing signal in which errors can easily be detected. In a CAN network, these two lines connect all participants. The electronics in the BHA and on the surface are also supposed to be connected in this way. Thus, actuators and sensors can exchange data with each other without a complicated algorithm. Synchronized processes can be organized in a decentralized way. In addition, several algorithms can retrieve data and place commands in the network independently. A practical example is an initialization, or an emergency stop command. A CAN message thus consists of several sections. In the beginning, there is the arbitration field which represents a sequential number. Depending on this number, only an individual module or all even modules are addressed. An emergency shutdown will have the number ”1”. Each module that does not receive this number will go into an error mode. This numbering also makes it possible to prioritize messages. If a sender wishes to send a message, it also listens to the bus lines simultaneously. If it randomly sends signals

simultaneously with a higher priority module, it automatically stops sending and waits for a new time window. Thus, important messages are exchanged very fast. The next data field of the CAN message determines the type of message. A distinction is made between data message, the message that transmits data from a module. The remote message requests data from a particular module and the error message signals to all participants that an error condition has been triggered. The overload message forces all participants to take a pause to stabilize the data traffic. Aligned behind it is the data field, which contains all the data that is to be sent. The CAN message is terminated by a CRC, a count sum to verify the correctness of the message. If this does not agree with the sum of the message, the message is considered unusable and the data is requested again.

6.2 Quick Data Query

To transmit large amounts of data from many sensors as fast as possible, a data acquisition protocol was designed, as shown in **Figure 6.2**.

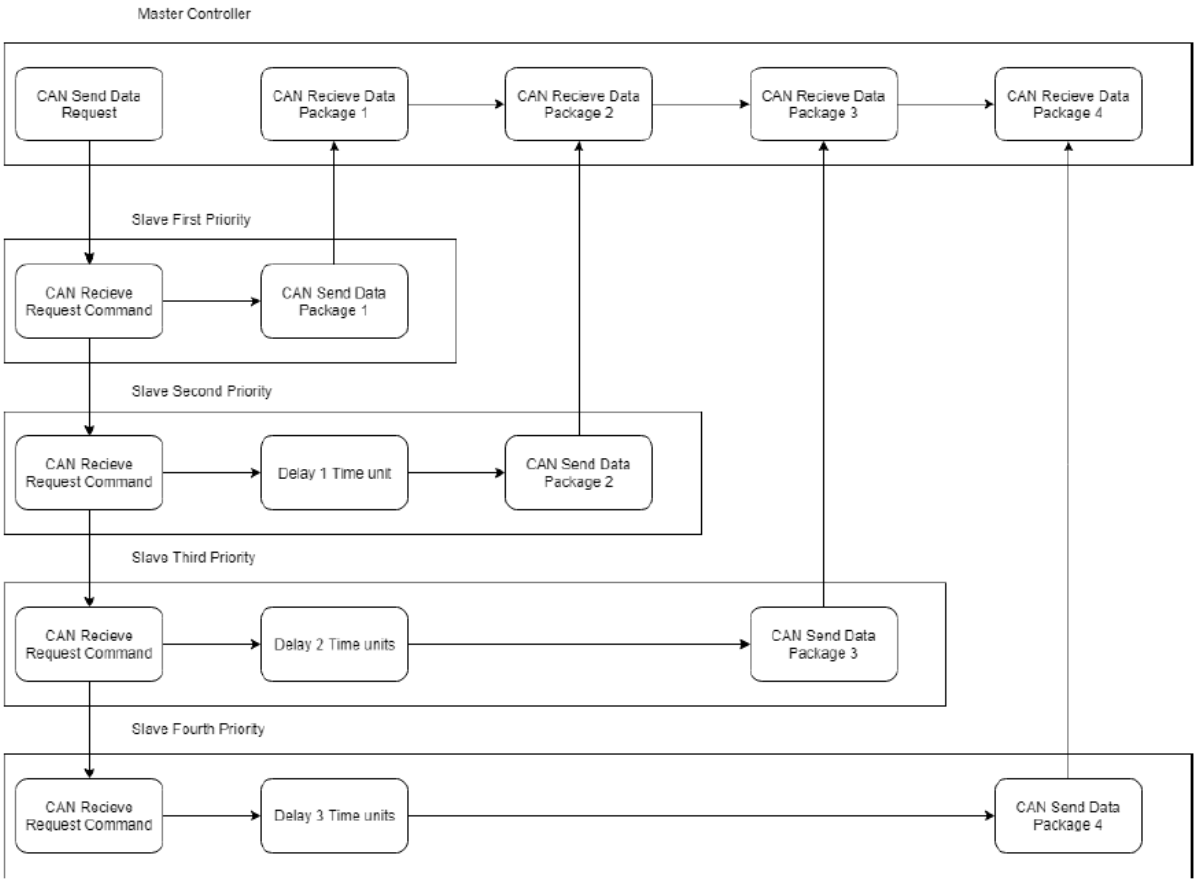

Figure 6.2: Quick data schematic

Normally an ECU would send a query message to a sensor and wait for a response. If this was received error-free, it would dedicate itself to the next sensor and again wait for an answer to the request. To avoid this waiting cascade, a trick is used. Each module that transmits data has a specific waiting time which corresponds to its own priority number. If a data acquisition message is imported into the network, all modules, which have no data to send, pause their communication. All modules, at which data are to be queried, go into a ”data sending mode” and wait for a specific time and, subsequently, send their data set. If this is successfully completed, the network returns to normal operation. Thus, the time required for the normal polling can be saved.

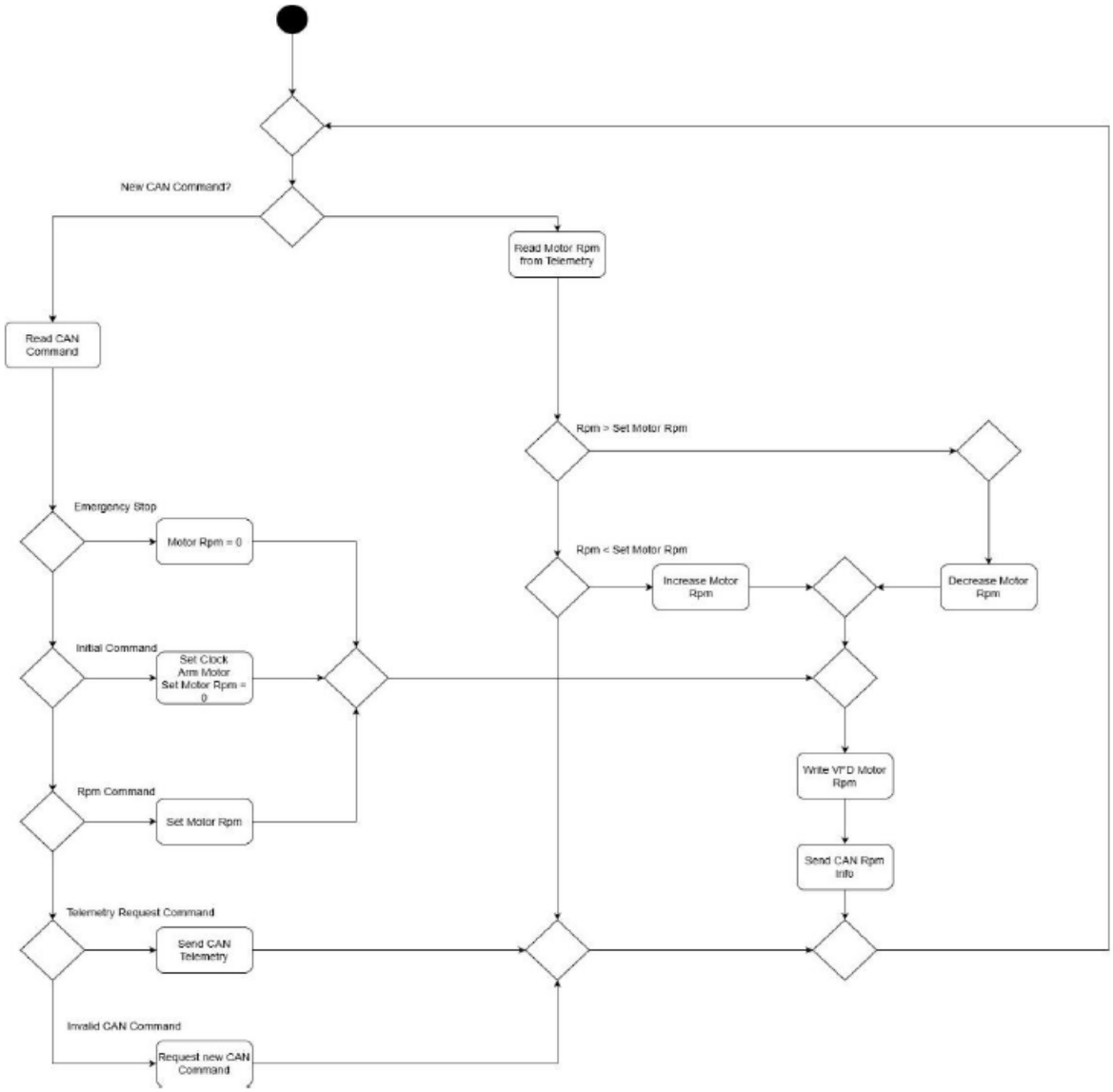

Figure 6.3: Motor control algorithm

6.3 Actuator Modules

6.3.1 Motor Control Unit

The motor control unit consists of several parts as shown in **Figure 6.4** and is located on the surface at the top of the spindle. The STM32 will process the telemetry data of the motor and has a CAN interface for bidirectional communication with the CAN bus.
To adjust the required speed of the main system, a small control loop runs on the STM32 as shown in the **Figure 6.3**. If the current speed is lower than required, the signal is amplified to increase the RPM, however, if the speed is too high, the control signal is reduced. In case the system requires data, current, voltage, speed and set control signal will be sent back. The servo motor type ihsv 60 is a closed unit consisting of a synchronous motor and a motor controller with feedback loop. The torque is specified with 1.27 Nm and the maximum speed with 3000 rpm. The motor is controlled with a step and direction signal. Due to the setting that 19200 pulses are needed per revolution and since the flex shaft can also be assumed as a damping element, the running of the bit is assumed to be smooth. If the motor reaches its set maximum torque, an extra io line is activated, which switches an interrupt inside the microcontroller and the speed is reduced by the STM 32 until the torque is back in the specified range. This avoids an overload of the flex shaft. If this is not the case within 100 ms, a blockage is assumed and the rotation is stopped completely. The control loop described here runs very quickly on the STM 32 in its own thread with a setting of 100 Hz and is independent of the control algorithm in order to be able to react as quickly as possible in the event of an error.

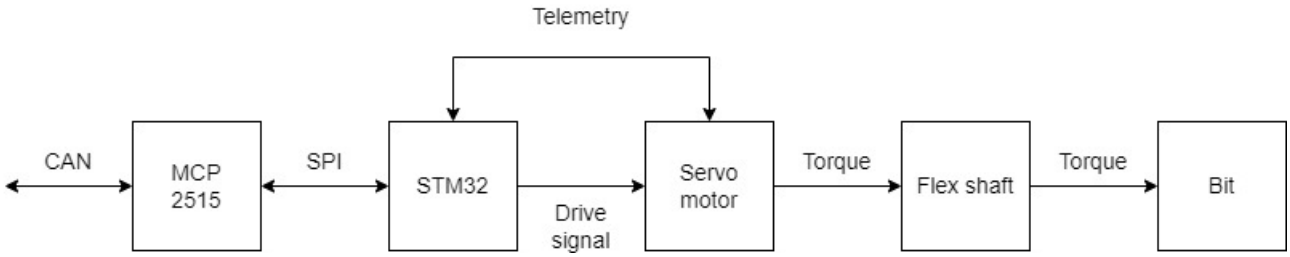

Figure 6.4: Motor control unit

Communication between the microcontroller and the motor controller takes place via Modbus. RS232 is a communication protocol that allows data exchange between a master and several slaves. The master device, the STM32, is connected to the slave device, the control unit. The Modbus protocol now allows the control of the connected devices and the transmission of the measurement data from the slave to the master. Basically, each

participant can send messages via the bus, where communication is usually initiated by the master.

6.3.2 Hydraulic Actuator Unit

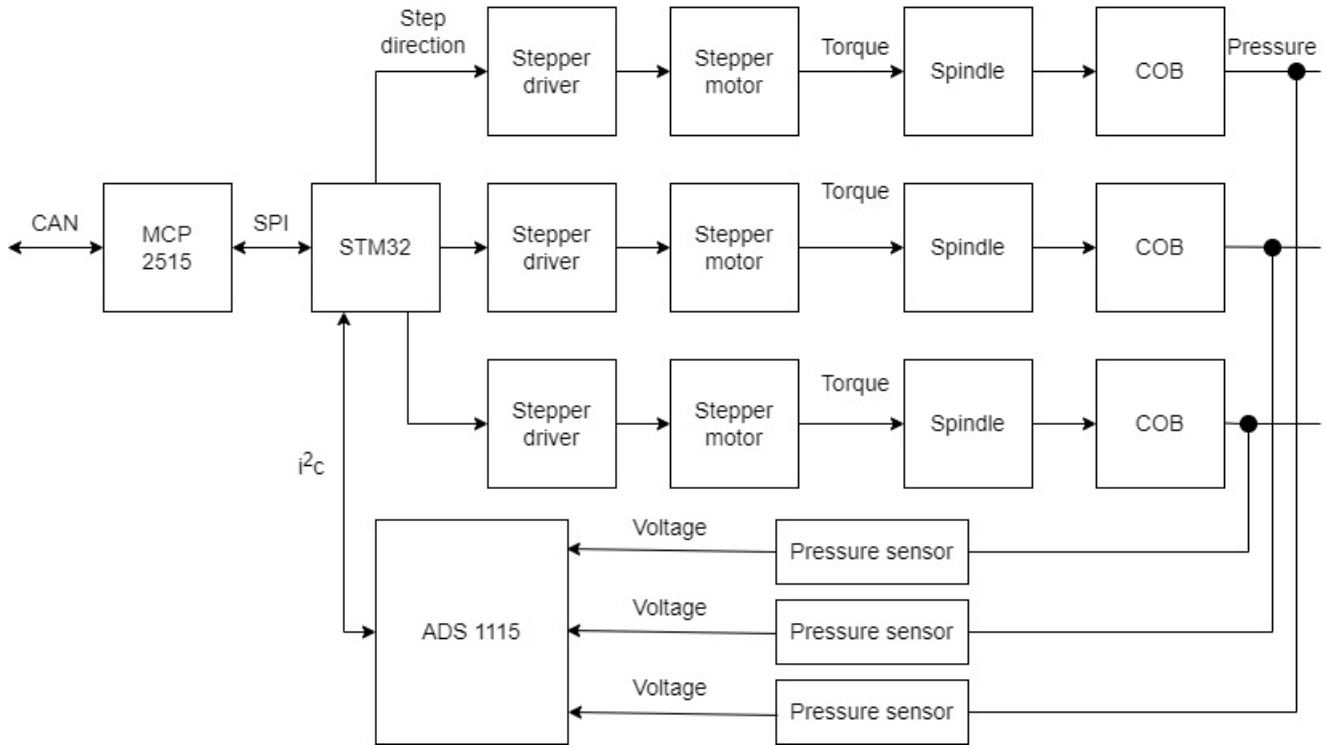

Figure 6.5: Hydraulic actuator unit

The steering unit is controlled by three offset wings, which are extended by a hydraulic system and controlled by adjusting the pressure as shown in the **Figure 6.5**. For each wing there is an associated stepper motor and stepper motor driver. The TMC2130 regulates the motors by adjusting the current. The stepper motors transmit a moment to the spindle, which in turn moves a cob that adjusts the pressure in the chamber. The deflection of each wing can be adjusted by the number of steps of the motor. The pressure within the system is measured with a pressure sensor and the data is passed on to the STM32. The microcontroller communicates with the pressure sensors and the TMC2130 via SPI. The STM32 transfers the data via CAN to the transceiver and further on the CAN bus. During initiation, the wings are moved to zero position, this is done by reading the pressure of the connecting lines. during homing, the spindles are moved back step by step until the wings are in contact and thus a negative pressure is drawn. Now the position is stored as zero and the module reports back as initiated. In normal operation, the module receives a

deflection force vector from the steering algorithm via the CAN bus. In order to be able to set this, the module must first move the wings evenly against the borehole walls and then approach the vector. To do this, all step motors are first moved out with the same number of steps until the pressure rises on all of them. Now the zero position is assumed. Next, a pressure ratio is set which corresponds to the force vector. The loop of the program queries the ADC with a frequency of 20Hz and first compares the calculated pressure value with the target value and then moves the steps in the right direction for correction. Since the step frequency of the motors is very low, in the event of a pipe rupture in the hydraulic lines, only a small flow of fluid will escape. Consequently, no hazards are expected as with a conventional hydraulic system.

6.3.3 Rotary Table Control

The rotary encoder control unit, as seen in the **Figure 6.6**, consists of a CAN transceiver and an ATmega 328p, which controls a stepper motor driver and assesses the absolute rotary encoder.

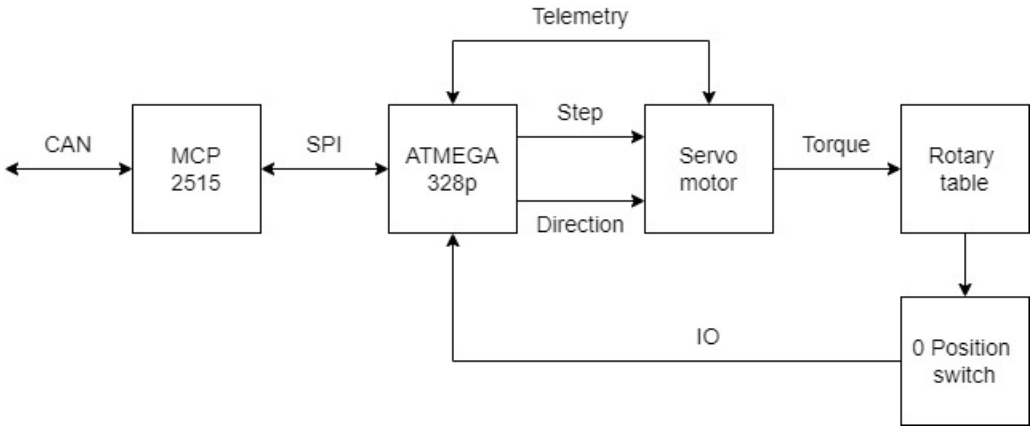

Figure 6.6: Rotary table control unit

The algorithm determines the current angle value and compares it with the desired angle. If a deviation is determined, the system moves in the opposite direction to correct the deviation to zero. As soon as the stepper motor moves, the motor current is additionally determined and compared with a previously defined maximum value. As soon as these values are exceeded, a warning message is generated.

6.3.4 Relay Switching Unit

The mechatronic system contains a CAN network controllable relay card which switches the pump. This unit consists of an ATMEGA 328p and a CAN transceiver as well as a relay card.

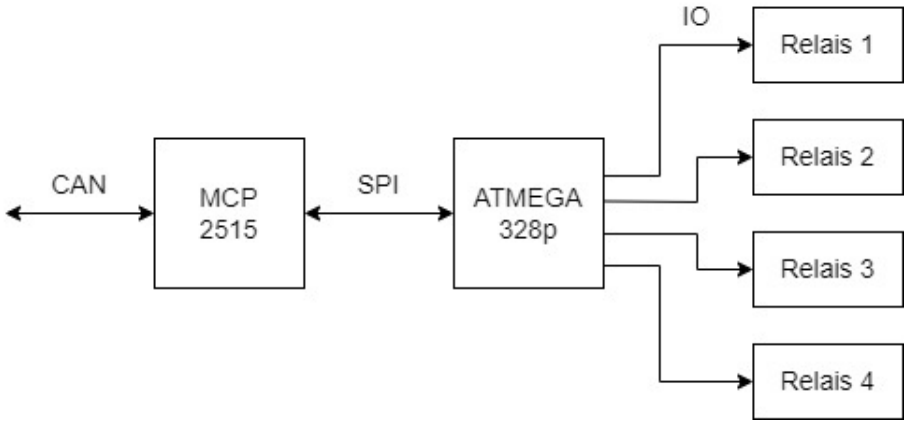

Figure 6.7: Relais switching unit schematic

6.3.5 Hoisting System Control Unit

This unit consists of a CAN transceiver and an ATMEGA 328p as well as switching inputs for the upper and lower limit switch of the hoist axis.

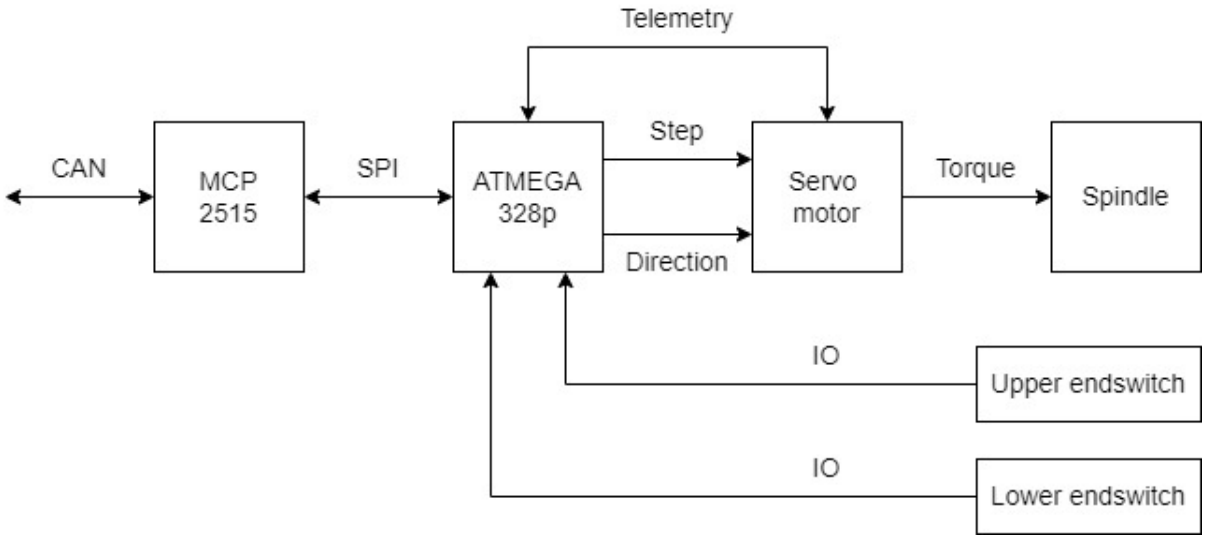

Figure 6.8: Hoisting system control unit schematic

The algorithm has in total two modes. In the first mode, N steps are driven in the pre-set direction. The second mode moves to a desired WOB and adjusts it with the hook load via the spindle. Since the controller has access to the data of the Downhole WOB module via CAN network, abnormal operating states can be determined by a comparison.

6.4 Sensor Units

6.4.1 MWD Sensor unit

To be able to determine the actual drilled path the azimuth and inclenation of the BHA has to be measured. The inclination is measured from the angle of the acceleration of gravity to the BHA, the azimuth is determined from the angle of the magnetic field of the magnetic coils to the BHA. These measurements are made in the MWD unit which consist of a magnetometer (LIS3MDL) and an accelerometer (LSM6DS33). As shown in the **Figure 6.9**, one central microcontroller is used for each sensor. Communication between the sensors and controller is enabled via SPI. The information is processed by the STM32 and transmitted to the transceiver via CAN communication. This forwards the data to the bus via a CAN protocol. With this design, the magnetic range magnetometer can use the magnetic field strength outside the BHA. To ensure that the data is measured and transmitted as accurately as possible, a low pass filter is implemented. The sensor unit consists of three smaller circuit boards arranged inside the sensor ring. The system consists of a LDO that supplies the entire unit with power. For this purpose, a voltage regulator is installed to regulate the voltages for the electronics down to 3.3V respectively. This board is standardized and used for all sensors. The unit will be inserted in the notch alongside the BHA. In addition, a standardized 4 pin jst connector is used, which is intended for data transfer and programming the STM32.
The sensor unit in the lower notch of the BHA will be located over the drill bit. Since the BHA is constantly flooded, it is necessary to shield the sensors from water or make them waterproof. Therefore, the two sensor modules are framed with epoxy resin or silicone. The plugs are laid from the housing to the inside, where the cables are also guided along. Another sensor unit is placed at the upper end of the BHA. The two rings make it possible to better determine references and deflections of the entire BHA. Another identical sensor unit is attached to the drill pipe to measure the vibration of the drill string.This is done via an embedded optimized FFT to compute the time discrete signal into the frequency domain. These values are included in the control algorithm. This allows a maximum value to be set at a point that must not be exceeded. If the value is exceeded an alarm will go off

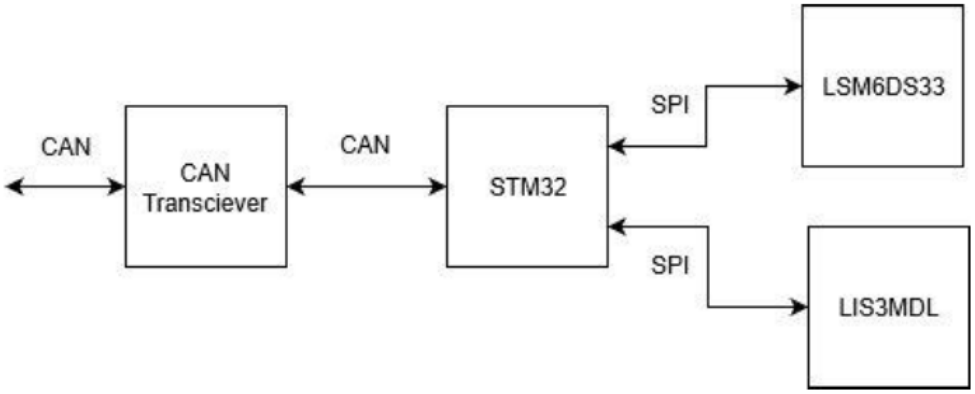

Figure 6.9: Electrical schematic of the Sensor Unit

and the RPM of the flexible shaft will be reduced. If an even higher threshold is reached, the drilling process will be stopped for safety considerations.

6.4.2 Flow-meter and pressure sensor

To control a crucial part of the cutting transport, it has to be ensured that a certain flow rate is constant getting pumped through the bit. As mentioned before, there is a pre-charge pump that feeds in the high-pressure pump, so they deliver a combined flow rate. In order to precisely control and monitor the values of the pump control system, the flow meter and the pressure sensor are installed between both pumps. The flow meter consists of sensors that measure the flow rate of the liquid that passes through, it captures an accurate output with built-in visual confirmation of the flow rate in the pipe. The vane cells in the flow sensor output a square wave signal proportional to the flow rate. These serial rectangular signals are counted by the counter 74HC590 in a certain interval. The data from the serial input shift register are transferred to the output register and converted as a parallel output. After the high pressure pump, a pressure sensor was connected that works up to a maximum of 10V and records pressure up to a maximum of 400bar. The pressure sensor is connected to the ADS1115 analog-digital converter, which has an internal signal amplifier that forwards the converted signal to the ATmega328p and finally forwards it to the CAN-BUS. It also has an alarm function that issues a warning if the set maximum pressure value is reached or exceeded. The communication between the two sensors and the micro controller shown in **Figure 6.10** takes place via SPI.

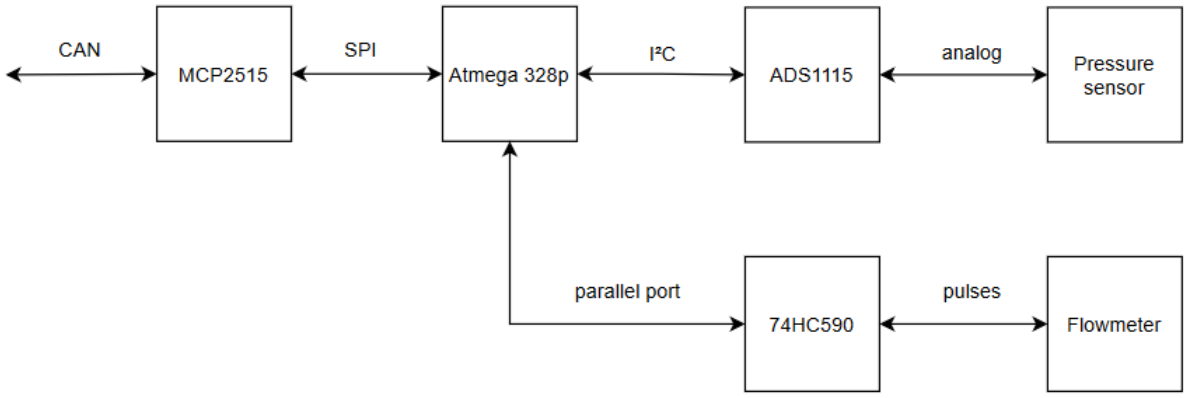

Figure 6.10: Flow-Meter and Pressure-sensor schematic

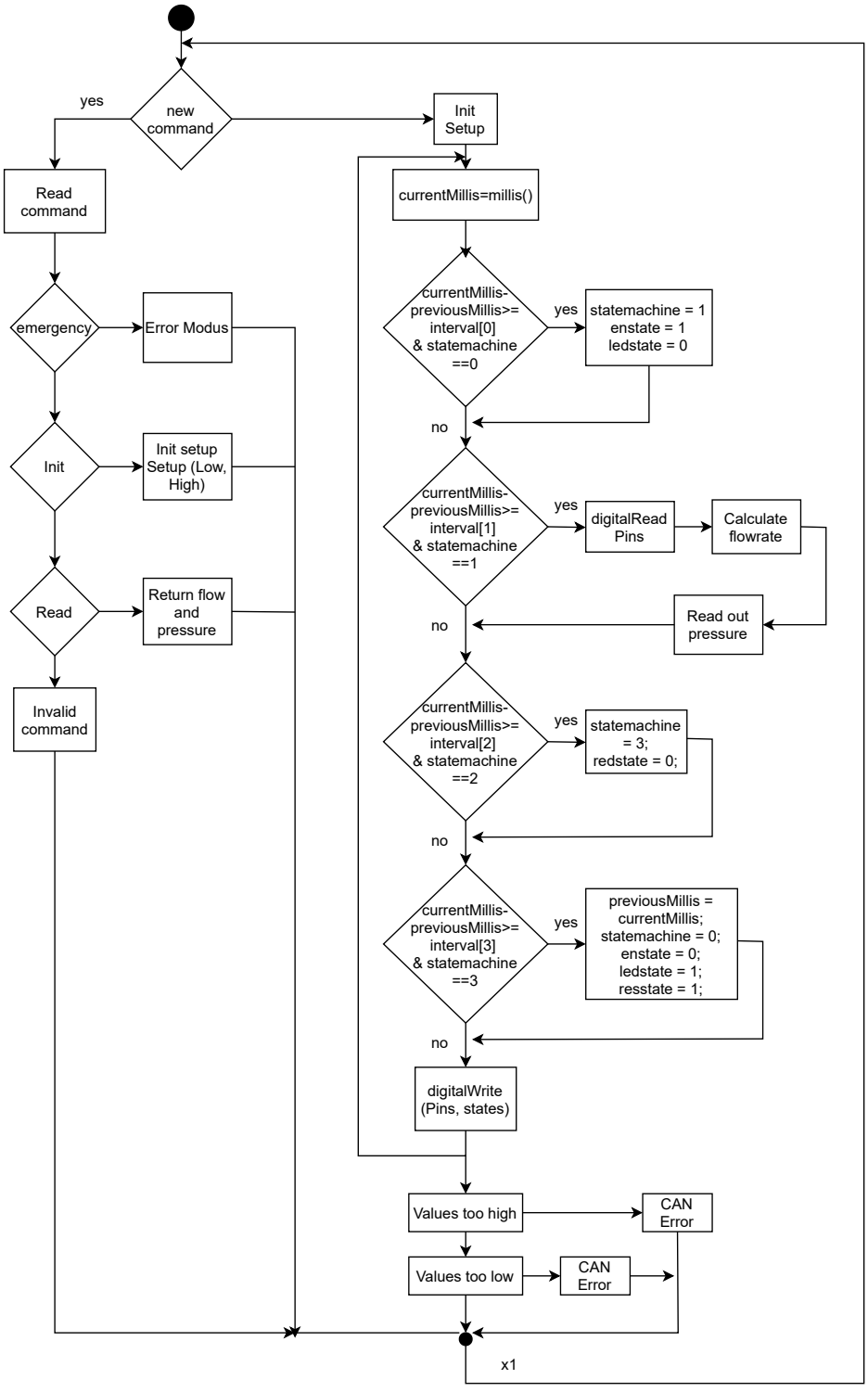

Figure 6.11: Flow-Meter and Pressure-sensor UML

6.4.3 WOB Measurement Unit

The Down hole WOB is measured by a strain gauge inside the BHA. The Hoockload is measured by a strain gauge glued to the mounting tube of the drill pipe. Both units have an Hx711 analog digital converter and a CAN transceiver which is controlled by a Atmega 328p micro controller. On request, the unit returns a WOB value or warning message if the set maximum value is reached or exceeded. In addition the units can receive a Tara command to set the output to zero.

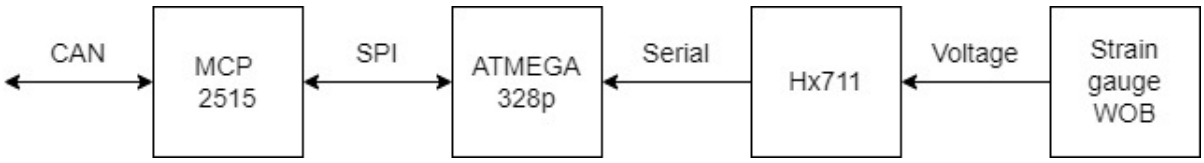

Figure 6.12: WOB Measurement module schematic

The measuring strips of the WOB unit are placed on the housing above the bit. The arrangement of the strain gauges is selected in such a way, that the influence of temperature and bending, as well as torsion, is compensated and the measuring bridge is only sensitive to strain. The measuring strips of the hook load sensor are configured in such a way that one Wheatstone bridge is measuring the axial strain and the other is measuring the torque. Due to the very small output values, an amplifier is needed. The HX711 has an internal signal amplifier which passes the amplified and converted output signal to the ATmega 328p and finally forwards it to the bus via CAN. In the sensor module, the measuring strips are mounted as a full bridge and half bridge as shown in **Figure 6.13**.

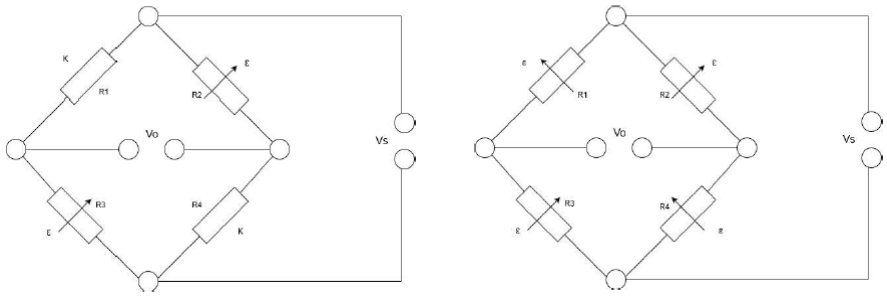

Figure 6.13: Wheatstone full and half bridge

On both controllers loops will run and query data permanently. For measuring normal elongation, the strain gauges are arranged as a diagonal bridge, each with 2 active and 2 passive measuring strips. This measures normal elongation independently of the bending strain. The strain is described by the following formula:

$$\epsilon = \epsilon_n = \frac{1}{2} * \frac{4}{k} * \frac{V_0}{V_s} \tag{6.1}$$

Where k is the K-factor of the measuring strips V_s and V_0 are the adjacent voltages. The equation can calculate the change in length that can be compared with the previously determined real values to find the critical values.
To measure the torsion, the strain gauges are installed as a full bridge, with four superimposed strips offset by 45°. The principle is like that of the half bridges and is described by the following formula:

$$\epsilon = \epsilon_d = \frac{1}{4} * \frac{4}{k} * \frac{V_0}{V_s} \tag{6.2}$$

6.5 Sensor Calibration

6.5.1 Accelerometer

The calibration process of the accelerometer involves two steps. These steps should eliminate the scale factor error and the bias offset. The bias offset is a simple offset of the initial zero position of the sensor. The scale factor error on the other hand describes a deviation between the input and the output of the sensor. These influences can be eliminated by pointing the x-axis towards the earth. The maximum read values of the sensor should then be used to calculate the bias offset error and the scale factor error for both negative and positive directions.

$$\begin{aligned} o_x &= \frac{x_{max} + x_{min}}{2} \\ s_x &= \frac{x_{max} - x_{min}}{2} \end{aligned} \tag{6.3}$$

The calibrated value can then be calculated by the following formula:

$$a_{x,corrected} = \frac{a_{x,measured-o_x}}{s_x} \tag{6.4}$$

This process should be repeated for all axes of the sensor unit.

6.5.2 Gyroscope

Like the accelerometer, the gyroscope needs to eliminate the bias offset and the scale factor error. However, the calibration approach differs in comparison to the other sensor. The bias offset $o_{x,y,z}$ of the gyroscope shifts after every restart which makes a static value for the bias offset useless. Therefore, the gyroscope needs a static starting sequence, where a certain amount of measurements is taken and averaged for all three axes. These averages can then be subtracted from the actual measurement to obtain the bias offset compensated value.

$$s_x = \frac{x_{max} - x_{min}}{2} \tag{6.5}$$

The compensation of the scale factor error $s_{x,y,z}$ is done by measuring the peak values of the gyroscope while its rotating around the x-axis at its maximum speed in both directions. The peak values during the maximum turning rate will be measured to calculate the scale factor error.The corrected characteristic curve of the gyroscope can then be calculated by the following formula:

$$\Omega_{x,corrected} = \frac{\Omega_{x,measured} - o_x}{s_x} \tag{6.6}$$

6.5.3 Magnetometer

The calibration process of the magnetometer is somewhat comparable to the other two sensors but to understand these compensation methods, one must look at the causes of the disturbances and why some disturbances cannot be corrected with the usage of filters and calibration procedures. The first possible error sources are 'Hard-Iron' interference's. These interference's emerge from static magnetic fields created by close by ferromagnetic objects or magnets. However, this error will simply act as an offset error $o_{x,y,z}$ which can easily be taken care of. This offset can be calculated by measuring the peak values for each axis in the negative and positive direction of the earth's magnetic field.

$$o_x = \frac{x_{max} + x_{min}}{2} \tag{6.7}$$

Secondly disturbances can arise from 'Soft-Iron' interferences. These influences distort the magnetic field and arise from nearby non-magnetic materials. These distortions can be adjusted with a proper rotation matrix which aligns the distorted measurements with the earths reference frame. The last possible negative influences for the sensor performance are dynamic magnetic fields. These can be emitted from electric devices such as DC motors and it is not possible to compensate for these disturbances with this algorithm. Therefore, the influence of these dynamic fields is avoided by placing the sensor as far away as possible.

6.5.4 Strain gauge

The calibration process of the strain gauges for the measurement of the WOB and the hook load are quite simple. To accurately measure forces with strain gauges an adequate bridge circuit should be chosen to for example compensate temperature influences (as seen in Chapter 7.3 WOB measurement unit). Since the voltage output of the strain gauges and the acting forces are proportional to each other, the calibration process of the strain gauges only needs two different measurements to accurately display the forces. One measurement must be taken in a static situation where no forces are applied, and the next measurement must be taken while a known force is applied to the strain gauge.

$$p_{prop} = \frac{F_{known} - F_0}{V_{known} - V_0} \tag{6.8}$$

With these measurements the proportionality factor p_{prop} between the acting forces and the voltage output can be calculated. The same procedure can be applied to measure acting torque on the strain gauges. If applying a force or torque is not applicable for the placement of the strain gauges, a shunt calibration method can also be used.

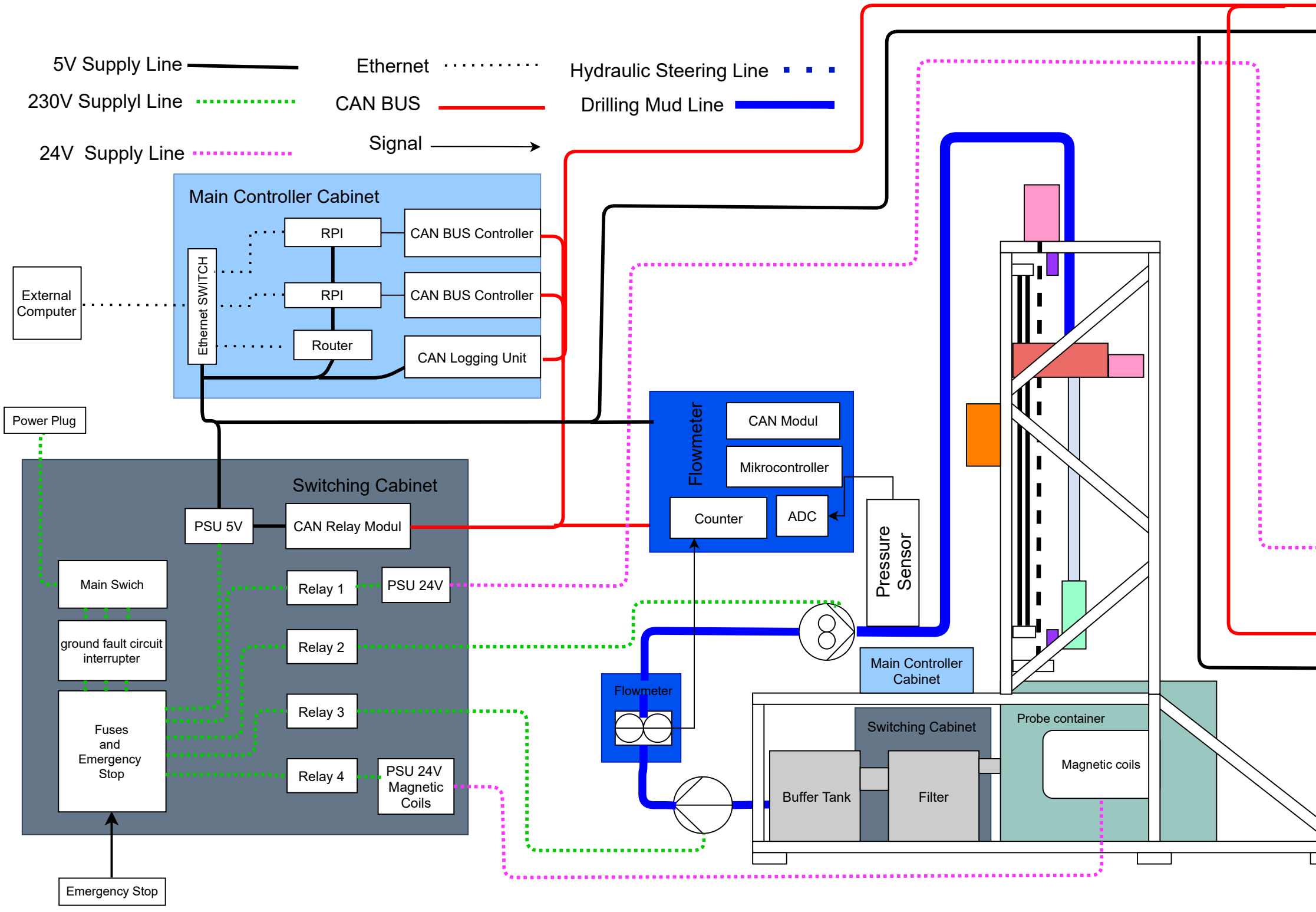
5V Supply Line
230V Supplyl Line
24V Supply Line
Ethernet
CAN BUS
Signal
Hydraulic Steering Line
Drilling Mud Line
Main Controller Cabinet
RPI
RPI
Router
CAN BUS Controller
CAN BUS Controller
CAN Logging Unit
Ethernet SWITCH
External Computer
Power Plug
Switching Cabinet
PSU 5V
CAN Relay Modul
Main Swich
ground fault circuit interrupter
Fuses and Emergency Stop
Relay 1
Relay 2
Relay 3
Relay 4
PSU 24V
PSU 24V Magnetic Coils
Emergency Stop
Flowmeter
CAN Modul
Mikrocontroller
Counter
ADC
Pressure Sensor
Flowmeter
Main Controller Cabinet
Switching Cabinet
Probe container
Magnetic coils
Buffer Tank
Filter

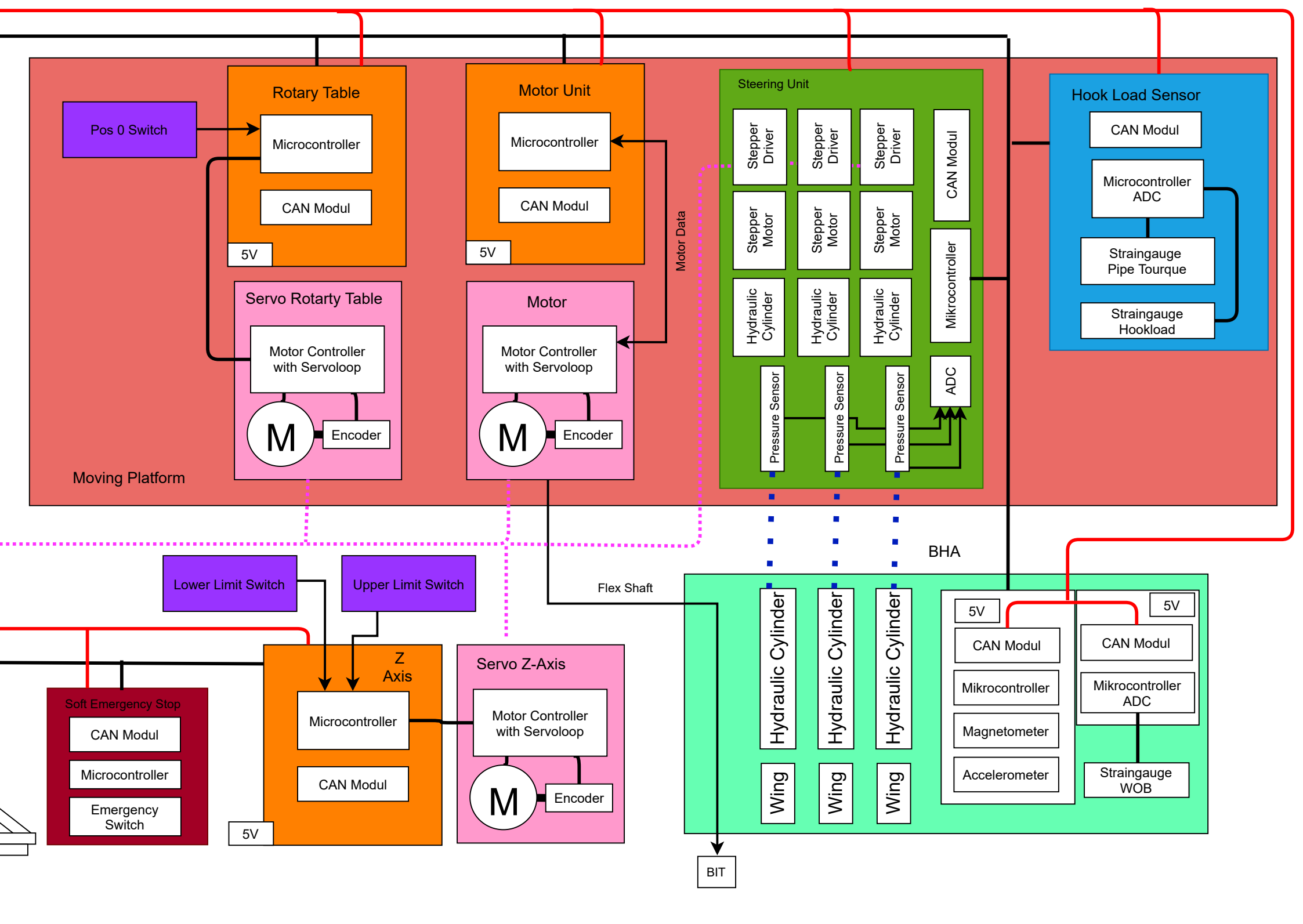
Moving Platform
Pos 0 Switch
Rotary Table
Microcontroller
CAN Modul
5V
Motor Unit
Microcontroller
CAN Modul
5V
Motor Data
Steering Unit
Stepper Driver
Stepper Driver
Stepper Driver
CAN Modul
Stepper Motor
Stepper Motor
Stepper Motor
Hydraulic Cylinder
Hydraulic Cylinder
Hydraulic Cylinder
Mikrocontroller
Pressure Sensor
Pressure Sensor
Pressure Sensor
ADC
Hook Load Sensor
CAN Modul
Microcontroller ADC
Straingauge Pipe Tourque
Straingauge Hookload
Servo Rotarty Table
Motor Controller with Servoloop
M
Encoder
Motor
Motor Controller with Servoloop
M
Encoder
Lower Limit Switch
Upper Limit Switch
Flex Shaft
BHA
Soft Emergency Stop
CAN Modul
Microcontroller
Emergency Switch
Z Axis
Microcontroller
CAN Modul
5V
Servo Z-Axis
Motor Controller with Servoloop
M
Encoder
Hydraulic Cylinder
Hydraulic Cylinder
Hydraulic Cylinder
Wing
Wing
Wing
5V
CAN Modul
Mikrocontroller
Magnetometer
Accelerometer
5V
CAN Modul
Mikrocontroller ADC
Straingauge WOB
BIT

7 Algorithmic

In the following chapter, the algorithmic which controls the robot - will be described. In addition, it will be clarified how the various sub-algorithms work together and which algorithm is executed where.

7.1 Overview

Figure 7.1 shows the conceptual diagram of the layered controlling approach. It can be seen that the sensors and actuators are connected via CAN bus to the first low level algorithm, which is running a raspberry pi. The individual modules are addressed hierarchically, so that the most important CAN messages such as the Z-axis drive commands and WOB data have a relatively low address with high priority. The software emergency shutdown has one of the highest priority addresses, "1". Sensor data and set points are communicated in the CAN network. The low level algorithm includes things like sequential execution of steps during a survey station or initiation of modules on the CAN bus, as well as the monitoring of machine data. It also represents the gateway to the outsourced high level algorithms, which are connected via Ethernet and TCP/IP protocol and are executed on a computer with sufficient power. These high level algorithms calculate the trajectory and optimal set points for drilling. These algorithms are described further in the following sections.

7.1.1 Synchronization and Timing

To ensure simultaneous data recording, the data query message initiates the transmission of all process data. This guarantees that the measurement data is recorded at the same time and also ensures synchronization of the modules. As described in **Figure 6.2**. an important point is the question of how much time elapses between the recording of a critical value and the action to avoid a critical situation. All module actuators and sensors which are responsible for critical parameters can send an error message to the can bus if a value exceeds or falls below a critical zone. This "critical zone" can be set by a can bus message. Experiments have shown that the CAN bus communication from controller to controller does not exceed one millisecond with a high-priority message. The programming philosophy of the individual modules prohibits a delay function. Thus, it can be estimated that the maximum time from the recording of a critical value to the shutdown of the actuator is 10 milliseconds. The team is aware that communication with external high level algorithms

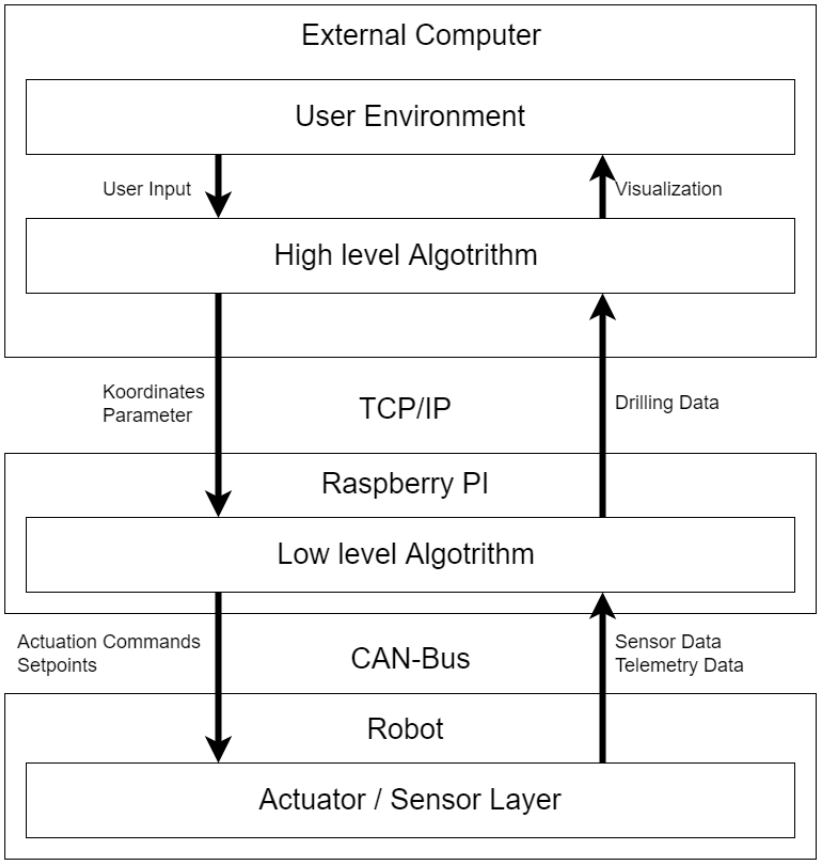

Figure 7.1: Algorithm Layering concept

connected via Ethernet cable may take longer. Due to the fact that these systems only provide set points and do not execute run commands, they are not taken into account in the time analysis.
In addition, the following table lists the target lead times and the sensors as such.

Sensor Value	Module	Resolution	inaccuracy	internal query frequency	Filter Type	Actual Sensor
WOB	WOB	24 bit	+-50 g	50Hz	Low pass 5 Hz	HX711
Hookload	Hookload	24 bit	+-50 g	50Hz	Low pass 5 Hz	HX711
Pipe Torque	Hookload	24 bit	+-50 g	50Hz	Low pass 5 Hz	HX711
Inclination	IMU	16 bit	0.122 $\frac{mg}{LSB}$	100Hz	Low pass 20 Hz	LSM6DS33
Azimuth	IMU	16 bit	0.48 $\frac{mgauss}{LSB}$	100Hz	Low pass 20 Hz	LIS3MDL
Vibration	Sensor Drillstring	16 bit	0.122 $\frac{mg}{LSB}$	200Hz	FFT	LSM6DS33
Rpm	Motor Unit	16 bit	+-1 Rpm	100Hz	-	IHS v60
Torque	Motor Unit	16 bit	+-0.01Nm	100Hz	-	IHS v60
Flow	Flowmeter		+-0.1 $\frac{l}{min}$	1Hz	-	74hS590
Pressure	Flowmeter	16 bit	+-0.1 Bar	10Hz	-	ADS1115
Pressure	Steering Unit	16 bit	+-0.1 Bar	20Hz	-	ADS1115

Table 7.1: Sensor Table

7.2 Steering algorithm

In the following the steering algorithm will be described. For path estimation and controlling disturbances the paper of Zhang et al.is used as guidance. This was chosen over the previous setup that was developed from scratch since this was a more sophisticated concept that did not need additional development time. However, if time is still available in the development phase, it will be tried to implement the previous concept of using Piecewise Hermite Interpolation Polynomial for trajectory calculation and develop a control algorithm from scratch to follow this trajectory accurately.

7.2.1 Components

All involved modules of the steering algorithm are described here. The steering algorithm which is described in the following section gives out setpoints for the steering unit and is described in **Chapter 6.3.2**. The Sensor Unit is described in **Chapter 6.4**.

7.2.2 Trajectory

One of the main tasks of the competition is to drill defined targets along a calculated trajectory in the stone. As a reference Mat and Jou was used.

Planing

The targets defined by the committee are first entered into the trajectory planning tool and then the Trajectory is calculated.

Trajectory Calculation and Control Algorithm

In the following section the Algorithm from et al.will be described. The goal of this algorithm is to connect two spatially separated points with a radius and not to create a rapid change to the previous trajectory. Before the actual algorithm can be explained a few values are needed to be defined. First, the maximum support force F_{max} and the minimum support force F_{min} of the three wings used to steer the drill bit is needed. Secondly the maximum usable steering force A_{max} must be calculated as well as the maximum dogleg γ_{max}

$$A_{max} = \frac{\sqrt{3}}{2} * (F_{max} - F_{min}) \tag{7.1}$$

After that the actual trajectory calculation of the desired path can begin. This calculation can be summarized by the following Figure

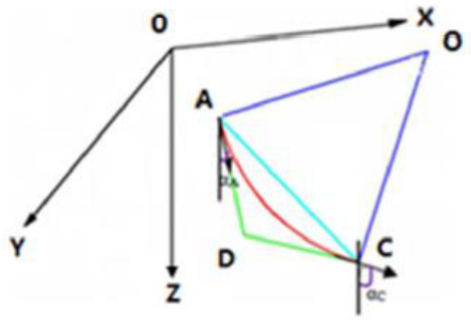

Figure 7.2: Starting point A and desired point C

To estimate the path between the given starting point A (given by the coordinates X_A,Y_A,Z_A) and the desired target point C (given by the coordinates X_C,Y_C,Z_C) one must simply calculate a constant radius between the points A and C. Additionally the angles of the starting point A (α_A and β_A) and the target point (α_c and β_c) must be calculated which can be done by using the tangent of the point in relation to the given reference frame. This procedure can be applied to several desired points to estimate the complete trajectory for an infinite amount of reference points. With these factors known the amplitude of the steering force A_k can be calculated. To determine that, the delta of the angle of inclination $\Delta\alpha_C$ and the delta of the azimuthal angle $\Delta\beta_{AC}$ as well as an average inclination angle α_0 is needed.

$$\begin{aligned} \Delta\alpha_{AC} &= \alpha_C - \alpha_A \\ \Delta\beta_{AC} &= \beta_C - \beta_A \\ \alpha_0 &= \frac{\alpha_A + \alpha_C}{2} \end{aligned} \tag{7.2}$$

After that the current dogleg γ can be calculated as follows:

$$\gamma = \frac{30 * 360 \left| sin(\frac{\sqrt{\Delta\alpha_{AC}^2 + \Delta\beta_{AC}^2 * sin(\alpha_0^2)}}{2} \right|}{\pi\sqrt{(X_C - X_A)^2 + (Y_C - Y_A)^2 + (Z_C - Z_A)^2}} \tag{7.3}$$

With both the current and maximum dogleg known, one can estimate the amplitude of the required steering force A_k.

$$A_k = \frac{\gamma}{\gamma_{max}} * 100\% \tag{7.4}$$

After the calculation of A_k one can calculate the direction of the steering . α_k For that, first the expected build rate $\Delta\alpha$ and the expected walk rate $\Delta\beta$ must be calculated. The variable ΔD_m in the following formulas describes the vertical depth between the points C and A in Figure 7.2

$$\Delta\alpha = 30 * \frac{\alpha_C - \alpha_A}{\Delta D_m} \tag{7.5}$$

$$\Delta\beta = 30 * \frac{\beta_C - \beta_A}{\Delta D_m} \tag{7.6}$$

With these values known one can calculate α_k. However, first it must be differentiated between 9 cases (for the exact 9 cases please refer to Zhang et al.). To determine which case is used to estimate the correct angle the expected build $\Delta\alpha$ and walk rate $\Delta\beta$ must be taken into account.

With the needed direction of the control force now known one can calculate the actual force F_i which is needed for all three wings. To calculate these forces the following two equations are given:

$$F * cos(\alpha_k) = F * cos(\alpha_1) + F_2 * cos(\alpha_1 + 240) + F_3 * cos(\alpha_1 + 120) \tag{7.7}$$

$$F * sin(\alpha_k) = F * sin(\alpha_1) + F_2 * sin(\alpha_1 + 240) + F_3 * sin(\alpha_1 + 120) \tag{7.8}$$

Since three variables are needed and only two equations are known, this problem cannot be solved with the given information. Therefore, the paper suggests setting one of the wings to maximum or minimum possible force. To determine which of these wings will be set to this value and if the force is maximum or not the system is divided into six sections for the azimuthal angle. The steering force is either in direction of the wings (favorable area f) or in the exact opposite direction (unfavorable area uf). Since all the six sections are equal in size, the tolerances for these areas are $\pm 30°$. To determine the missing third equation, the paper suggests that if the directional force lies in a favorable area the force F_i is equal to F_f and if it lands in an unfavorable area F_i is equal to F_{uf}

The forces F_f and F_uf are calculated as follows:

$$F_f = \frac{F_{max} + F_{min}}{2} + \frac{F_{max} - F_{min}}{2} * A_k \tag{7.9}$$

$$F_f = \frac{F_{max} + F_{min}}{2} - \frac{F_{max} - F_{min}}{2} * A_k \tag{7.10}$$

It needs to be noted that an initial condition is needed for the start of the algorithm where

F_j is equal to the initial force F_{ini}

$$F_{ini} = \frac{F_{max} + F_{min}}{2} \tag{7.11}$$

At last the relative direction of the steering force $\dot{\alpha}_k$ can be calculated. The resulting value can be divided into the two following results.

$$\begin{aligned} \dot{\alpha}_k &= \alpha_k - \alpha_1; \quad \alpha_k \geq \alpha_1 \\ \dot{\alpha}_k &= \alpha_k - \alpha_1 + 360; \quad \alpha_k \leq \alpha_1 \end{aligned} \tag{7.12}$$

To calculate the actual forces F_1, F_2 and F_3 of the wings the calculations are divided into six different cases which depend on the actual value of $\dot{\alpha}_k$(for the exact six cases please refer to Zhang et al.). With the forces F_1, F_2 and F_3 now known the actual force needs to be calculated, that is needed to move the hydraulic pistons. The piston forces F_{ki} depend on the wing position and the required wing contact force. By means of the geometrical relations the pivot angle ϕ_i can be calculated as a function of the piston position via an approximate function (polynomial). With the help of the pivot angle the necessary piston force can be calculated to achieve the required wing contact force.

$$\begin{aligned} F_{k1} &= \frac{F_1 * L_{k0} * cos(\phi_1)}{cos(\beta_1) * R} * sin(\beta_1 + \phi_1) \\ F_{k2} &= \frac{F_2 * L_{k0} * cos(\phi_2)}{cos(\beta_2) * R} * sin(\beta_2 + \phi_2) \\ F_{k3} &= \frac{F_3 * L_{k0} * cos(\phi_3)}{cos(\beta_3) * R} * sin(\beta_3 + \phi_3) \end{aligned} \tag{7.13}$$

For the entire step by step explanation of the **Equations 7.13** please refer to Appendix.

Recording of the trajectory

To determine where the actual drilled trajectory is, the drilling process is stopped after a defined drilled distance and the angle of the drill head to the acceleration due to gravity and the artificially generated magnetic field is measured. Thus, with the drilled length and the measured azimuth and the inclination of the BHA, a point in space can be calculated, starting from the last survey station. To increase precision and minimize sensor noise, a digital low-pass filter is applied to the sensor data of the accelerometer and the magnetometer.
Figure 7.10 describes the procedure of a survey station details are given in **Chapter 7.5.3**

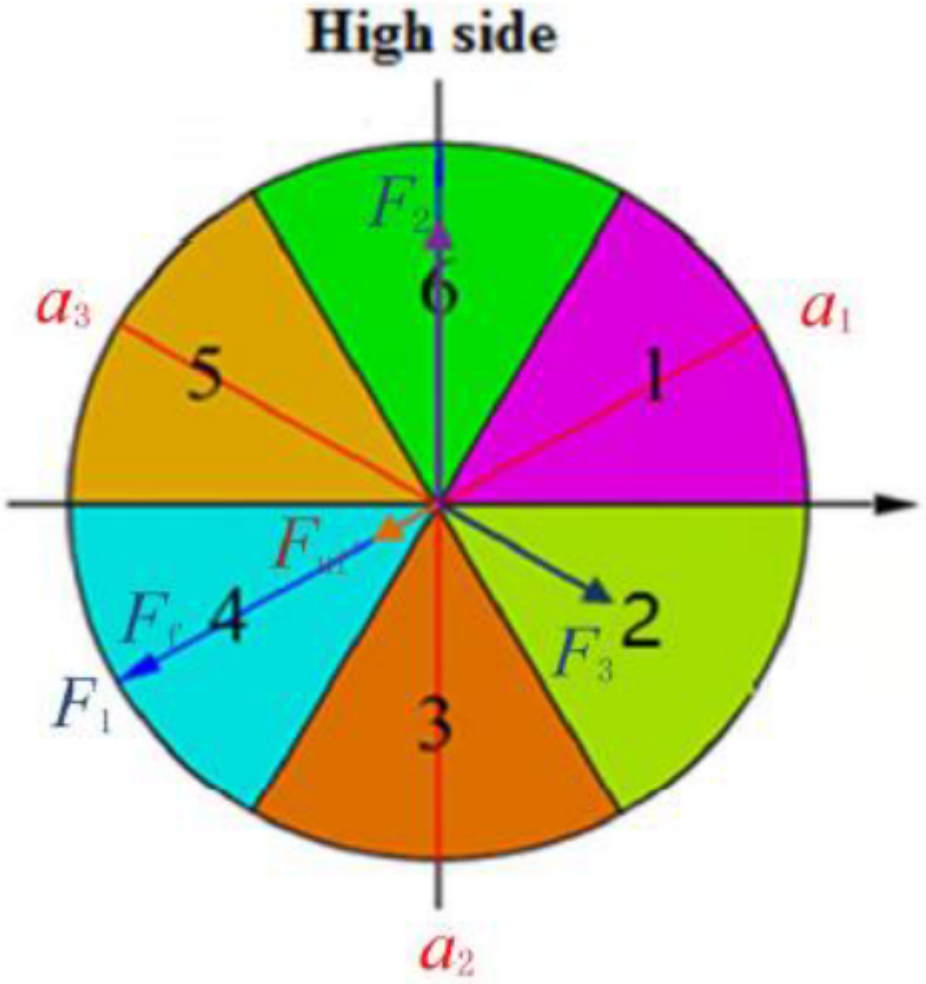

Figure 7.3: Six areas of favorability based on the angle between the directions of each wing force and the required steering force

Countermeasures in the event of deviation from the trajectory

During the first survey station, the actual position of the BHA is determined and compared to the position it should be at. If there is a deviation, a correction vector must be calculated and applied to hit the target anyway. To accomplish that, the same calculation as previous is used, but in this case the last known survey station position will be set as new start point and the new trajectory is calculated from S_1 to E. This mechanism is repeated until the originally planned trajectory is followed again.

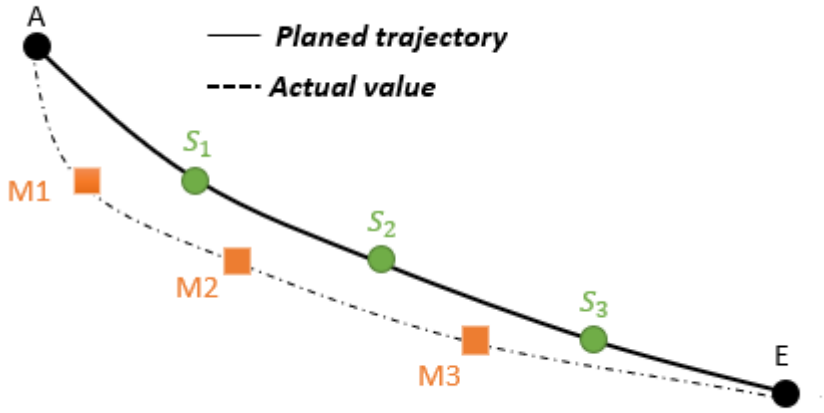

Figure 7.4: Trajectory deviation

To make sure that the target point E will be reached, when a deviation is detected, it is possible to operate the wings at max. force to get the maximum possible correction angle α as shown below.

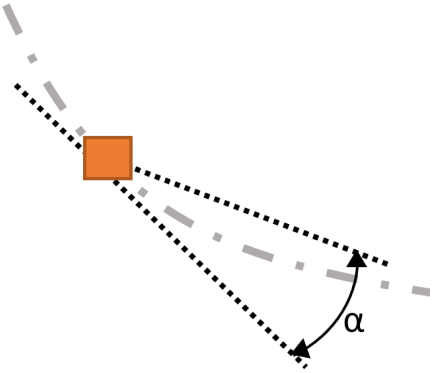

Figure 7.5: Maximum deviation angle

7.3 WOB algorithm

The algorithm for the calculation of the WOB is initially executed and is to adjust the parameters speed and WOB. First, several settings of the WOB are applied at a fixed speed for a fixed time interval, so that the ROP can be calculated for this setting. Now a curve is plotted through the data points from ROP and WOB and then the maxima of the curve is determined. This maxima represents the most optimal setting of the WOB. The algorithm is only executed at the beginning of the drilling process. As the sandstone is considered to be largely homogeneous, the optimum should not change significantly.

7.3.1 Drilling Performance Optimizations

One objective of the competition states that the hole should be drilled as fast as possible by the autonomous drilling rig. In other words, the rate of penetration (ROP) should be as high as possible. To achieve a high ROP, it is planned to use an algorithm that optimizes the mechanical specific energy (MSE) of the drilling process. Alternatively, a machine learning approach will be followed and implemented if time is on hands as shown in **Chapter 7.3.3**.

7.3.2 Mechanical Specific Energy

The mechanical specific energy describes the amount of energy required to remove a certain volume of material during a drilling operation. The best efficiency of drilling (high ROP) is given when the minimum mechanical specific energy is reached (R. (2011)).

$$MSE = \frac{Total\ Energy\ Input}{Volume\ Removed} \tag{7.14}$$

Volume of a drill hole is simply cross-sectional area multiplied by depth of penetration (Δh) and Work Energy can be described as force multiplied by distance. In drilling there are two forces acting on the bit: Weight on Bit (axial force) and Torque (rotational force). These are additive to MSE, so there are two terms in the MSE Equation.

$$\begin{aligned} MSE &= \frac{Vertical\ Energy\ Input}{Volume\ Removed} + \frac{Rotational\ Energy\ Input}{Volume\ Removed} \\ MSE &= \frac{WOB * \Delta h}{Area * \Delta h} + \frac{Torque * 2 * \pi * Rotations\ per\ time}{Area * \Delta h} \end{aligned} \tag{7.15}$$

The distance travelled by the bit (Δh) during a given interval is the penetration per time (ROP) divided by rotations per time. This is also known as depth of cut or as Penetration per Revolution.

$$\Delta h = \frac{Penetration\ per\ Minute}{Rounds\ per\ Minute} + \frac{ROP}{RPM} = P \tag{7.16}$$

This results in

$$MSE = \frac{WOB * \Delta h}{Area * \Delta h} + \frac{2 * \pi * RPM * Torque}{Area * ROP} \tag{7.17}$$

In this equation the MSE is a function of the WOB, the torque and the Penetration per Revolution. In order to find the minimum of the MSE, the equation is only set in dependence of one variable, the WOB. Therefore, the Torque and the Penetration per Revolution must be expressed as function of the WOB. This is possible with two assumptions. The higher the axial force, the higher the penetration rate and the torsional force. Therefore, the MSE is only displayed as a function of the axial force, i.e. the WOB. WOB and torque have a linear relationship. With these assumptions, the penetration per revolution can be described as a quadratic function of the WOB.

$$\begin{aligned} Torque = f(WOB) &= A_0 + A_1 * WOB \\ P = g(WOB) &= B_2 * WOB^2 + B_1 * WOB + B_0 \\ P &= \frac{ROP}{RPM} \\ MSE &= \frac{WOB * \Delta h}{Area * \Delta h} + \frac{2 * \pi * Torque}{Area * P} \end{aligned} \tag{7.18}$$

The parameters A_0, A_1, B_0, B_1, B_2 are determined by making test bores in which the WOB, the torque and the penetration per revolution are measured. The insertion in the function of the MSE results in the following equation.

$$MSE = \frac{WOB}{Area} + \frac{2 * \pi * f(WOB}{Area * g(WOB} = \frac{WOB}{Area} + \frac{2 * \pi (A_0 + A_1 * WOB)}{Area * B * WOB^2 + B_1 * WOB + B_0} \tag{7.19}$$

7.3.3 Machine Learning Approach

With the help of machine learning it is possible to set up and train an algorithm which uses complex statistics to predict a desired value. The basis of any machine learning algorithm is always the availability of a large data set, needed to train the algorithm. On this dataset the algorithm learns the specific relationships between the different values and how they influence the outcome. The greater the dataset and the more diverse, the better the algorithm will get. Ideally, the algorithm can, after being trained, predict the correct outcome from data it has never seen before. In the scope of the drilling optimization process, it is desired to increase the ROP by influencing the drilling parameters WOB and RPM as shown in **Figure 7.6** from **Git**. To determine the best combination of set points for these values a machine learning algorithm could be used. If the mechanical set up of the rig and BHA is finished in adequate time before the competition, a drilling data set could be created by drilling a sandstone sample with a variety of different combinations of drilling parameters for different hole inclinations. For each combination the ROP is measured and added to the data set. A machine learning algorithm, e.g. a Random Forest regressor, could then be set up and be trained on the dataset. Implemented on the rig the algorithm would predict the ideal drilling parameters for a high ROP and provide the system with the values to be used for these parameters.

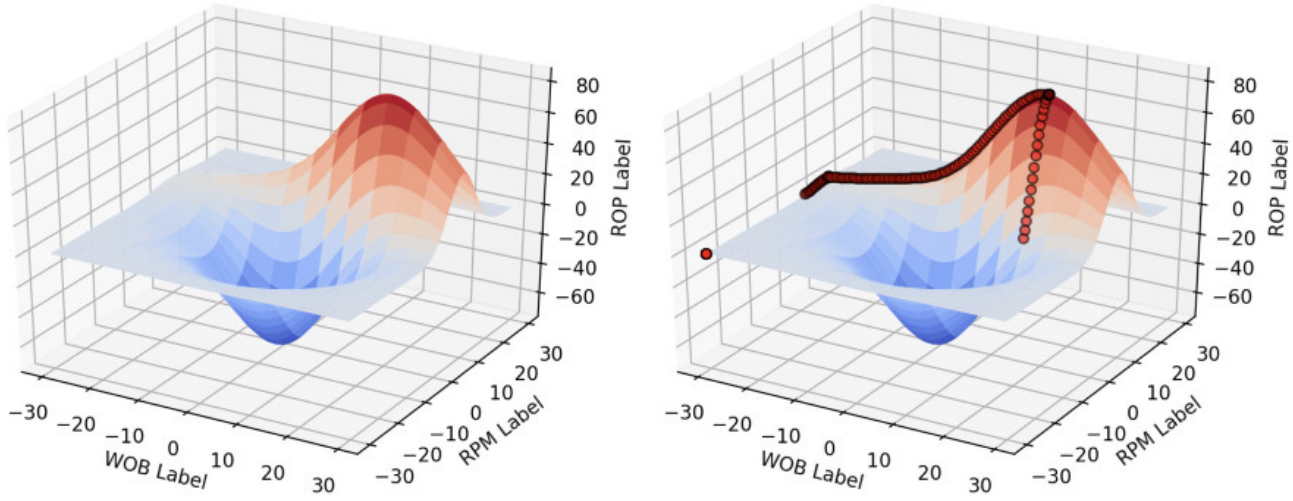

Figure 7.6: ROP Optimization

A possible protocol to determine the optimal WOB is shown in the following figure, the process will be started during the drilling procedure exactly when the initial set point for WOB was communicated to the robot. First the torque will be set to a fixed value and the ROP is recorded for a given time, so that a data point is generated. The algorithm goes through different settings and thus takes a field of data points to generate a surface plot. This surface will differ with each material that will be drilled and the spaces between the measured points will be extrapolated. To get the maximum ROP, different finding algorithms can be used but the best algorithm with the least amount of iterations is the Column-row search algorithm which is shown in **Figure 7.6**. The last step in the algorithm is to check if WOB and RPM are in the defined range and if they are, the new WOB and RPM is applied as a fixed value as the medium is considered homogeneous.

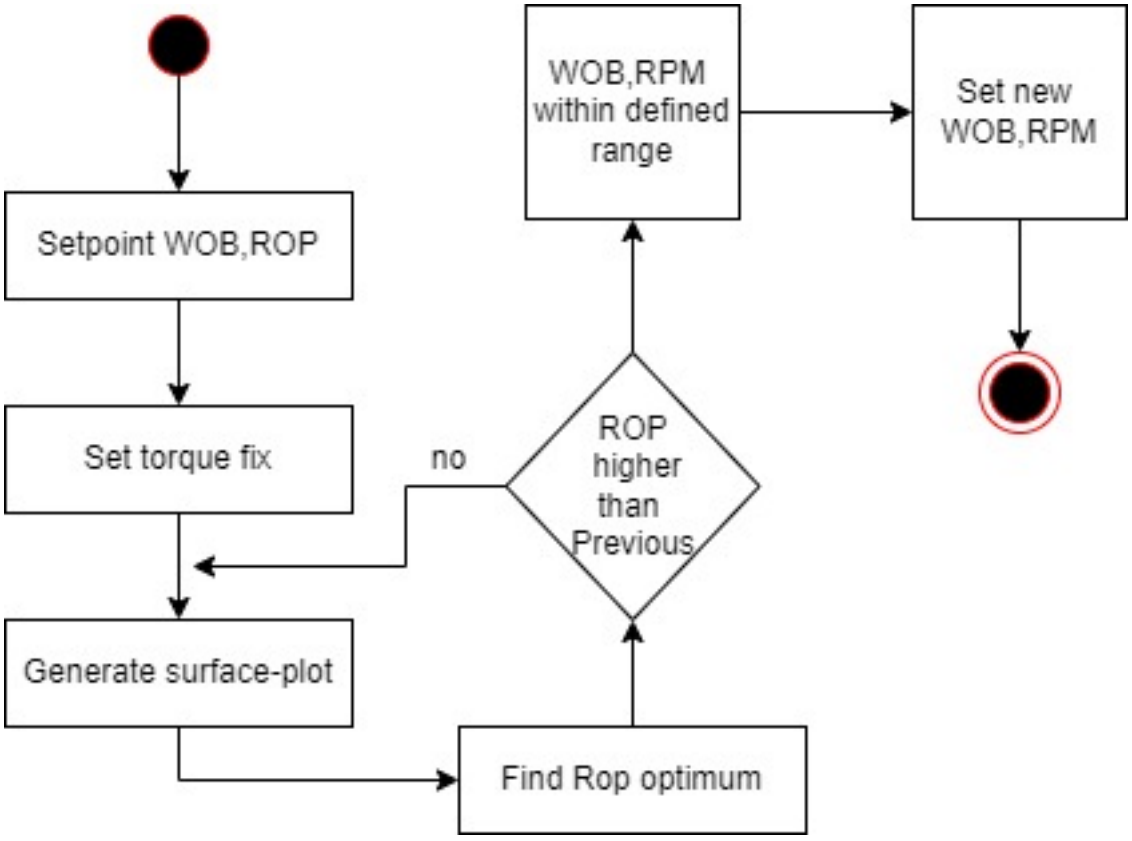

Figure 7.7: ROP Optimization UML

7.4 Data Visualization

Monitoring the data during the drilling process is crucial for accurate and smooth operations. Data that will be monitored is used for example to observe the heading of the system. This can be done by plotting the values of the accelerometer and the sensor fusion data. With these datasets the current path of the system can be observed by the user. This is especially important for the testing phase of the system since the actual path of the well can be compared with the desired path and will most certainly be helpful to improve the trajectory control-algorithm. Other values that will be displayed are vibrations and stress of the drill string. These are vital for secure operations of the system since surpassing certain thresholds can be a safety hazard for the system or the user. The classic drilling parameters, like ROP, WOB, RPM, standpipe pressure, torque and flowrate will also be visualized on a display in a typical manner. These parameters will be displayed in a graphic user interface (GUI) that is like the ones on large scale rigs. The team will monitor these parameters to make sure everything is going as planned. In that way it is ensured that even if the rig works fully autonomous, the current condition of the drilling operation can always be observed and monitored. As an example of what the GUI could look like, some sketches on **Page: 70-71** are included.

7.5 Visualization of software parts and other systems

For the entire drilling process, the system can be divided into 4 compartments, each of which is shown individually in the UML diagrams below. Starting with the initialization, which is initiated by pressing the main switch and command to start the protocol. Then to the drilling protocol combined with the Steering algorithm, which first switches on all the machines and begins the actual drilling process, and finally the survey station protocol which stops the drilling process every few sections on the Z-axis in order to query and measure data

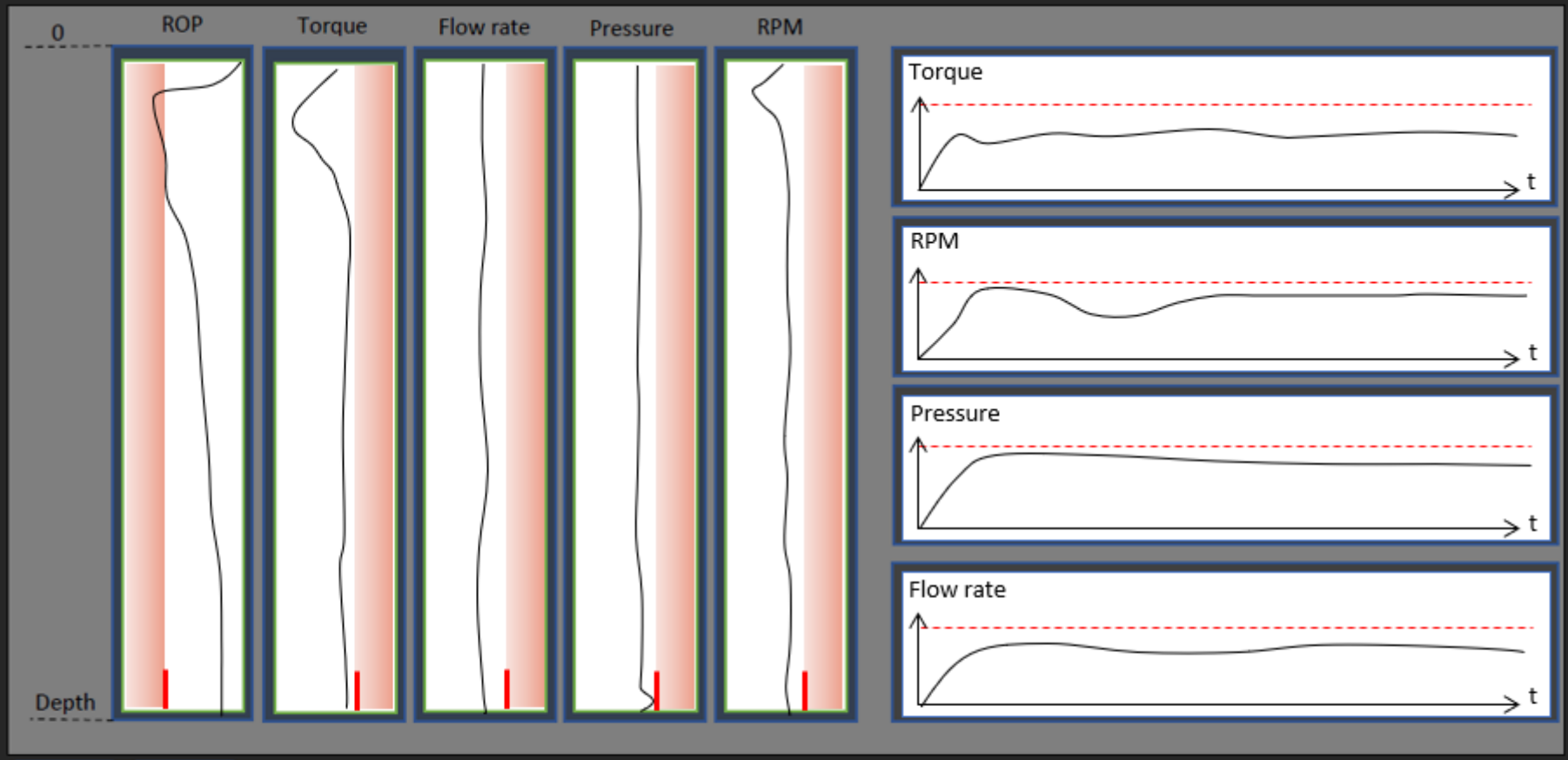

Start

Stop

Init

Manuel

Bus Communication

Switch

RPM in range

Pressure in range

Flow rate in range

Torque in range

All modules in range

Survey Mode

Load Configuration

Torque:

WOB:

Pressure:
max: min:

Flow:
max: min:

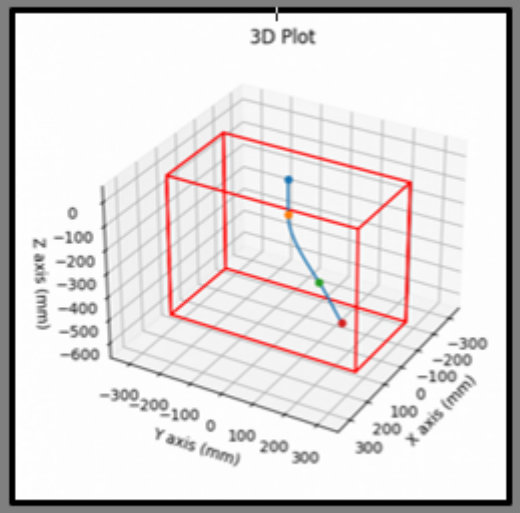

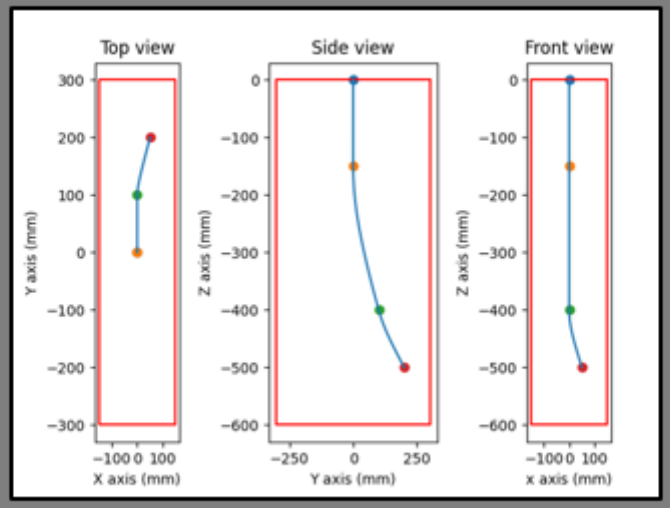

	X	Y	Z
Target:			
Start:			
Point 1:			
Point 2:			

Steps for Survey S.:

ROP Torq. Flow Pres. RPM

Current Position:

Current Trajectory:

N

Start | Stop

Init | Manuel

Bus Communication

Switch

RPM in range

Pressure in range

Flow rate in range

Torque in range

All modules in range

Survey Mode

Load Configuration

Torque:

WOB:

Pressure: max: min:

Flow: max: min:

7.5.1 Initialization

By activating the main switch, the 5V power supply turns on and all modules start up, waiting in standby mode. The next phase is initiated via a user input which is telling all modules to start their protocol. In the first step it is checked if all the modules are active and if they send an answer back through the BUS, if all modules are up and running the User gets notified. When the User initiates the homing phase, the relays connects mains to the 24v psu, only now can the motors drive the axes. The Z-axis and Rotary table are starting to home. After that the Magnetometer and Accelerometer are getting set to zero. The magnetcoils are switched on and Rotary table rotates the BHA while the magnetometer is querried. With that maneuver, the relative angle of the BHA to the rotary table is detected and the BHA azimuth is driven to stone north. Further, the Hook load and WOB will be set to zero as well and the Z-axis moves down to find Rock zero. If the Hook load and WOB are plausible, the Z-axis drives to the park position, where it waits for further User-input.

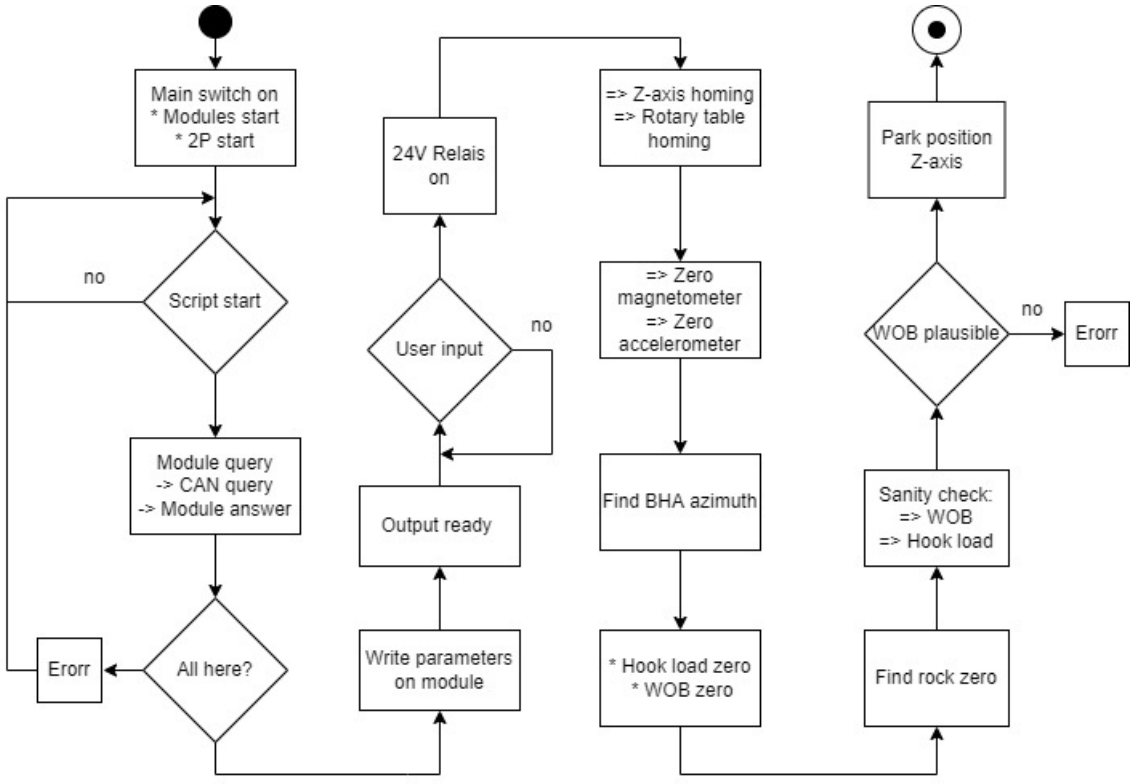

Figure 7.8: Initialization UML

7.5.2 Drilling

For initiating the drilling protocol, the user is required to put in the coordinates for the trajectory. If the coordinates are valid, the planner calculates a trajectory. If all Systems are ready to go the user can start the actual drilling process. With that the Relay module activates the circulation system. The flow meter then proves if there is a fluid flow and if the Pressure builds up in a valid range. If there is a fluid flow and pressure is neither too low nor too high, the motor starts and RPM and torque are measured. If there is no error like for example when the torque goes up and the rpm stays low, the z-axis applies WOB and the rig starts drilling. During drilling, the machine views all data and checks if everything is within range. The machine now enters the drilling loop and checks every iteration whether a survey station has to be executed. The criteria for this is met if a defined delta has been drilled. Then the loop starts over again with setting WOB.

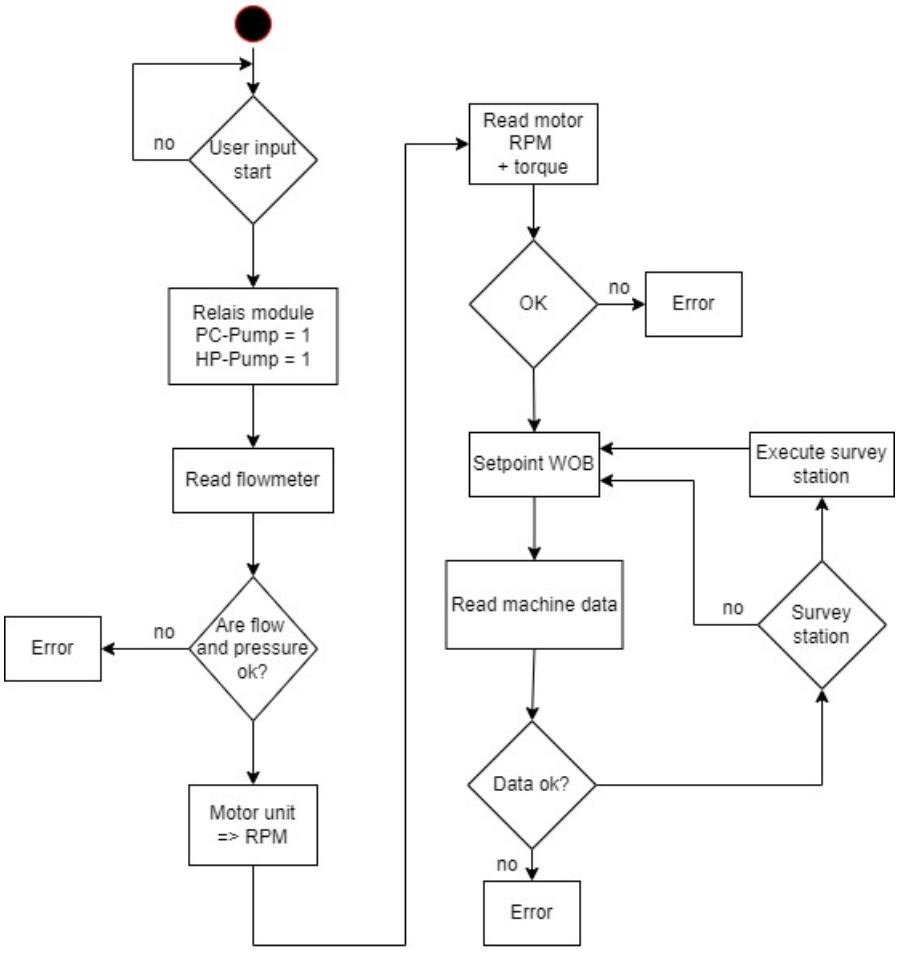

Figure 7.9: Drilling UML

7.5.3 Survey station

The first step when entering the survey station mode is setting the RPM to zero, so there is no unnecessary vibration during measurement. The next step is to drive 5 mm back on the z-axis (survey state) and wait until the hole is cleaned by the drilling fluid. For the first measurement it is needed to apply WOB again and measure WOB and Azimuth (not rotating), after that the z-axis drives back again to start the rotation of the bit again. Finally, WOB is applied again, and the drilling can go on.

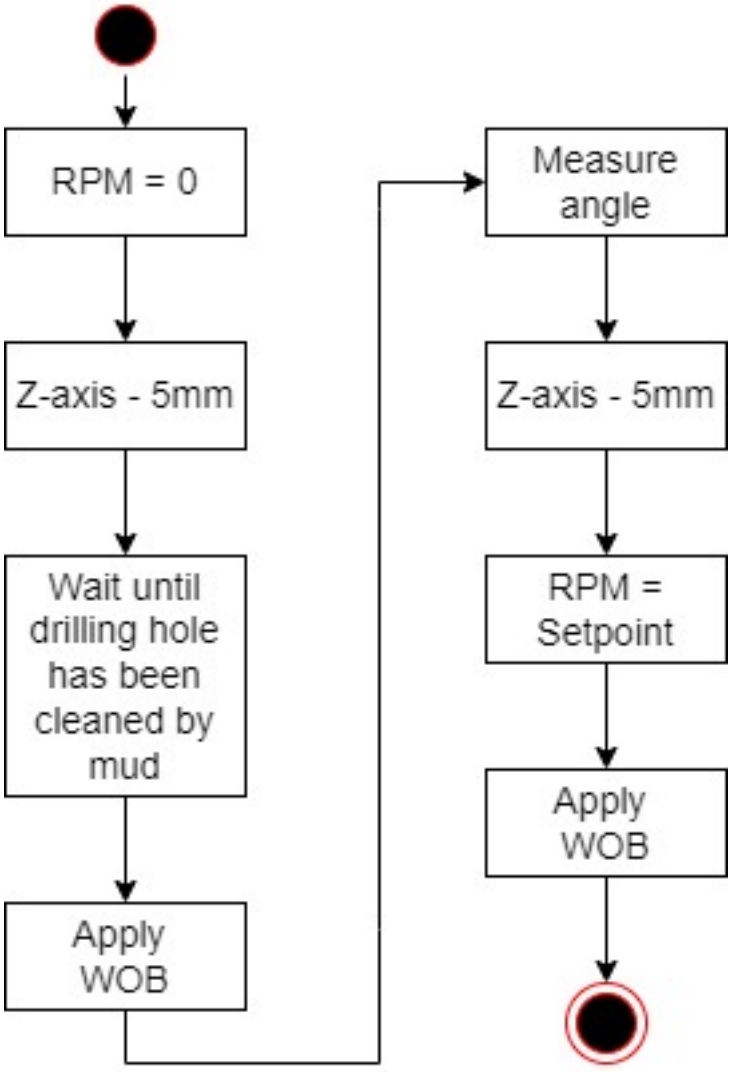

Figure 7.10: Survey station UML

7.5.4 Steering algorithm

After checking if the input data is valid, the steering unit protocol starts planing the trajectory and points for the survey stations. If the connection is stable and the robot is ready, the drilling starts, and the z-depth is queried. If the defined z delta has been drilled then a survey station is initiated. In the survey station the current angle is queried and the actual trajectory is computed. To check if the actual trajectory is deviating from the planned one, the date is analyzed. If that is the case, the correction vector needs to be calculated, which then gets sent to the steering unit to correct the drilled trajectory.

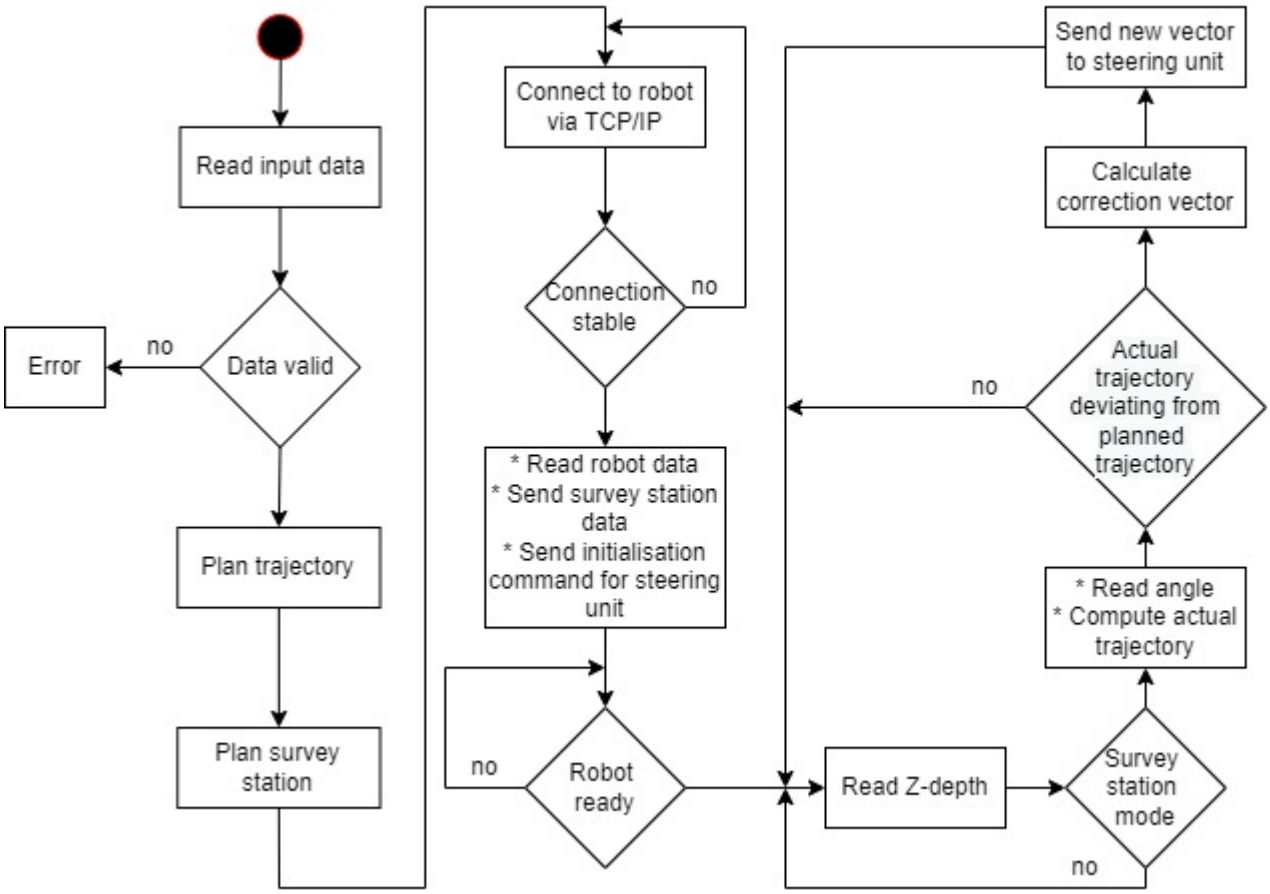

Figure 7.11: Steering unit UML

7.6 End of Well Report

Basic information like geological data will be manually entered into the drilling rig. Further, all positional data and drilling data will be saved iterative every three seconds with a time stamp in a text file. Based on this information, an end of well report will be automatically created after the drilling process is over.
The report will be divided into these categories: Operations summary, geologic summary, well data summary, wellbore schematic, time vs. depth graph, drilling program, mud program and directional program. In the operation summary, the different activities that were performed will be stated. These include an overview of starting and ending times, drilled and measured depth, kickoff point, build up ratio and an overview over the NPT. The geologic summary will describe the rock that was drilled as well its dimensions. The well summary data will show parameters such as RPM, WOB, pump rate, torque, measured depth, true vertical depth, and standpipe pressure. This data will be collected and transferred into an excel file to be attached to the end of well report.
The wellbore schematic will show the trajectory that was taken during drilling and the different coordinate points given. A Time vs Depth graph will show how much time was taken to get to each depth, all activities will be recorded in this time frame. The drilling program will explain in detail the drilling plan. The mud program will state the mud that is used to drill the rock with its rheological values. The directional program will show the different data collected by the BHA sensors near the bit that affect the trajectory. The NPT/Incident report will describe in full detail any problematic shown during the drilling procedure that caused the operation to be delayed or come to a stop.
This report will be used at the end of the competition to create a lesson learned and make a team review of what it was done, what worked and what needs to be improved.

7.7 Third-Party Interface

If the user chooses to steer the drill system remotely, it is planed to implement a manual interface where the direction of the drill bit, RPM and WOB can be specified by the user. This can be simply done by ignoring the trajectory control- and optimization-algorithm of the WOB and sending the commands directly over the CAN-bus towards the specified actuators. If enough time is at hand an implementation of an additional joystick for intuitive steering will be investigated. Since the high level algorithms communicate with the low level algorithm via tcp/ip, this can also be done at separate locations. This tcp/ip interface can therefore also be regarded as a third party interface. In addition, a video transmission

system must be provided. For security reasons, it must be insisted that at least one person is on site to activate the manual emergency stop in case of a failure.

8 Further Rig Considerations

8.1 Power Consumption

The following values were recorded for the electronics of the entire drilling machine:

Device	Perfomance [kW]	Performance [HP]
Hydraulic Pump	1.6	2.16
Hoisting Motor	0.18	0.243
Rotary Table Motor	0.18	0.243
Top Drive	1	1.35
Low Hydraulics	0.5	0.675
Remaining Electronics	0.1	0.135
Total	**3.56**	**4.806**

The drilling machine thereby consumes less than one fifth of the maximally allowed 25 horsepower of electrical power.

8.2 Rig Handling

To be able to transport the rig in a practical way, the hoisting traverse is designed to be removable. All electric and hydraulic supply lines are fitted with quick release couplings to reduce preparation time and to prevent the setting of incorrect connections. Once the hoisting traverse is removed, it can be mounted horizontally on the supporting rig structure for transportation. In that manner the rigs dimensions are 1600 mm (63 inch) in height, 2050 mm (80.7 inch) in length and 950 mm (37.4 inch) in width. The overall weight of the rig is 250 Kg (551 lbs.) and the chargeable weight 500 Kg (1102 lbs.).

8.3 Rock sample Handling

To get the rock sample into the rock sample receiver, the decision was made to not build an additional crane into the rig. The workshop at the institute is already equipped with a big crane hanging from the ceiling which makes it possible to load and unload the rock sample receiver very easily, the same thing applies for the drilling simulator in Celle. If it is

difficult to use, a motorized crane can be used to manipulate the test stone. So a built-in crane is not needed.

8.4 Funding Plan and Price List

The majority of the components already existed, and we only had to invest in some small parts to complete the build. The team would like to take this opportunity to thank the generous sponsor ITE Engineering GmbH. Without the active donation the project would not come to realization.

Table 8.1: Price list

Part	Price estimated
Safety housing	350€
Makrolon sheets	
Aluminium Profile	
Machine Parts	500€
Screws	
Bearings	
Semi Finished Products	
Seals	
Electrical Components	500€
PCBs	
Controller	
Sensors	
Router	250€
New Pump	600€
Total	2200€

8.5 Rig Upscaling

Due to the small scale at which the Drillbotics® rig is operated, the opportunity was taken to try out ways of transmitting data, fluids and power that might be foreign to the oil and gas industry. In contrary to real applications in the field it was decided do conduct information, hydraulic fluids, and the drilling fluid to the downhole area via cables and hydraulic hoses that are attached to the drill pipe. Since the depth of the borehole is relatively small compared to the diameter of the BHA, this method is applicable. This can be compared to the concept of a wired drill pipe. Here the cables are sealed within the pipe, but the idea of a direct connection is basically the same. But in the end even this

technology reaches its limitations, when facing very deep drilling applications with multiple connections. The torque for the drill bit will be transmitted by a rotating shaft that runs within the drill pipe and is greased to mitigate friction between the surfaces of the two metals. The rotation will be adapted to the needed RPM for the bit by a gearbox seated in the BHA. This might also be considered as very unorthodox. The application of this idea in the field seems not very realistic. The lubricant would not be allowed to flow down the inner annulus and therefore would have to have quite good thixotropic characteristics in the case of downtime. On top of that the additional weight of the rotating shaft would come with additional hook load and stresses inside the drill pipe and shaft would be too high and lead to failure. Considering the inclination of the BHA in the borehole got inspired by real applications and mirrors the common push-the-bit rotary steerable systems used in many applications. Wings at the side of the BHA that can be extended according to the desired direction are used. The difference to the field application lies in the way those wings are controlled. Though they are also moved hydraulically, the hydraulic fluid is pumped from the surface and not integrated into the BHA.

9 Safety Consideration and Risk Analysis

9.1 Safety Plan

The Teams safety plan is based around preventing any kind of accident that could happen to one of the Team members and to people near the operating zone of the rig. As it is impossible to predict where and how an accident can occur, the focus was set on what actions immediately could be taken in the event of an accident. First and foremost, everyone that is working on the rig got a safety briefing and no one is allowed to work alone on the rig without supervision. Before the work on the rig starts, it must be assured that the power is turned off and it is strictly forbidden to turn the power back on until the personnel around the rig is informed. Also, during testing and drilling, it is prohibited to touch or to move close to the rig. If, despite all these precautions, an accident should occur and immediate action is required, there is an emergency stop switch that immediately cuts off the power supply. To secure the area around the rig, there are not only going to be barriers in the form of safety tape at a sufficiently large safety distance but also acrylic glass cladding that are surrounding any moving, Rotating and Pumping parts. For communication purpose the office and workspace is equipped with a phone that makes it possible to contact the teams supervisors and advisor immediately in the event of an accident. Further considerations are listed in the tables below.

9.1.1 Technical safety

Riskname	**Risk Description**	**Risk control strategy**
Drilling fluid (water) leaking	Drilling fluid leaks from hose or circulation system	Use suitable hose and circulation system (e.g. hose with appropriate pressure rating capacity). The circulation system will be checked before and while testing.

Pumps working at high pressures	Pumps and hoses where the drilling fluid is flowing through may cause serious damage to personnel and equipment if there is any kind of leaking due to the high pressures.	Pumps and valves will be pressure tested before starting any operation, 5 min at low pressure and 10 min at high pressures. At this time only authorized personnel will be allowed to be near the drilling rig. A zone will be set up for visitors or other competitors to not pass through during this time.
String wobbling	String vibration/wobbling	Start drilling at low RPM then increase gradually after reaching a certain depth e.g. 1/4". Set the limit of the RPM in algorithm. During this time the string will be observed for any non-normal operations and the vibrations will be recorded to see any abnormalities.
Bit walking	Bit drills deviated away from the trajectory plan. This risk is also associated with string wobbling.	Install a guide shoe or riser/casing at rotary table above the rock sample thus limiting the drill string wobbling. Install downhole sensors, which are accelerometer and gyro, and integrates the acquisition data with algorithm to self-control the drilling trajectory.
Drill string stuck	Drill string stuck due to unclean hole or cutting is not circulated properly from the hole	Apply minimum flow rate according to minimum cutting transport velocity estimation. Apply also minimum drill string rotation speed (RPM) according to design calculation to help hole cleaning.

Loss verticality of hole section	Drill directional hole or deviated trajectory away from the plan	Install downhole sensors (accelerometer and gyro) and integrates acquisition data with algorithm program. Apply algorithm program to maintain verticality to selfcontrol string while drilling.
Drill string buckling and twist off	The weakest part along the drill string is drill pipe. Another potential weak part is connection. Buckling and twist off could occur during the drilling.	Use high strength connection type for all parts of the drill string, particularly the drill pipe. Calculations are made to avoid going over the critical buckling load and set the WOB limit and RPM Estimate the limit strength of drill pipe then limit the WOB and RPM to avoid the failure according to the design calculation. Set the WOB and RPM limit in the algorithm. Avoid going over the critical buckling load. In case much vibration occurs, alert (alarm) system will be active thus students can respond.

Cutting and drilling fluid spill and disposal	During the drilling, cutting, and drilling fluid will flow out of the well to the surface and must be disposed properly.	Safety containment will be installed around the rock sample and rig structure (below), thus the cutting and drilling fluid circulation (outflow) can be stored properly. The safety containment will be made from transparent material (e.g. plastic, etc.), thus the drilling process can still be observed. Additional storage containment will be installed also to store more cutting and drilling fluid circulation out of the well or rock sample. The cutting and drilling fluid outflow circulation will be recorded and disposed according to regulations (university and state regulations), particularly if there is chemical content. A general procedure will be included together with HSE procedure.
Electric cables and water hoses	Cables and hoses lying around which is a serious tripping hazard. Damaging of the equipment, tool failures and health restrictions might be consequences	Cable shafts for electric cables as well as hose guards will be laid to gather the loose components. Additionally, clearly visible warning labels will be put up to make people aware of the hazard

Table 9.1: Technical safety

9.1.2 Human safety

Riskname	Risk Description	Risk control strategy
Short circuit and/or electrical hazard	The risk is associated with electrical cable or source	Proper handling of electrical cable shall be applied, especially the avoidance from liquid (water). All electrical systems must be set up properly, soldered, installed, and connected to power source carefully and if it is possible enclosed system (use protector) and contained in one place. All the steps associated with setting up electrical must be done with safety concerns and safety protector (if applicable). Minimum safety equipment (e.g. safety glasses, gloves, etc.) must be worn during the electrical installation. No electrical connections should be made when connected to power. Every casing that has electrical components should be grounded to avoid any electrical injury to personnel.

Mechanical construction risk	During build up and/or testing, risk associated with pinch points, punctures, lacerations, cutting debris etc., could cause damage and hazard.	Proper handling of material and pieces during building up the rig structure, particularly it is mandatory to wear the proper HSE equipment according to minimum standard (e.g. safety shoes, safety glasses, gloves, etc.). Students will also work from a certain height during building up the rig structure, thus precautions must be taken to prevent injuries. A certain range of zone isolation must be set thus nonrelated person will be allowed to pass the zone. A general working procedure (Standard Operating Procedure/SOP) will be set before rig construction work. The connection of all parts and pieces of rig structure must be checked properly during and after rig construction to confirm the solid rig structure, thus avoiding the loose pieces during the drilling or test. All the sharp edges in rig structure will be covered or protected with protector to avoid human injures. Any items that could potentially fall from any height or loosen through vibrations or high rpm should be secured with a string to some other part, to ensure that no part flies out or falls

Hazard during drilling or testing	Accident and hazard during drilling or testing could occur.	The drilling automation (through algorithm and computer control) is set up thus less or even no human intervention is needed during the test. However, supervision during the test is still needed. Before the test or drilling is started, safety meeting will be held to discuss the procedure and any potential hazard. Emergency shutdown is included in algorithm program and will active in case serious hazard occurs. The emergency shutdown can also be activated manually (intervention from human) in case the self-control program does not work properly. In case there is obstacle or restriction in circulation system that causing increase of the pressure, emergency shutdown system will be activated (included in algorithm) at certain limit of pressure and relief valve is installed to release the pressure. A general testing procedure (Standard Operating Procedure/SOP) will be set before drilling or testing. Minimum HSE equipment standard must be worn (e.g. safety glasses, hearing protection, etc.). A certain range of zone isolation must be set thus unauthorized person will not be allowed to pass the isolation zone. A fire extinguisher will be available on location in case fire occurs due to overheating of electronic components or motor, etc. The hoisting system has locking mechanism to stop the movement in case lost control happens.

Flying debris	Debris that breaks free when cleaning the hole can be unsafe during the drilling process	To maintain the debris confined in the drilling area and to avoid any flying debris to harm anyone around the drilling area, a plastic cover will be installed to protect the personnel around it.
Mobility of the rig		The mobility of rig is incorporated in the design. The rig structure will be placed above the table and wheels will be installed below the table; thus, the rig can be mobilized. A brake system will be included in wheels to prevent undesired rig movement during drilling or testing due to vibration. Proper handling system will be installed so the rig can be moved safely and in convenient way. Modular design will be considered and as far as possible applied in the rig construction, such as electrical, computer, pump and disposal storage that can be disassembled or separated. This will make the mobilization and transportation more convenient and safer.
Rig transport	Pinching of fingers due to handling the rig	To avoid finger pinching the rig will be always handled with a forklift or a portable crane. Wood pieces will be placed on the bottom and sides of the rig when securing it for transportation in case it needs to be handle with the hand to accomplish the correct position. It is prohibited to put a hand under the rig when its being lifted.

Rock sample handling	Personnel can get injured by improperly handling the rock sample	The rock sample will be lifted by a lifting crane, thus avoiding any manual handling from personnel. While lifting the rock sample safety shoes and high impact gloves are to be worn. No other work is to be performed at the time of lifting and unauthorized personnel will be instructed to step back.

Table 9.2: Human safety

9.1.3 Communication safety

Riskname	Risk Description	Risk control strategy
Communication error	Failure during data acquisition due to communication system error	Correct system communications will be controlled by someone in the personnel to ensure good data acquisition and communication between the different systems. System restart will be designed, so whenever data is failed to be acquired, by restarting the system, data acquisition can work properly.
Sensor error	Failure during data acquisition due to sensor failure	The sensors will be tested before and after installation. After each test or drilling, maintenance will be performed to confirm whether the sensors can still function properly.

Table 9.3: Communications safety

10 Future applications

10.1 What this is about

In this chapter potential future applications are presented. Those designs are not going to be implemented in this year's competition.

10.2 Filter

The MARG filter used for the combination of the tri-axis accelerometer, magnetometer and gyroscope data is an efficient combination of compensation and heading algorithms which can compete with similar methods for IMU sensors like a Kalman-filter approach. This filter will only be explained briefly in this report since a deep explanation and discussion was already made by its creator Sebastian O. H. Madgwick in 'An efficient orientation filter for inertial and inertial/magnetic sensor arrays' (FIL and Mad). First and foremost, to understand the working principle of the algorithm one must look at the different methods of rotating different coordinate reference frames. This is important since the coordinate system of the sensor system will most certainly not align with the desired reference system of the drilling rig. This rotation of reference frames can be achieved by either the Euler method, which is considerably easier to understand, and the Quaternion approach. The Quaternion based method was chosen since it was already used in the depicted filter algorithm in Figure 10.1. The Quaternion based method is essentially an expansion of the complex number System to make it applicable to three-dimensional problems. This is represented by extending the complex numbers from one imaginary part $b * i$ to three imaginary parts represented by $b * i$, $c * j$ and

$$q = a + b * i + c * j + d * k \tag{10.1}$$

This method is preferred in comparison to the Euler approach since the rotation of a reference frame with a Quaternion based method can be done by the Quaternion product. This Quaternion product, denoted by the operator $\otimes$, uses only basic arithmetic operations like subtractions and multiplications. This results in a considerably faster operating speed compared to the rotation matrix used by the Euler method which relies on trigonometric functions like sine and cosine.

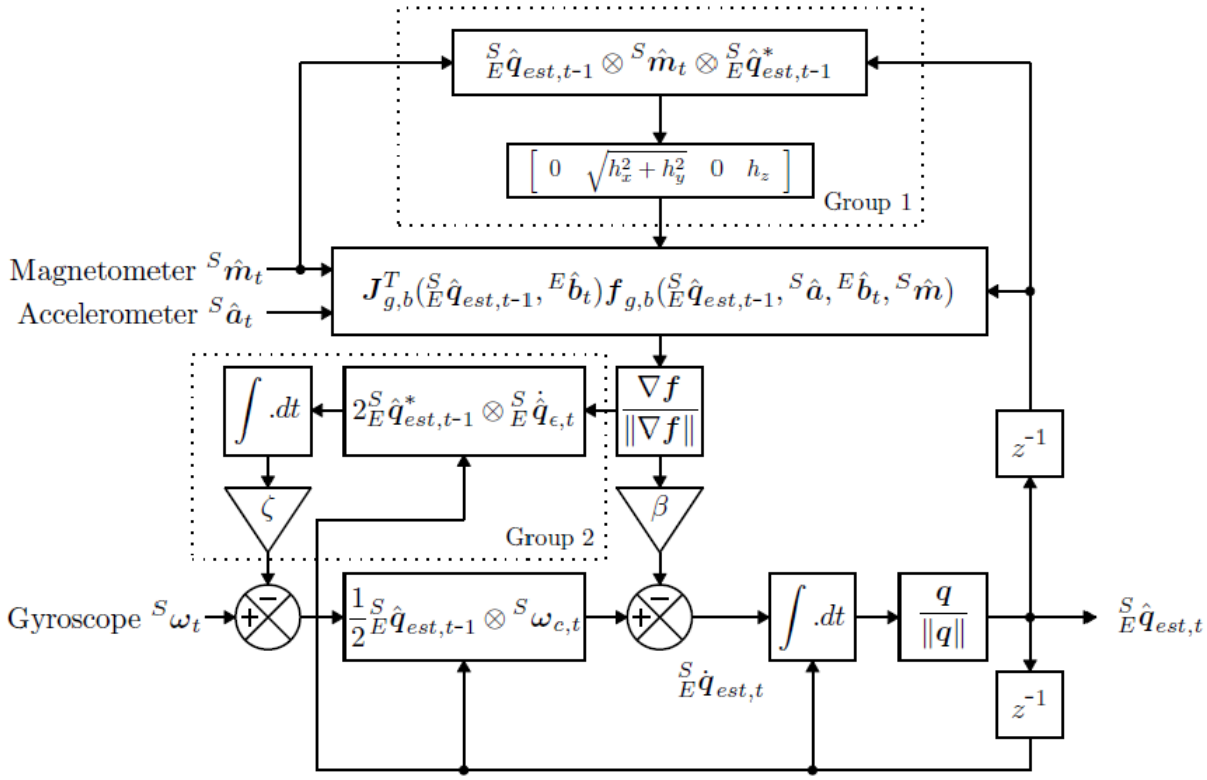

Figure 10.1: Block diagram of the MARG-Filter with gyroscope drift and soft iron distortion compensation modules

The block diagram depicted in Figure 10.1 explains the working principle of the MARG filter in a compact manner. The unfiltered measurements of the Magnetometer ${}^{S}\hat{m}_t$ and accelerometer ${}^{S}\hat{a}_t$ enter the block with the functions $J^{T}_{g,b}({}^{s}_{E}\hat{q}_{est,t-1}, {}^{E}\hat{b}_t)$ and $f_{g,b}({}^{S}_{E}\hat{q}_{est,t-1}, {}^{S}\hat{a}_t, {}^{E}\hat{b}_t, {}^{S}\hat{m}_t)$ is block basically describes the function gradient ∇f the magnetometer and accelerometer measurements. This is needed as a part of the gradient descent algorithm which is used to align the sensor frame S with the earth frame E. For the first iteration of this algorithm the term ${}^{s}_{E}\hat{q}_{est,t-1}$ needs an initialization value. This value will be set to ${}^{s}_{E}\hat{q}_{est,0} = [1, 0, 0, 0]$. The block above the function gradient ∇f (highlighted by the dotted box 'Group 1') is solely used to compensate the soft iron influences on the measurements of the magnetometer by rotating the magnetometer measurements ${}^{S}\hat{m}_t$ by the estimated orientation of the sensor ${}^{s}_{E}\hat{q}_{est,t-1}$ (the index * denotes the conjugate of a Quaternion which is similar to the conjugate of a complex number and describes a rotation in the opposite direction). This rotated vector ${}^{E}\hat{h}_t$ then needs to be adjusted for inclination errors. This is done by normalizing the values h_x and h_y of the vector ${}^{E}\hat{h}_t$. The newly constructed vector ${}^{E}\hat{b}_t$ only uses the previously calculated norm and the h_z values for the earths frame in the x and z axis.

The lower half of the algorithm shows that the gyroscope measurements ${}^{S}\omega_t$ enter a summation block where the gyroscope bias drift error ${}^{S}\omega_{b,t}$ is subtracted from the actual measurements ${}^{S}\omega_t$. The block outlined with the description 'Group 2' shows the working principle of this compensation method. To accurately estimate the orientation error, one must use the norm of the gradient function $\frac{\nabla f}{||\nabla f||}$ of the magnetometer and accelerometer data. This value represents the rate of change in orientation ${}^{s}_{E}\hat{q}_{\epsilon,t*}$ After that the product of ${}^{s}_{E}\hat{q}_{\epsilon,t}$ and ${}^{s}_{E}\hat{q}_{\epsilon,t-1}$ needs to be integrated. This calculation leads to the DC component ${}^{S}\omega_t$ of the bias error. This error then needs to be subtracted from the actual measurements with an appropriate gain ζ The result of these subtractions are gyroscope measurements ${}^{S}\omega_{t,c}$ which will not be influenced by an overtime increasing drift. After that the corrected gyroscope values must be rotated towards the earths current reference frame ${}^{s}_{E}\hat{q}_{est,t-1*}$. The actual fusion of all three sensor measurements occurs in the lower half of block diagram. The normalized rate of change of the magnetometer and accelerometer $\frac{\nabla f}{||\nabla f||}$ is multiplied by the factor β which describes the divergence rate of the gyroscope. This product is then subtracted from the drift free gyroscope measurements ${}^{s}_{E}\hat{q}_{\omega,t*}$ The result then needs to be integrated to get the current heading. After that the unit quaternion $\frac{\nabla q}{||\nabla q||}$ must be calculated. This last operation leaves the user with a unit quaternion of the current heading of the sensor ${}^{s}_{E}\hat{q}_{est,t}$ which will then be used for the next iteration to update the current heading to repeat the process (this is represented by the block z^{-1} which is the conjugate of the unit Quaternion $\frac{\nabla q}{||\nabla q||}$). These Quaternions then must be transformed into useable representations which would be Euler angles. These transformations can be done by the

following formulas:

$$\psi = atan2(2bc - 2a, 2a^2 + 2b^2 - 1) \tag{10.2}$$

$$\theta = -sin^{-1}(2bd + 2ac) \tag{10.3}$$

$$q = atan2(2cd - 2ab, 2a^2 + 2d^2 - 1) \tag{10.4}$$

The function atan2 in the above-mentioned Equations 10.2describes an expansion of the inverse of the tangent function. This function needs two real arguments with which it can calculate an angle in the complete range of 360 degrees. In consideration for a performance increase of the sensor are an additional low pass filter (or other high frequency suppressing filters) to decrease the influence of vibrations of the accelerometer measurements ${}^{S}\hat{a}_t$. However, to accurately program the low pass filter, the cut off frequency needs to be estimated which can only be done after measurements have been taken with the drilling rig.

10.3 Safety Clutch

Since the flex shaft can only transmit a maximum torque of 6 Nm before permanent damage is imminent, a way had to be found to prevent failure. This can happen if the drill bit seizes up and the energy stored in the inertia is suddenly transferred to the flex shaft in the form of excessive torque. In order to avoid such a scenario in operation, it was decided to use a clutch which rotatably separates the flex shaft from the drill bit when the torque exceeds a certain level, so that damage to the shaft, which is difficult to replace, is avoided. The clutch (**Figure 10.2**) is designed in such a way that three balls under spring pre-tension engage in bores which are located radially in the clutch bell and thus the torque is transmitted via the shear forces. If the transmitting torque increases in a forcible manner, the balls slip out of the slightly smaller bore holes and the clutch allows the Flex shaft to rotate freely. In order to achieve the best possible performance in later operation, an adjusting screw has been designed to adjust the preload of the spring. In this way an optimum can be determined experimentally. In addition, the speed of the main shaft is determined by the sensor module and the algorithm recognizes the triggering of the clutch and thus also a seizing of the bit, so that countermeasures can be taken. Due to its complex design, it is still under discussion if the safety clutch will be implemented or if a workaround can be found.

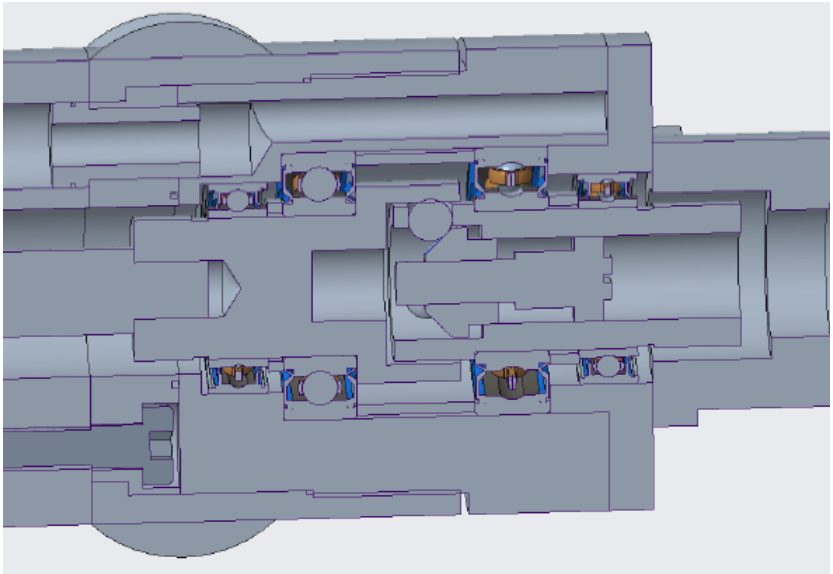

Figure 10.2: Safety Clutch

11 Appendix

11.1 A: Data and Assumptions

Based on the 2022 Drillbotics competition guidelines, some assumptions and basic information for calculation and engineering design are summarized:

Table 11.1: Drilling hole and rock data

Drilling hole and rock data	Field unit	Metric unit
Hole diameter (d_h)	1.5 in	38.1 mm
Rock strength	2-5 ksi	13.8-34.5 MPa
Cutting concentration (C_{conc})	1.5%	1.5%
Height of rock	24 in	0.6 m
Cutting density (ρ_s)	165.43 lb ft^{-3}	2650 Kg m^{-3}
Diameter cutting (d_s)	0.004 -0.04 in	0.1-1mm
ROP	0,8 ft/hr	0.24 m/hr

Table 11.2: Drilling fluid data

Drilling fluid data	Field unit	Metric unit
Water viscosity	1 cp	0.001 Pas
Water density	8.33ppg	1000 Kgm^{-3}

Table 11.3: Drill pipe data

Steel drill pipe data	**Field unit**	**Metric unit**
Ultimate Tensile Strength	73244 psi	505 MPa
Yield strength (Ys)	31183 psi	215 MPa
Modulus of elasticity (E)	$2.901 * 10^7$ psi	200 GPa
Weight	0.1493 lb/ft	0.2233 Kg/m
Outside diameter (d_p)	0.393 in	10 mm
Outside radius (r_o)	0.1968 in	5 mm
Inside diameter (id_p)	0.31496 in	8 mm
Inside radius (r_i)	0.15748 in	4 mm
Wall thickness (t)	0.0787 in	2 mm
Length (L_{dp})	36 in	0.91 m
Roughness	0.0006 in	0.0152 mm

Table 11.4: Stabilizer / downhole BHA data

Stabilizer/downhole BHA data	Field unit	Metric unit
Outside diameter (d_d)	1.46 in	37 mm
Diameter Flowline	0.15in	4 in
Length Flowline	3.14in	124 mm
Diameter shaft	0.19 in	5 mm
Length shaft	0.19 ft	60 mm
Length (L_{dw})	7.28 in	185 mm
Roughness	0.0039 in	0.1 mm
Inside diameter (id_d)	0.6 in	15.2 mm
Wall thickness (t)	0.1 in	2.54 mm
Length (L_{dw})	3.5 in	8.9 cm
Roughness	0.0006 in	0.0152 mm

Table 11.5: Bit data

Bit data [DSATS provided]	Field unit	Metric unit
Bit diameter	1.5 in	38.1 mm
Nozzle diameter	0.118 in	3 mm
Discharge coefficient	0.95	0.95

Table 11.6: Calculation Results

Parameter	Symbol	Calculated Result	
		Field Units	Metric Units
Critical buckling load	Pbcr	151.92 lbf	675.77 N
Burst limit	Pburst	8326.04 psi	574.06 bar
Torsional Stress limit	τ	218.25 in.lbf	24.66 Nm
Flow rate	Q	1.84 gpm	7 Lpm
Pump pressure	Ppump	118.76 psi	29.7 bar
Pump horsepower	HPP	0.12 HP	0.46HP

Table 11.7: Used formulas

Calculations	Formula	Reference
Reynolds number	$Re = \frac{928*\rho*v*id}{\mu}$	Reynolds number (Moore,1986)
Friction factor	$f = 0.25[log_{10}(\frac{\epsilon}{3.7*id} * \frac{5.74}{Re^{0.9}})]^{-2}$	(Mitchell und Miska, 2011)
Pressure losses	$P = \frac{f*\rho*v^2*L}{25.8*id}$	(Mitchell und Miska, 2011)
Total area of nozzle	$A = 2 * \frac{\pi}{4} * d^2$	Calculation of an area
Pressure loss at bit	$P_{bit} = \frac{Q^2*\rho}{12031*A^2}$	(Bourgoyne Jr., et al., 1991)
Pressure loss in the BHA	$P_{BHA} = P_s + P_{ho} + P_dp$	(Bourgoyne Jr., et al., 1991)
Jet impact force	$F_j = 0.01823 * C_d * Q * \sqrt{\rho * P_{bit}}$	(Bourgoyne Jr., et al., 1991)
Jet velocity of bit	$v_{bit} = \frac{Q}{A}$	(Bourgoyne Jr., et al., 1991)
Total downhole pressure loss	$P_{downhole} = P_{bit} + P_{BHA}(+P_a)$	(Bourgoyne Jr., et al., 1991)
Velocity in hose	$v_h = \frac{Q}{2.448*id_h^2}$	(Bourgoyne Jr., et al., 1991)
Friction factor determination on Fanning chart	$\frac{\epsilon}{id_h}$	Fanning friction factor (Bourgoyne jr., et al., 1991)
Total Pressure loss along entire system	$P_{loss} = P_{downhole} + P_h$	(Moore, 1986) (Bourgoyne Jr., et al., 1991)
Requirement horsepower for pump	$\frac{P*Q}{1714}$	(Mitchell und Miska, 2011)
Torsional Limit	$T_{max} = \frac{\pi}{16} * \sigma_m ax * \frac{(d_p^4 - id_p^4)}{d_p}$	
Burst Limit	$P_{burst} = \frac{2*Y_p*t}{d_p*Sf}$	
Buckling load	$P_{bcr} = \frac{\pi^2*E*I}{(K*L)^2}$	
current dogleg	$\gamma = \frac{30*360\left\lvert sin(\frac{\sqrt{\Delta\alpha_{AC}^2 + \Delta\beta_{AC}^2 * sin(\alpha_0^2)}}{2})\right\rvert}{\pi\sqrt{(X_C - X_A)^2 + (Y_C - Y_A)^2 + (Z_C - Z_A)^2}}$	

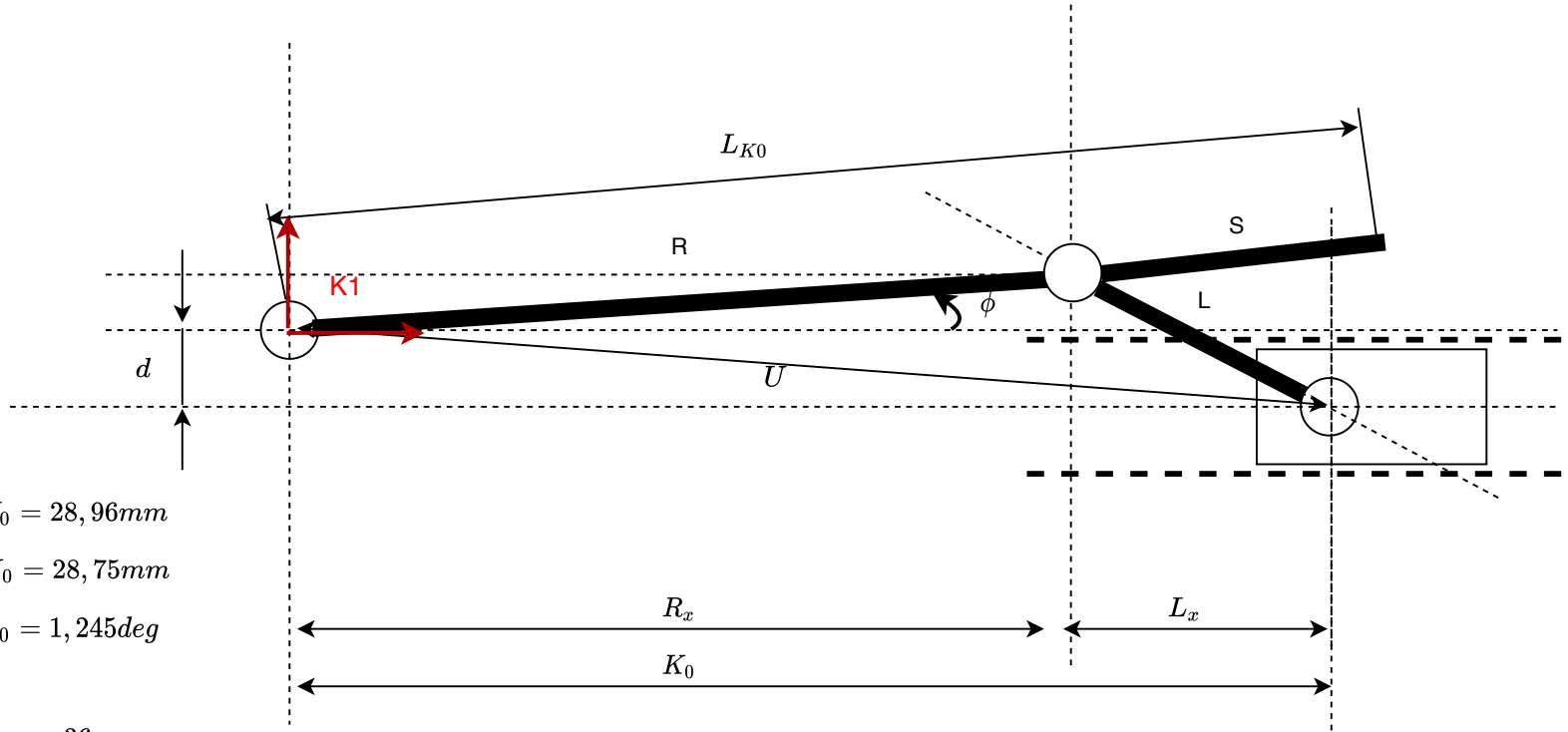

$U_0 = 28,96mm$

$K_0 = 28,75mm$

$\phi_0 = 1,245deg$

$L_{K0} = 36mm$

$R = 23mm$

$L = 7mm$

$d = 3,5mm$

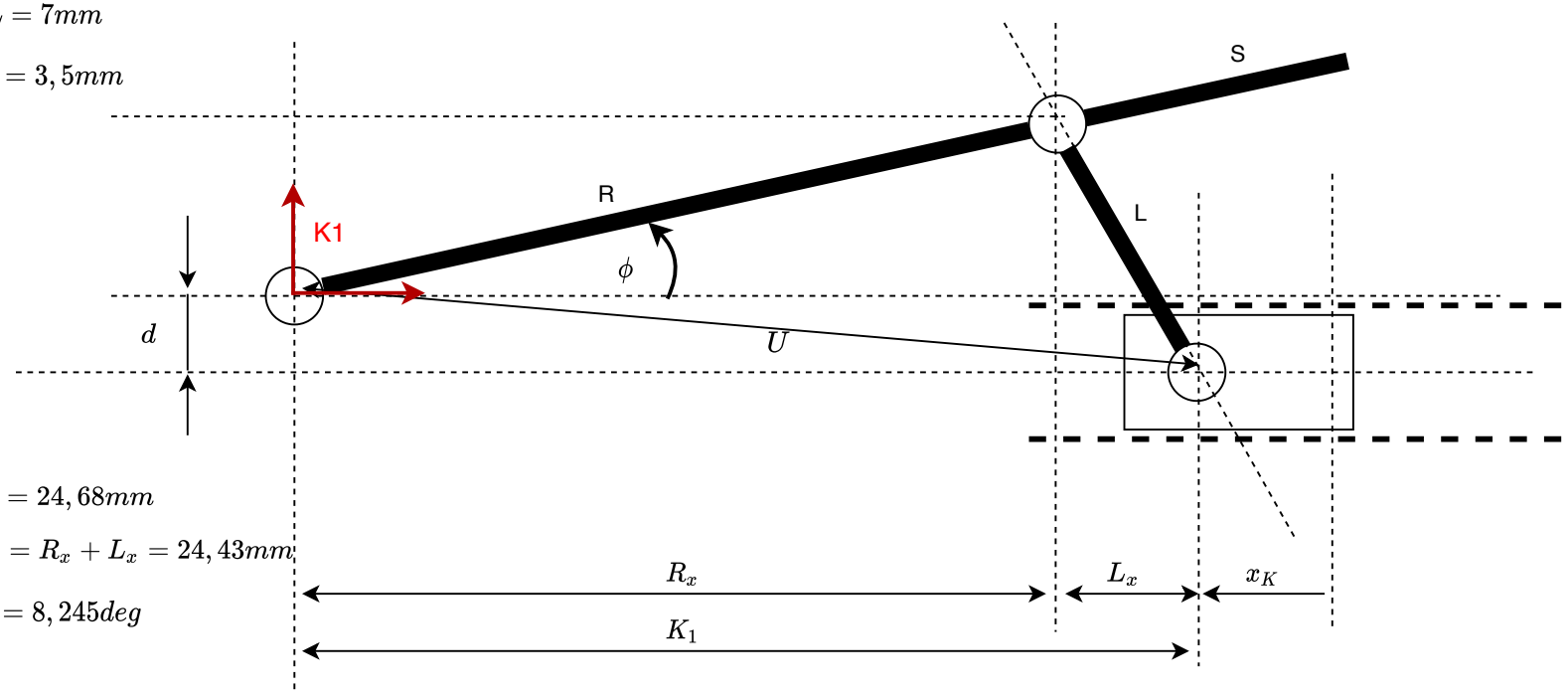

$U_1 = 24,68mm$

$K_1 = R_x + L_x = 24,43mm$

$\phi_1 = 8,245deg$

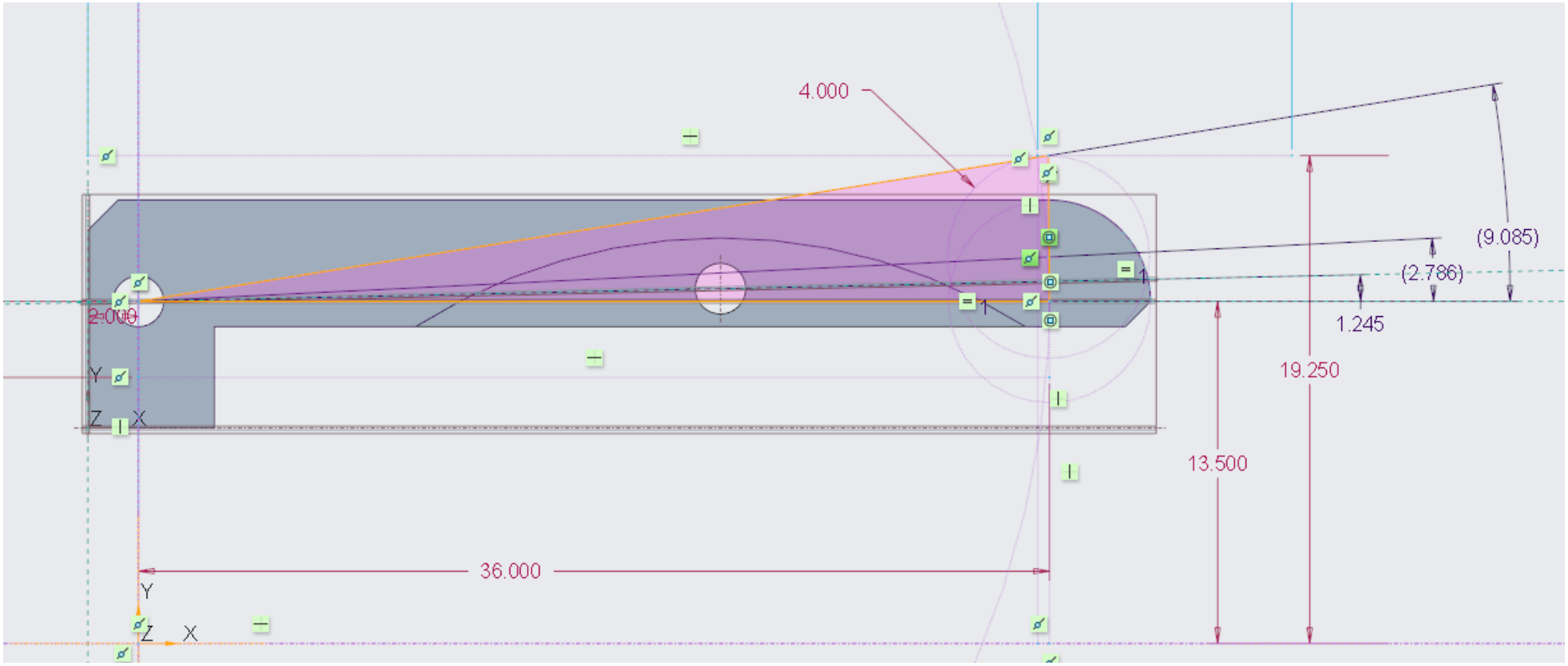
4.000
(9.085)
(2.786)
1.245
19.250
13.500
36.000
Y
Z
X

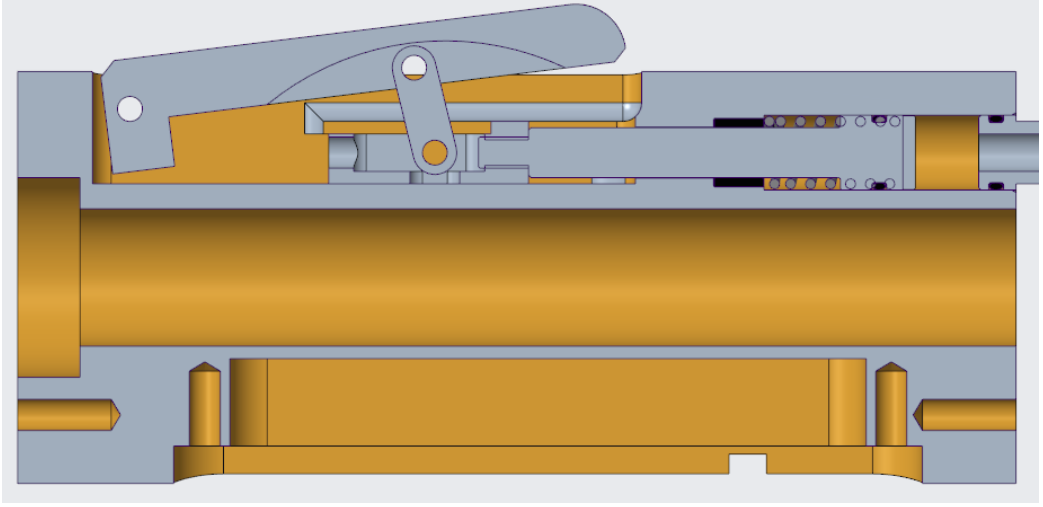

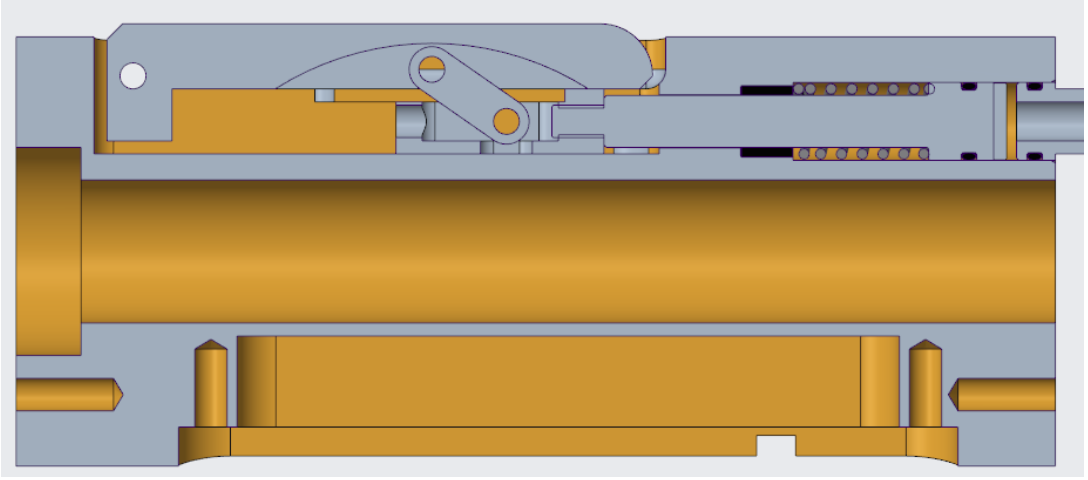

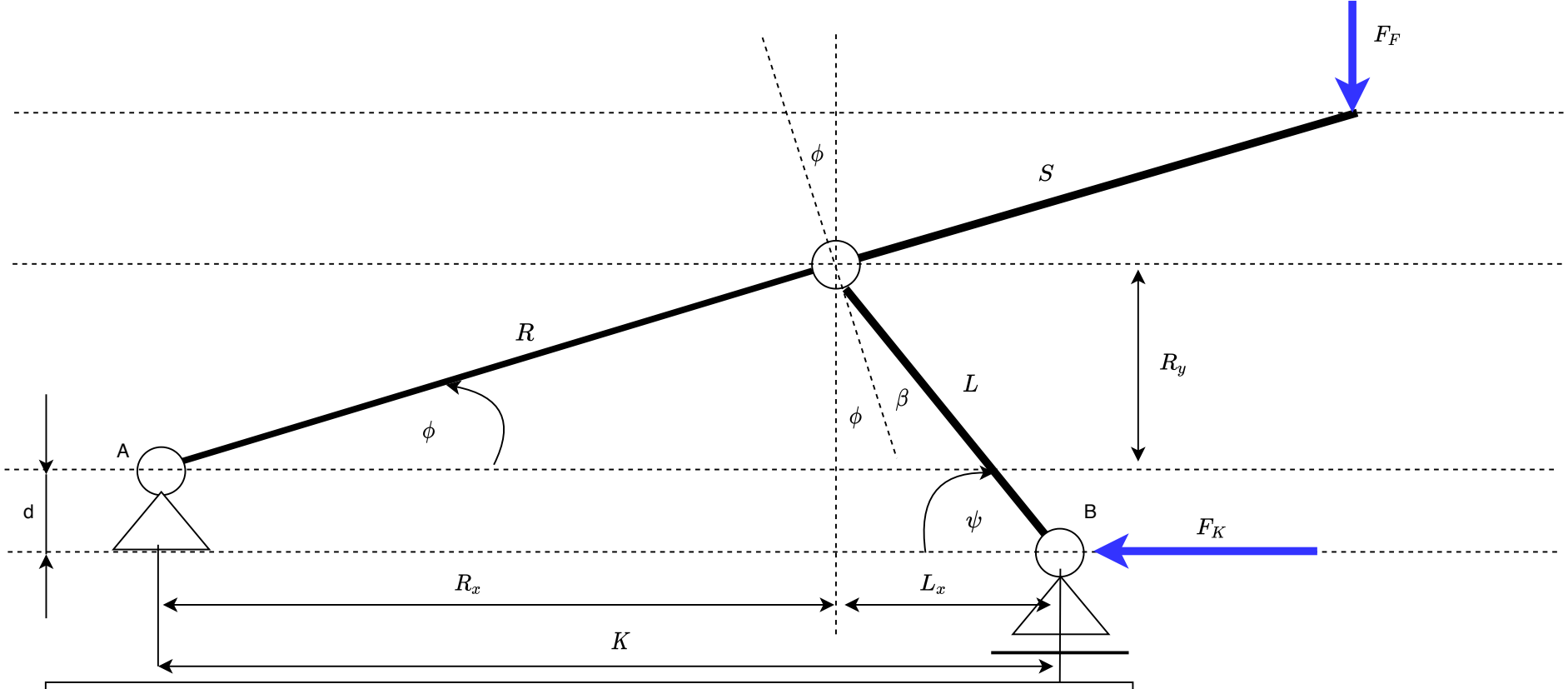

$$K = R \cdot \cos(\phi) + \sqrt{L^2 - (d + R \cdot \sin(\phi))^2}$$

Step 1: Calculate angle β

$$\psi = \sin^{-1}\left(\frac{R_y + d}{L}\right) = \sin^{-1}\left(\frac{R\sin(\phi) + d}{L}\right)$$

$$\beta = 90^\circ - \phi - \psi$$

Step 2: Transformation from reference frame K1 to K2

$$\vec{e}_{1x} = \cos(\phi) \cdot \vec{e}_{2x} - \sin(\phi) \cdot \vec{e}_{2y}$$

$$\vec{e}_{1y} = \sin(\phi) \cdot \vec{e}_{2x} + \cos(\phi) \cdot \vec{e}_{2y}$$

$$\vec{e}_{2x} = \cos(\phi) \cdot \vec{e}_{1x} + \sin(\phi) \cdot \vec{e}_{1y}$$

$$\vec{e}_{2y} = -\sin(\phi) \cdot \vec{e}_{1x} + \cos(\phi) \cdot \vec{e}_{1y}$$

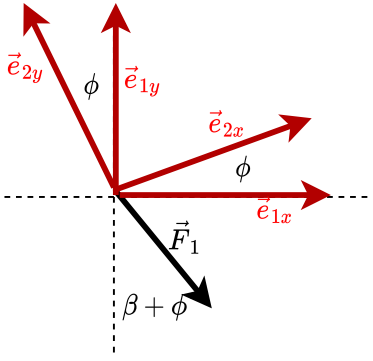

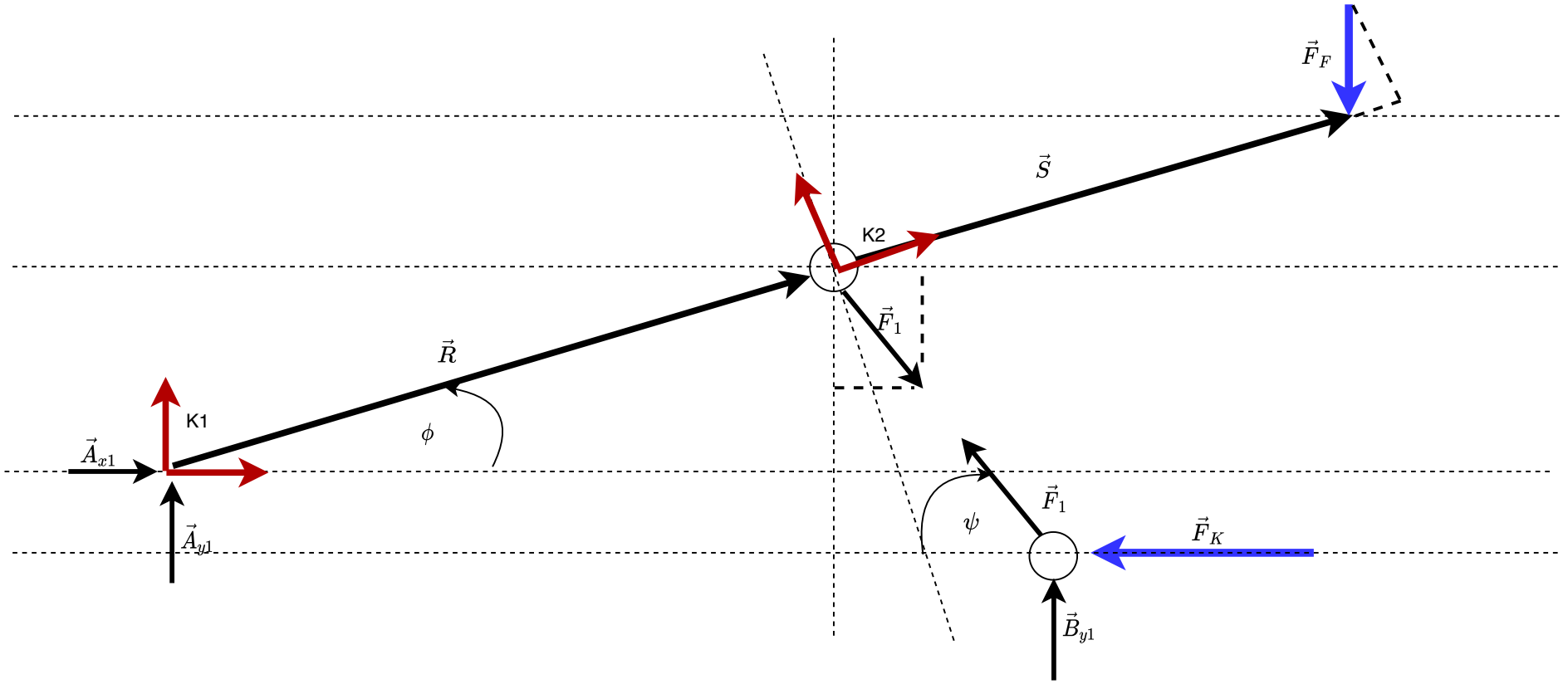

Step 3: Denote active forces in component notation for reference frame K1 and K2

$$\vec{F}_F = -|\vec{F}_F| \cdot \vec{e}_{1y} = -|\vec{F}_F| \cdot (\sin(\phi) \cdot \vec{e}_{2x} + \cos(\phi) \cdot \vec{e}_{2y})$$

$$\vec{F}_1 = |\vec{F}_1| \cdot \sin(\beta) \cdot \vec{e}_{2x} - |\vec{F}_1| \cdot \cos(\beta) \cdot \vec{e}_{2y} = |\vec{F}_1| \cdot \sin(\beta) \cdot (\cos(\phi) \cdot \vec{e}_{1x} + \sin(\phi) \cdot \vec{e}_{1y}) - |\vec{F}_1| \cdot \cos(\beta) \cdot (-\sin(\phi) \cdot \vec{e}_{1x} + \cos(\phi) \cdot \vec{e}_{1y})$$

Step 4: Define equilibrium of forces for the pads

$$\sum \vec{F} = 0: \quad \vec{A} + \vec{F}_1 + \vec{F}_F = \vec{0}$$

Step 5: Define equilibrium of torque of the pad around A

$$\sum \vec{M}_A = 0: \quad \vec{R} \times \vec{F}_1 + \vec{S} \times \vec{F}_F = \vec{0} \qquad |\vec{S}| = L_{K0}$$

Step 6: Define equilibrium of forces for the lever

$$\sum \vec{F} = 0: \quad \vec{B} + \vec{F}_1 + \vec{F}_K = \vec{0} \qquad \vec{F}_K = -|\vec{F}_K| \cdot \vec{e}_{x1}$$

$$\vec{B} = |\vec{B}| \cdot \vec{e}_{y1}$$

Step 7: Define equilibrium of torque for the lever

$$\sum \vec{M}_B = 0: \quad \vec{0}$$

Step 7: Define force and position vectors in reference frame K1

$$\vec{A} = \begin{bmatrix} A_{x1} \\ A_{y1} \\ 0 \end{bmatrix}^T \cdot \begin{bmatrix} \vec{e}_{x1} \\ \vec{e}_{y1} \\ \vec{e}_{z1} \end{bmatrix} \qquad \vec{B} = \begin{bmatrix} 0 \\ B \\ 0 \end{bmatrix}^T \cdot \begin{bmatrix} \vec{e}_{x1} \\ \vec{e}_{y1} \\ \vec{e}_{z1} \end{bmatrix}$$

$$\vec{F}_F = \begin{bmatrix} 0 \\ -F_F \\ 0 \end{bmatrix}^T \cdot \begin{bmatrix} \vec{e}_{x1} \\ \vec{e}_{y1} \\ \vec{e}_{z1} \end{bmatrix} \qquad \vec{S} = \begin{bmatrix} L_{K0}\cos(\phi) \\ L_{K0}\sin(\phi) \\ 0 \end{bmatrix}^T \cdot \begin{bmatrix} \vec{e}_{x1} \\ \vec{e}_{y1} \\ \vec{e}_{z1} \end{bmatrix}$$

$$\vec{F}_1 = \begin{bmatrix} F_1\sin(\beta+\phi) \\ -F_1\cos(\beta+\phi) \\ 0 \end{bmatrix}^T \cdot \begin{bmatrix} \vec{e}_{x1} \\ \vec{e}_{y1} \\ \vec{e}_{z1} \end{bmatrix} \qquad \vec{R} = \begin{bmatrix} R\cos(\phi) \\ R\sin(\phi) \\ 0 \end{bmatrix}^T \cdot \begin{bmatrix} \vec{e}_{x1} \\ \vec{e}_{y1} \\ \vec{e}_{z1} \end{bmatrix}$$

$$\vec{F}_K = \begin{bmatrix} -F_K \\ 0 \\ 0 \end{bmatrix}^T \cdot \begin{bmatrix} \vec{e}_{x1} \\ \vec{e}_{y1} \\ \vec{e}_{z1} \end{bmatrix}$$

Step 8: Insert force and position vectors in the equilibrium equations

$$\vec{F}_1 = -\vec{A} - \vec{F}_F = -\begin{bmatrix} A_{x1} \\ A_{y1} \\ 0 \end{bmatrix}^T \cdot \begin{bmatrix} \vec{e}_{x1} \\ \vec{e}_{y1} \\ \vec{e}_{z1} \end{bmatrix} - \begin{bmatrix} 0 \\ -F_F \\ 0 \end{bmatrix}^T \cdot \begin{bmatrix} \vec{e}_{x1} \\ \vec{e}_{y1} \\ \vec{e}_{z1} \end{bmatrix}$$

$$\left(\begin{bmatrix} R\cos(\phi) \\ R\sin(\phi) \\ 0 \end{bmatrix}^T \cdot \begin{bmatrix} \vec{e}_{x1} \\ \vec{e}_{y1} \\ \vec{e}_{z1} \end{bmatrix}\right) \times \left(-\begin{bmatrix} A_{x1} \\ A_{y1} \\ 0 \end{bmatrix}^T \cdot \begin{bmatrix} \vec{e}_{x1} \\ \vec{e}_{y1} \\ \vec{e}_{z1} \end{bmatrix} - \begin{bmatrix} 0 \\ -F_F \\ 0 \end{bmatrix}^T \cdot \begin{bmatrix} \vec{e}_{x1} \\ \vec{e}_{y1} \\ \vec{e}_{z1} \end{bmatrix}\right) + \left(\begin{bmatrix} L_{K0}\cos(\phi) \\ L_{K0}\sin(\phi) \\ 0 \end{bmatrix}^T \cdot \begin{bmatrix} \vec{e}_{x1} \\ \vec{e}_{y1} \\ \vec{e}_{z1} \end{bmatrix}\right) \times \left(\begin{bmatrix} 0 \\ -F_F \\ 0 \end{bmatrix}^T \cdot \begin{bmatrix} \vec{e}_{x1} \\ \vec{e}_{y1} \\ \vec{e}_{z1} \end{bmatrix}\right) = \vec{0}$$

$$\vec{F}_K = -\vec{B} - \vec{F}_1 = \begin{bmatrix} -F_K \\ 0 \\ 0 \end{bmatrix}^T \cdot \begin{bmatrix} \vec{e}_{x1} \\ \vec{e}_{y1} \\ \vec{e}_{z1} \end{bmatrix} = -\begin{bmatrix} 0 \\ B \\ 0 \end{bmatrix}^T \cdot \begin{bmatrix} \vec{e}_{x1} \\ \vec{e}_{y1} \\ \vec{e}_{z1} \end{bmatrix} - \left(-\begin{bmatrix} A_{x1} \\ A_{y1} \\ 0 \end{bmatrix}^T \cdot \begin{bmatrix} \vec{e}_{x1} \\ \vec{e}_{y1} \\ \vec{e}_{z1} \end{bmatrix} - \begin{bmatrix} 0 \\ -F_F \\ 0 \end{bmatrix}^T \cdot \begin{bmatrix} \vec{e}_{x1} \\ \vec{e}_{y1} \\ \vec{e}_{z1} \end{bmatrix}\right) = \begin{bmatrix} -A_{x1} \\ -B_{y1} + A_{y1} - F_F \\ 0 \end{bmatrix}^T \cdot \begin{bmatrix} \vec{e}_{x1} \\ \vec{e}_{y1} \\ \vec{e}_{z1} \end{bmatrix}$$

Step 9: Set up systems of equations

$$-\begin{bmatrix} A_{x1} \\ A_{y1} \\ 0 \end{bmatrix}^T \cdot \begin{bmatrix} \vec{e}_{x1} \\ \vec{e}_{y1} \\ \vec{e}_{z1} \end{bmatrix} - \begin{bmatrix} 0 \\ -F_F \\ 0 \end{bmatrix}^T \cdot \begin{bmatrix} \vec{e}_{x1} \\ \vec{e}_{y1} \\ \vec{e}_{z1} \end{bmatrix} - \begin{bmatrix} F_1 \sin(\beta+\phi) \\ -F_1 \cos(\beta+\phi) \\ 0 \end{bmatrix}^T \cdot \begin{bmatrix} \vec{e}_{x1} \\ \vec{e}_{y1} \\ \vec{e}_{z1} \end{bmatrix} = \vec{0} = \begin{bmatrix} -A_{x1} - F_1 \sin(\beta+\phi) \\ -A_{y1} + F_F + F_1 \cos(\beta+\phi) \\ 0 \end{bmatrix}^T \cdot \begin{bmatrix} \vec{e}_{x1} \\ \vec{e}_{y1} \\ \vec{e}_{z1} \end{bmatrix} = \vec{0}$$

$$-\begin{bmatrix} 0 \\ B_{y1} \\ 0 \end{bmatrix}^T \cdot \begin{bmatrix} \vec{e}_{x1} \\ \vec{e}_{y1} \\ \vec{e}_{z1} \end{bmatrix} - \left(-\begin{bmatrix} A_{x1} \\ A_{y1} \\ 0 \end{bmatrix}^T \cdot \begin{bmatrix} \vec{e}_{x1} \\ \vec{e}_{y1} \\ \vec{e}_{z1} \end{bmatrix} - \begin{bmatrix} 0 \\ -F_F \\ 0 \end{bmatrix}^T \cdot \begin{bmatrix} \vec{e}_{x1} \\ \vec{e}_{y1} \\ \vec{e}_{z1} \end{bmatrix} \right) - \begin{bmatrix} -F_K \\ 0 \\ 0 \end{bmatrix}^T \cdot \begin{bmatrix} \vec{e}_{x1} \\ \vec{e}_{y1} \\ \vec{e}_{z1} \end{bmatrix} = \begin{bmatrix} -A_{x1} + F_K \\ -B + A_{y1} - F_F \\ 0 \end{bmatrix}^T \cdot \begin{bmatrix} \vec{e}_{x1} \\ \vec{e}_{y1} \\ \vec{e}_{z1} \end{bmatrix} = \vec{0}$$

$$\begin{bmatrix} 0 \\ 0 \\ F_F R\cos(\phi) - A_{y1} R\cos(\phi) + A_{x1} R\sin(\phi) \end{bmatrix}^T \cdot \begin{bmatrix} \vec{e}_{x1} \\ \vec{e}_{y1} \\ \vec{e}_{z1} \end{bmatrix} + \begin{bmatrix} 0 \\ 0 \\ -F_F L_{K0} \cos(\phi) \end{bmatrix}^T \cdot \begin{bmatrix} \vec{e}_{x1} \\ \vec{e}_{y1} \\ \vec{e}_{z1} \end{bmatrix} = \begin{bmatrix} 0 \\ 0 \\ F_F R\cos(\phi) - A_{y1} R\cos(\phi) + A_{x1} R\sin(\phi) - F_F L_{K0} \cos(\phi) \end{bmatrix}^T \cdot \begin{bmatrix} \vec{e}_{x1} \\ \vec{e}_{y1} \\ \vec{e}_{z1} \end{bmatrix} = \vec{0}$$

$$\begin{bmatrix} -1 & 0 & -\sin(\beta+\phi) & 0 & 0 \\ 0 & -1 & \cos(\beta+\phi) & 0 & 0 \\ -1 & 0 & 0 & 0 & 1 \\ 0 & 1 & 0 & -1 & 0 \\ R\sin(\phi) & -R\cos(\phi) & 0 & 0 & 0 \end{bmatrix} \cdot \begin{bmatrix} A_{x1} \\ A_{y1} \\ F_1 \\ B \\ F_K \end{bmatrix} = \begin{bmatrix} 0 \\ -F_F \\ 0 \\ F_F \\ -F_F(R\cos(\phi) - L_{K0}\cos(\phi)) \end{bmatrix}$$

$$F_1 = \frac{F_F \cdot L_{K0} \cdot \cos(\phi)}{\cos(\beta) \cdot R} \qquad A_{x1} = F_K = -\frac{F_F \cdot L_{K0} \cdot \cos(\phi)}{\cos(\beta) \cdot R} \cdot \sin(\beta+\phi) \qquad A_{y1} = \frac{F_F \cdot L_{K0} \cdot \cos(\phi)}{\cos(\beta) \cdot R} \cdot \cos(\beta+\phi) + F_F \qquad B = \frac{F_F \cdot L_{K0} \cdot \cos(\phi)}{\cos(\beta) \cdot R} \cdot \cos(\beta+\phi)$$

$$\vec{F}_K = \begin{bmatrix} \frac{F_F \cdot L_{K0} \cdot \cos(\phi)}{\cos(\beta) \cdot R} \cdot \sin(\beta+\phi) \\ 0 \\ 0 \end{bmatrix}^T \cdot \begin{bmatrix} \vec{e}_{x1} \\ \vec{e}_{y1} \\ \vec{e}_{z1} \end{bmatrix}$$

$$\psi = \sin^{-1}\left(\frac{R_y + d}{L}\right) = \sin^{-1}\left(\frac{R\sin(\phi) + d}{L}\right)$$

$$\beta = 90^\circ - \phi - \psi$$

$$\phi = \phi_0 + \Delta\phi$$

Relevant equations

$$x_K = R \cdot \cos(\phi_0 + \Delta\phi) + \sqrt{L^2 - (d + R \cdot \sin(\phi_0 + \Delta\phi))^2} - K_0$$

$$\Delta\phi(x_K) = a_3 x_K^3 + a_2 x_K^2 + a_1 x_K + a_0$$

$\Delta\phi$ must be determined by an interpolation polynomial. The polynomial can be determined from the course of the function x_K.

F_K is the force that must be applied to the piston to apply a defined force F_F to the borehole wall. Thus, the angle correction in the horizontal and vertical planes must be calculated depending on the nominal and actual position of the BHA. The BHA geometry can be used to calculate the displacement vector (location vector at the origin of K0). The direction of the displacement vector is also the direction of the resulting force vector, composed of the three position vectors of the wings. In order to make a change of course now, the individual wing forces must be adjusted so that the resulting force points in the direction of the displacement vector. At the same time, the wings must be adjusted so that no jamming occurs.

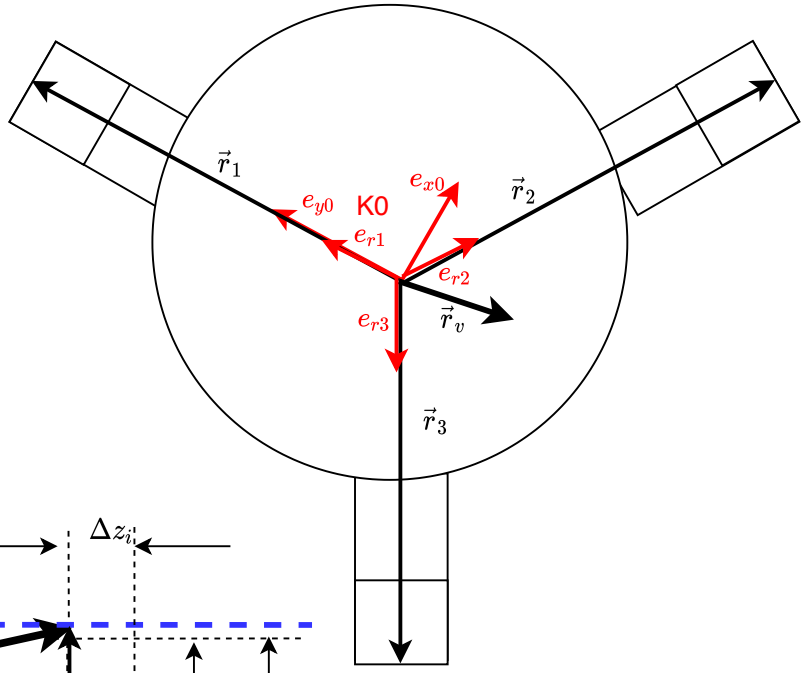

$\vec{r}_{v0} = displacement$

$\phi = \phi_0 + \Delta\phi$

$\Delta z_i \approx 0$ $\quad \Delta r_i \approx \tan(\Delta\phi_i) \cdot L_{K0}$ $\quad |\overrightarrow{r_i}| = s_0 + \Delta r_i$ $\quad \overrightarrow{r_i} = |\overrightarrow{r_i}| \cdot \overrightarrow{e_i}$

Δz_i

borehole wall

K2

$\vec{S}$

$\vec{R}$

K1

$\Delta\phi_i$

K2

Δr_i

$\overrightarrow{e_{r1}} = \overrightarrow{e_{y0}}$

$\overrightarrow{e_{r2}} = \cos(30^\circ)e_{x0} - \sin(30^\circ)\overrightarrow{e_{y0}}$

$\overrightarrow{e_{r3}} = -\cos(30^\circ)e_{x0} - \sin(30^\circ)\overrightarrow{e_{y0}}$

$\frac{D_B}{2} = 19,25mm$

$\vec{r}_i$

Symmetry axis of the BHA

$s_0 = 17,5mm$

e_{y0}

$L_{K0} = 36mm$

K0

e_{z0}

In this case it is assumed in a simplified way that over the entire swivel range $\Delta(z_0)$ is very small. Thus, the position vectors of the wing attack points always lie in the xy-plane.

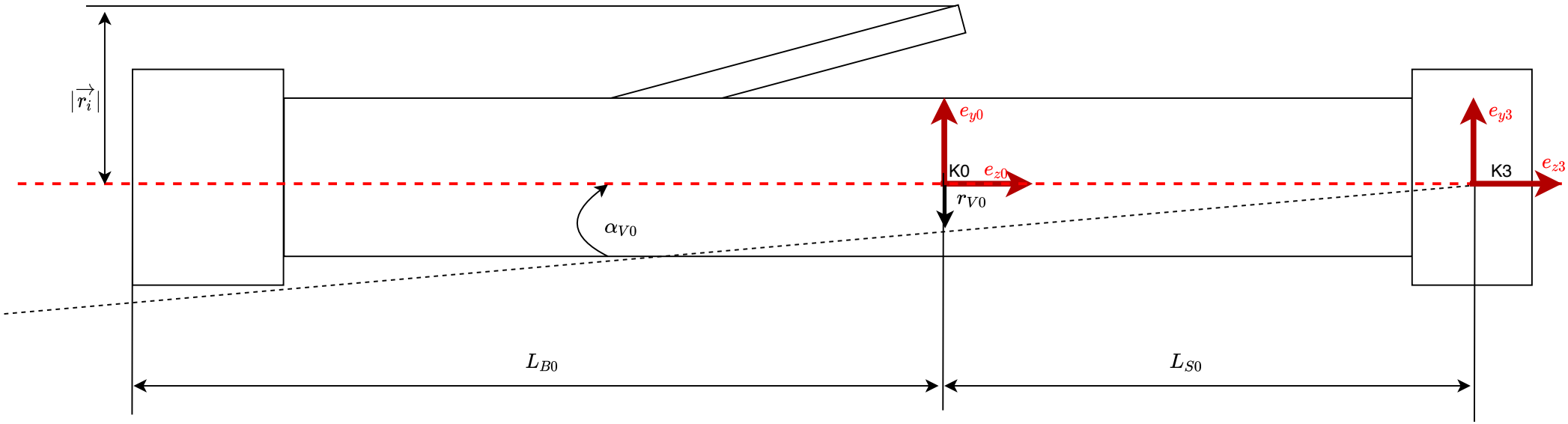
$|\overrightarrow{r_i}|$
e_{y0}
K0
e_{z0}
r_{V0}
α_{V0}
e_{y3}
K3
e_{z3}
L_{B0}
L_{S0}

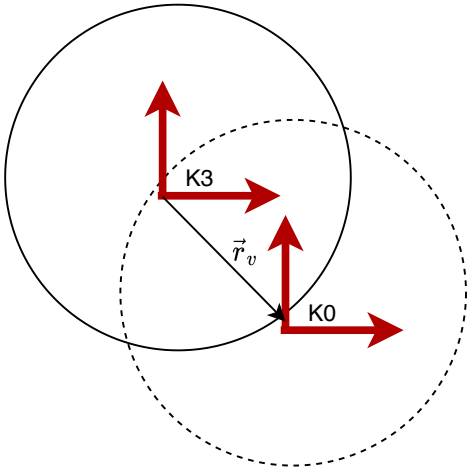
K3
$\vec{r}_v$
K0

A Bibliography

[Jou] *Analysis and optimization of control algorithms for RSSTSP for horizontal well drilling*

[Mad] *An efficient orientation filter for intertial and intertial/magnetic sensor arrays*

[Mat] *Interpolation*

[FIL] *Lagebestimung durch Sensorfusion mittels Kalmanfilter*

[Git] *ROP search algorithms*

[5C3 1994] 5C3, API B.: *Bulletin on formulas and calculations for casing, tubing, drill pipe, and line pipe properties* -. 6th. American Petroleum Institute, 1994

[Aadnoy 2006] Aadnoy, Bernt S.: *Mechanics of Drilling* -. Aachen : Shaker, 2006. – ISBN 978–3–832–24861–1

[Bourgoyne 1986] Bourgoyne, Adam T.: *Applied Drilling Engineering* -. Society of Petroleum Engineers, 1986. – ISBN 978–1–555–63001–0

[Bruno 2005] Bruno, Michael S.: *Fundamental Research on Percussion Drilling - Improved Rock Mechanics Analysis, Advanced Simulation Technology, and Full-scale Laboratory Investigations.* United States. Department of Energy, 2005

[Construction 2011] Construction, American Institute of S.: *Steel Construction Manual* -. American Institute of Steel Construction, 2011. – ISBN 978–1–564–24060–6

[Fairhurst 1956] Fairhurst, C. L. W.: *Some principles and developments in hard rock drilling techniques* -. Minnesota Uni, 1956

[Hearn 1997] Hearn, E.J.: *Mechanics of Materials 2 - The Mechanics of Elastic and Plastic Deformation of Solids and Structural Materials.* Amsterdam : Elsevier, 1997. – ISBN 978–0–080–52400–9

[Mitchell u. Miska 2011] Mitchell, Robert F. ; Miska, Stefan: *Fundamentals of Drilling Engineering* -. Society of Petroleum Engineers, 2011. – ISBN 978–1–555–63207–6

[Moore 1986] Moore, Preston L.: *Drilling Practices Manual* -. PennWell Publishing Company, 1986. – ISBN 978–0–878–14292–7

[PhD u. Liu 2011] PhD, Boyun G. ; Liu, Gefei: *Applied Drilling Circulation Systems - Hydraulics, Calculations and Models*. Orlando, Florida : Gulf Professional Publishing, 2011. – ISBN 978–0–123–81958–1

[R. 2011] R., Hamrick T.: *Optimization of Operating Parameters for Minimum Mechanical Specific Energy in Drilling*. West Virginia University Morgantown West Virginia (2011), 2011